Helicopter drive train modelling for manoeuvre load alleviation

B. van Bruchem

Technische Universiteit Delft

TU Delft

This page is intentionally left blank.

Helicopter drive train modelling for manoeuvre load alleviation

by

B. van Bruchem

to obtain the degree of Master of Science

at the Delft University of Technology,

to be defended publicly on Thursday August 24, 2017 at 2:30 PM.

Student number:	1365223	
Project duration:	September 1, 2015 – August 24, 2017	
Thesis committee:	Dr. Ir. M. Voskuijl,	TU Delft, supervisor
	Ir. J. A. Melkert,	TU Delft, chairman
	Dr. F. Yin,	TU Delft
	Dr. Ir. S. Hartjes,	TU Delft

Thesis registration number: 144#17#MT#FPP

An electronic version of this thesis is available at http://repository.tudelft.nl/.

TU Delft

This page is intentionally left blank.

Acknowledgements

This report marks the end of a journey that began with my internship at the Condition Based Maintenance center of the University of South Carolina. The knowledge about rotorcraft maintenance and operations that I have gained during this time proved invaluable for this research project.

I wish to thank various people for their contribution to this thesis. First and foremost, I would like to thank my supervisor Mark Voskuijl for his guidance and support throughout the project. His insights proved indispensable for this work and his willingness to give his time so generously has been very much appreciated. I would like to offer my special thanks to Travis Edwards and Dr. Bayoumi from the Condition Based Maintenance center for their assistance with the drive train experiment. I would also like to thank the LORD corporation for providing the TorqueLink sensor. Furthermore, the practical insights of Martin Keaney and pilots from the South Carolina Army National Guard into helicopters operations are very much appreciated.

I am grateful to my family and friends for supporting me and making this journey possible. I wish to thank my parents and my brother Maarten for their support and encouragement throughout my study. Special thanks go to Johan and Rozemarijn Nederend for so generously providing me with a place to say in Delft when I came back from South Carolina. Furthermore, I would like to thank my friend and fellow student Pieter Danneels for the many interesting conversations during the time we worked together. I also want to express my gratitude to the friends who helped me with this project. Thank you Edwin Wijnja en Martin van Meijeren for proofreading the report and making it better. Finally, I would like to thank Taco Postma for guiding me and helping me finish this graduation project.

B. van Bruchem
Delft, August 18, 2017

This page is intentionally left blank.

Abstract

Helicopters are complex and expensive aircraft with a level of technology that is immature compared to fixed-wing counterparts. Helicopters suffer from vibratory loads stemming from the main rotor and exhibit control and stability problems in the low-speed flight regime. Operating a helicopter near the limits of its flight envelope may result in unacceptable high structural loads which adversely affects wear and tear of drive train components. Conservative safety regulations lead to high operating cost where a significant part can be attributed to maintenance. Manufacturers and operators therefore strive to make helicopters more capable and reliable in an effort to reduce operating cost. Structural load alleviation offers an attractive option to achieve this goal by reducing component damage accumulation and subsequent required maintenance.

This thesis investigates structural load alleviation in the tail rotor drive train of the UH-60 Black Hawk. The Black Hawk provides a compelling case for load alleviation research because of its ever growing operational weight and resulting increase of drive train load levels. Furthermore, the lifetime of the UH-60 is to be extended so that it will fly for many years to come. Current research and applications of rotorcraft structural load alleviation focus on the main rotor but less attention is given to tail rotor drive train components. This project seeks to address this knowledge gap by investigating manoeuvres that result in critical dynamic loads in the UH-60 tail rotor drive train. A survey of pertinent literature and interviews with helicopter pilots indicate that pedal inputs for left-hand turns in hover lead to high dynamic loads in the UH-60 tail rotor drive train.

A flight simulation model is constructed that offers the novel capability to predict dynamic loads in tail rotor drive shafts. This model consists of an available high fidelity engine model and existing rotor models coupled by a multi body dynamics tail rotor drive train model with properties that are based on component measurements and CAD drawings. Experiments are conducted to determine the relation between manoeuvre aggressiveness and dynamic loads in tail rotor drive shafts. Based on the results a manoeuvre load alleviation control strategy is devised to reduce dynamic loads while ensuring applicable Level 1 handling quality requirements. Application of this control strategy will decrease dynamic loads during left-hand yaw manoeuvres in hover. Furthermore, the results highlight what reduction in loads can be achieved for varying levels of manoeuvre aggressiveness. These findings may aid in the design of flight control systems that incorporate tail rotor drive train load alleviation objectives.

This page is intentionally left blank.

Table of Contents

List of Tables

This page is intentionally left blank.

List of Figures

List of Symbols

Arabic symbols

A	Surface area	m^2
a	Lift curve slope	$1/rad$
a_0	Tail rotor precone	rad
B	Blade tip loss factor	–
c	Blade chord	m
c	Torsional damping constant	$Nm/(rad/s)$
C_D	Drag coefficient	–
C_L	Lift coefficient	–
C_M	Pitching moment coefficient	–
C_T	Thrust coefficient	–
D	Derivative controller gain	
dt	Time step	s
E	Endurance	min
F	Force	N
f	Frequency	Hz
G	Material shear modulus	Pa
g	Gravitational acceleration	m/s^2
h	Flight altitude	m
$\dot{h}$	Rate of climb	m/s
I	Integral controller gain	
I	Mass moment of inertia	kgm^2
J	Polar moment of inertia	m^4
K	Step steepness, height response constant	–
k	Torsional stiffness, spring constant	Nm/rad
K_1	Pitch flap coupling tangent	rad
L	Length	m
M	Moment	Nm
m	Mass	kg
N	Number of occurrences	-
n	Eigenmode number	-
n	Load factor	-
P	Proportional controller gain	

p	Roll rate	rad/s
Q	Torque	Nm
q	Pitch rate	rad/s
Q_l	Load quickness metric	
R	Rotor radius, blade span	m
r	Yaw rate	rad/s
r^2	Coefficient of determination	–
S	Range	km
T	Thrust	N
t	Time	s
t_p	Time to first peak	s
u	Generalized (angular) position or displacement	
u	Velocity component x-axis	m/s
V	Velocity	m/s
v	Velocity component y-axis	m/s
W	Weight	N
w	Velocity component z-axis	m/s

Greek symbols

α	Angle of attack	rad
β_0	Coning angle	rad
β_{1c}	Lateral flapping angle	rad
β_{1s}	Longitudinal flapping angle	rad
δ_p	Pedal deflection	in
γ	Flight path angle	rad
γ	Lock number	-
λ	Inflow ratio	-
Ω	Rotational speed	rad/s
ω_n	Angular eigenfrequency	rad/s
ϕ	Roll angle	rad
ψ	Azimuth angle	rad
ρ	Air density, material density	kg/m^3
σ	Rotor solidity	-
τ	Time delay	s
θ	Shaft rotation angle	rad
θ_t	Linear blade twist	rad
θ_0	Collective pitch angle	rad
θ_{1c}	Lateral cyclic pitch angle	rad

θ_{1s}	Longitudinal cyclic pitch angle	rad
ξ	Damping ratio	–
ξ	Lead-lag angle	rad

Sub- and superscripts

b	blade(s)
cr	critical, cruise
des	desired
e	element(s)
eq	equivalent
est	estimated
f	flap
fus	fuselage
gg	gas generator
i	induced, index
in	inner
m	mean
max	maximum
min	minimum
mr	main rotor
n	eigenmode number
out	outer
p	pedal
s	sampling
sc	service ceiling
ss	steady state
t	twist
tot	total
tr	tail rotor
xyz	XYZ axes

This page is intentionally left blank.

List of Acronyms

AC Aerodynamic Centre. 70
ADS Aeronautical Design Standard. 7, 11, 23, 25, 27, 29, 31–35, 46, 50, 68
ADT Actuator Disk Theory. 71
AFCS Automatic Flight Control System. 1, 7
AH Attack Helicopter. 12
API Application Programming Interface. 21, 57, 67
ASW Anti-Submarine Warfare. 15, 17

BEM Blade Element Momentum theory. 5, 70, 72

CAD Computer-Aided Design. 59
CBM Condition-Based Maintenance. 12, 20, 49, 50, 59, 62
CCW Counter Clockwise. 3, 11, 21, 37
CFD Computational Fluid Dynamics. 6
CG Centre of Gravity. 35–38, 41–47, 50, 70, 71, 75

DOF Degree(s) of Freedom. 5, 9, 18, 20, 23–25, 46, 49, 50, 57, 59

FAR Federal Aviation Requirements. 32
FEM Finite Element Method. 5, 6
FGR FLIGHTLAB Generic Rotorcraft. 5, 22, 24, 25, 50, 70, 71
FPP Flight Performance and Propulsion. 6, 7, 9, 50

GSP Gas Turbine Simulation Program. 6, 9, 19, 21, 49–51, 57, 67, 70

HMU Hydro Mechanical Unit. xi, 21, 67, 68
HQ Handling Quality. 7, 31, 33, 40, 42, 44, 46, 50
HQR Handling Quality Rating. 18, 46
HUMS Health and Usage Monitoring System. 12

IGB Intermediate Gearbox. 13, 14, 20, 40, 59, 60, 62
IP Instructor Pilot. 15, 17
ISA International Standard Atmosphere. 57, 73

JAR Joint Aviation Requirements. 32

LAF Load Amplification Factor. 33, 34, 40, 42, 44, 46, 50

MBD Multi Body Dynamics. 5–7, 9, 19–22, 34, 49, 50, 59, 62, 64, 69, 70, 72, 73
MGB Main Gearbox. 1, 12, 16, 20, 21, 40, 59, 60, 67, 69, 70
MR Main Rotor. 2, 4, 11, 14, 19, 21–25, 29, 34, 35, 37, 40, 49, 51, 57, 69–71, 75
MTE Mission Task Element. 31
MTOW Maximum Take-Off Weight. 4

NASA National Aeronautics and Space Administration. 5, 12, 49

OGE Out of Ground Effect. 4, 15, 17

PID Proportional-Integral-Derivative. 67

RC Rate of Climb. 4, 71
RPM Revolutions Per Minute. 4, 20, 21, 59, 62, 63, 67

SAS Stability Augmentation System. 24
SCARNG South Carolina Army National Guard. 12–15
SLA Structural Load Alleviation. 1–3, 5, 7, 9, 10, 33, 34, 37, 44, 46, 47, 49–51

TGB Tail Rotor Gearbox. 13, 14, 20, 40, 59, 60
TR Tail Rotor. 2, 4, 11, 12, 14, 18, 19, 22–25, 29, 31, 34–37, 40, 42, 44, 49, 57, 73–76
TRDT Tail Rotor Drive Train. 2, 5–7, 9–20, 23, 31–33, 36, 37, 44, 46, 49–51, 59, 62, 64, 65

UH Utility Helicopter. 3, 15, 20, 32
US United States. 3, 5, 7, 31
USC University of South Carolina. 12, 20, 49, 50, 59, 62

1 Introduction

Helicopters have been around for more than 70 years now, offering unique capabilities such as hover and vertical take-off. They are well established in the military, providing troop and equipment transport, ground attack, as well as search and rescue capabilities. Rotorcraft in the civil market are mainly used for VIP transportation, emergency services, and personnel transport in the oil and gas industry. Helicopters have matured over the years to full-fill a range of operational roles that no other platform can offer. However, these advancements do not mean that the helicopter is a fully developed product. Despite the progress made, helicopter technology is immature compared to fixed-wing aviation because of the complexity of rotorcraft aero-physics, a much smaller helicopter market, and simply because rotorcraft developments started later than that of fixed-wing aircraft. [2] [13]

The helicopter faces a number of challenging problems. First and foremost, vibrations stemming from the main rotor and its interaction with the fuselage form one of the most common and disruptive challenges for rotorcraft development and operation today. [13] An example is the recent world-wide grounding of the Airbus H225 fleet because of fatigue cracks in the Main Gearbox resulting in two helicopter crashes. [31] The challenge is to understand and prevent these vibrations at an early stage to increase reliability and operational availability, but also controllability and passenger comfort.

Secondly, rotorcraft are very expensive in terms of operations and cost of ownership. Conservative safety regulations have led to stringent and costly maintenance requirements that also affect operational availability. Maintenance reportedly accounts for almost a quarter of total helicopter operating cost. [38]. As a result, operators seek to reduce operating costs and increase helicopter utilisation rates. New helicopters are introduced which offer greater capabilities and performance, utilisation of helicopters currently in service is increased, and the operational lifetime of existing airframes is extended. For the military, this translates to ever heavier loaded helicopters, operating airframes beyond the originally envisioned lifetime, and adapting helicopters to perform roles they were not designed for. [3] For example, the operational lifetime of the UH-60 Black Hawk is to be extended by re-engining the aircraft and adding other upgrades. [28]

A third issue is that helicopter stability and control characteristics are inherently poor compared to fixed-wing aircraft, especially near hover and at low speeds. [61] [15] Also, operating a helicopter near the limits of its flight envelope may result in unacceptable high structural loads. Pilots have to make sure these limits are not exceeded by monitoring appropriate load indicators in the cockpit. These factors impose extra workload on the pilot and adversely affect handling qualities.

Driven by these challenges and operational demands, manufacturers are developing technology to improve overall efficiency and enhance rotorcraft capabilities. Helicopter controllability has improved and pilot workload has been reduced over the last decades with the advent of computer aided control systems. This development has led to Automatic Flight Control Systems (AFCSs) with functions that can go from basic stabilization to advanced envelope protection schemes and autopilots. [15] [61] Using active control based on the system state, one could potentially utilize the maximum helicopter performance capabilities in a safe manner without exceeding structural limits. [62] The reduction of structural loads in the rotor system, drive train and fuselage by means of control is known as Structural Load Alleviation (SLA).

Successful application of Structural Load Alleviation will lower damage accumulation and elongate the lifetime of structural components. SLA has the potential to reduce maintenance cost and improve helicopter component reliability for both current and new rotorcraft. Recent examples of SLA applications include main rotor yoke bending alleviation for the Bell-Boeing V-22 Osprey and tail rotor load alleviation for the new Bell 525 Relentless. [35] [34] SLA seems well suited to increase the lifetime of existing helicopters such as for the UH-60 Black Hawk.

The topic of this thesis is UH-60A Black Hawk drive train modelling for manoeuvre load alleviation. The reason for selecting this helicopter is threefold. Next to the aforementioned desired operational lifetime extension, there is a wealth of research data available about this helicopter which will aid in the research here. Furthermore, the gross weight of the UH-60 has increased significantly over the years. However, only the main transmission and engines have been upgraded while other drive train components have remained the same. This results in a higher average stress level in the drive train and associated risk of structural damage. [3] These three reasons combined make a compelling case to investigate SLA in the UH-60 drive train. Specifically, the loads in the Tail Rotor Drive Train (TRDT) will be investigated because much attention has been given to Main Rotor (MR) load alleviation but less so to tail rotor drive trains.

This documents reports the work that has been done on helicopter drive train modelling for manoeuvre load alleviation. Chapter 2 provides the reader with an overview of the UH-60 Black Hawk as well as a background on relevant rotorcraft research and developments. Chapter 3 details the scope and objective of this research project. Next, the identification of critical manoeuvres for the UH-60 TRDT is discussed in chapter 4. A UH-60 flight simulation has been constructed to calculate loads in the TRDT during critical manoeuvres. The various components of this flight simulation model and the way in which these are coupled is detailed in chapter 5. The experiment set-up and approach to investigate the feasibility of Structural Load Alleviation are the topic of chapter 6. Chapter 7 contains the results of these simulations. The last part of the report body is chapter 8 where conclusions are drawn and recommendations for future work are given.

Furthermore, the report contains a number of appendices that provide more technical background on the component models used in the constructed UH-60 flight simulation model. First, Appendix A provides technical information on the flight simulation model and instructions on how to use it. Next, Appendix B details the constructed UH-60 and AH-64 tail rotor drive train models, and describes the experiment that has been used to validate the constructed TRDT models. Lastly, more technical details on the Main Rotor and Tail Rotor component models are provided in Appendix D and Appendix E respectively.

2

Background

This research project concerns load alleviation in the tail rotor drive train of the UH-60 Black Hawk. An overview of the UH-60 Black Hawk is presented in section 2.1 to familiarize the reader with this helicopter and its drive train components. Next, section 2.2 discusses the results of a literature review about relevant research and developments pertaining to drive train modelling and Structural Load Alleviation.

2.1. Sikorsky UH-60 Black Hawk

The UH-60 Black Hawk is a medium-lift Utility Helicopter (UH) built by Sikorsky, see Figure 2.1 for an overview of this helicopter. The US Army is the main operator of the UH-60. It uses the Black Hawk for troop transport. The UH-60 can carry a crew of three and eleven troops. Other roles of this helicopter include medevac (medical evacuation), reconnaissance, and cargo transport for which a cargo hook is available. Multiple variants of the Black Hawk have been developed, including the SH-60 Sea Hawk and the upgraded UH-60M Black Hawk. The data provided here apply to the UH-60A variant. For the sake of simplicity, the UH-60A Black Hawk will simply be referred to as UH-60 in the rest of this report.

The UH-60 has a four-bladed articulated main rotor rotating Counter Clockwise (CCW) (viewed from above), and a four bladed, top aft rotating canted tail rotor puller propeller to provide directional control and addi-

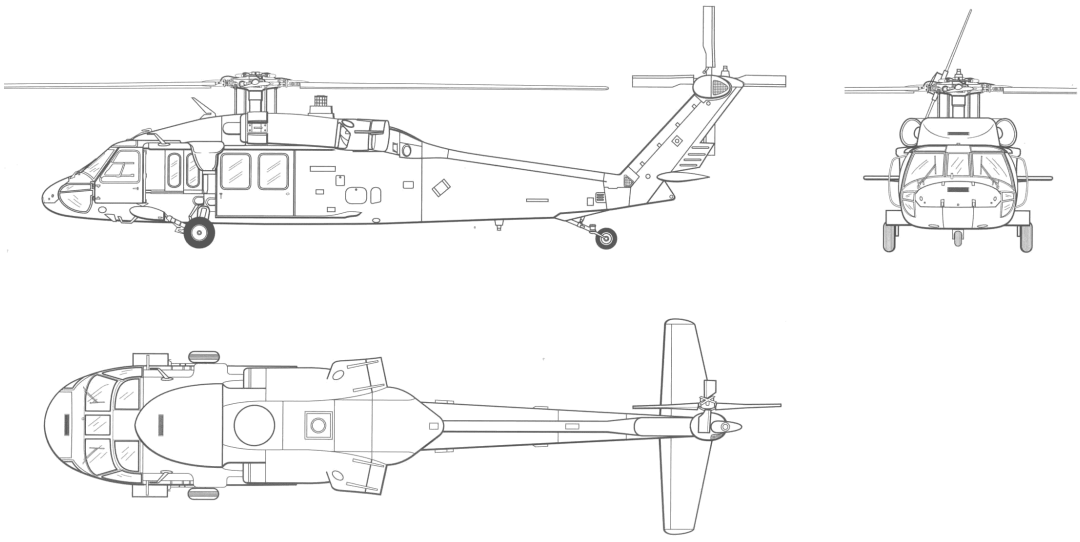

Figure 2.1 – Overview of the Sikorsky UH-60 Black Hawk. Saranga [53]

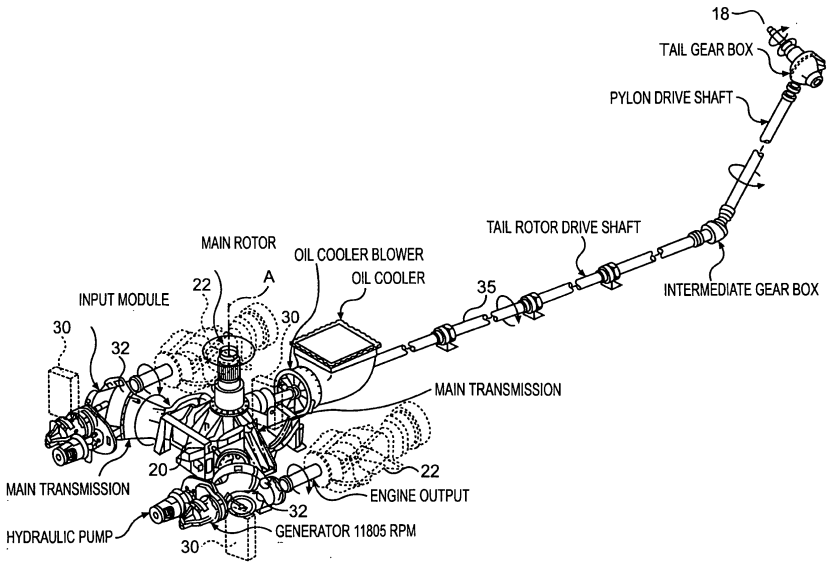

Figure 2.2 – Overview of the UH-60 drive train. [64]

tional lift. The Black Hawk is powered by two T700-GE-700 turboshaft engines generating 1,560 shp each.The UH-60 features a typical drive train layout where the engines are connected to the main transmission via a number of gear reductions. The main transmission powers the main and tail rotor, changes the engine drive angle, reduces drive shaft RPM, and powers accessory modules. Power is transferred to the tail rotor by means of a system of drive shafts that run along the upper part of the tail boom, flexible couplings, bearings, and gearboxes. Figure 2.2 shows the complete UH-60 drive train and the location of these components. The main characteristics of the Black Hawk are listed in Table 2.1.

Table 2.1 – Main characteristics of the UH-60A Black Hawk. [30]

Parameter	Symbol	Value
Number of MR & TR blades [-]	$N_{b,mr}$, $N_{b,tr}$	4, 4
Main Rotor radius [m]	R_{mr}	8.178
Tail Rotor radius [m]	R_{tr}	1.676
Overall length [m]	L_{tot}	19.76
Fuselage length [m]	L_{fus}	15.26
Empty weight [kg]	W_{empty}	5118
Maximum Take-Off Weight [kg]	W_{MTOW}	7708
Maximum gross weight [kg]	W_{gross}	9185
Maximum internal payload [kg]	W_{payload}	1197
Maximum external payload [kg]	W_{slung}	3629
Cruise speed [kn]	V_{cr}	140[a]
Maximum speed [kn]	V_{max}	160[b]
Rate of Climb [m/min]	RC	115[c]
Cruise range [km]	S_{cr}	590[d]
Endurance [min]	E	136
Service ceiling [m]	h_{sc}	5700
Hover ceiling [m]	h_{OGE}	1645[e]

[a] At 4,000 ft, 35°C
[b] At sea level
[c] At 7620 kg, 1220 m, and 35°C
[d] At MTOW with 30 min fuel reserve
[e] In OGE conditions at 35°C

2.2. Literature review

New rotorcraft technology is enabled by advances in research and developments conducted by manufacturers and research institutions. The aim of this literature study is to determine what research is relevant for this structural load alleviation feasibility study, and to benefit from the knowledge that is available. Literature on the following areas have been surveyed: flight simulation tools, helicopter loads, component modelling methods, load alleviation and limit protection, and handling qualities. A synthesis of the findings from this study is provided at the end of this section.

2.2.1. Flight simulation tools

A flight simulation tool is needed to simulate critical manoeuvres for the UH-60 TRDT. This tool should be able to predict dynamic loads in the drive train for the purpose of Structural Load Alleviation research. A review of literature shows there are a number of software packages available to simulate helicopter flight. These options are listed below together with a short description of software capabilities.

NASA NDARC The NASA NDARC (NASA Design and Analysis of Rotorcraft) tool has been developed to provide the US government with up to date rotorcraft simulation tools. [33]. It is intended for the design and sizing of rotorcraft for specific missions and/or flight conditions, and to analyse flight performance in off-design conditions. The software can model a broad range of existing and new rotorcraft configurations such as the tilt rotor. It combines a set of component models such as propulsion, fuselage, wings, tails, and rotor models to create a complete simulation model. The helicopter drive train is modelled as a set of gear ratios, the rotor is modelled using the Blade Element Momentum theory (BEM), and the engines are represented by a parametrized turboshaft engine model. The tool can be used for low fidelity performance analysis, although work is under way to include higher fidelity component models.

FLIGHTLAB FLIGHTLAB is a well-known commercial flight dynamics modelling simulation software package. [45] It includes the FLIGHTLAB Generic Rotorcraft (FGR) which is a non-linear model representative of the UH-60 Black Hawk which consists of control systems and physics-based element models. The Multi Body Dynamics (MBD) main rotor is modelled with controlled hinges and rigid blades to which quasi-steady airloads calculated using the BEM are applied. The tail rotor is modelled using a Bailey rotor. [8] Furthermore, a turboshaft engine model is included. The aerodynamics of airframe components are determined using look-up tables. The FGR does no include a tail rotor drive train model. Applications of the FGR include load alleviation and handling qualities research [45] [61]

GenHel Howlett [27] has created a full non-linear UH-60A simulation model based on Sikorsky's GenHel to provide the United States (US) Army with a performance analysis and handling qualities evaluation capability. The resulting verified engineering simulation 6-Degree(s) of Freedom (DOF) model is built up from physics based element models such as a BEM main rotor and a Bailey tail rotor that only calculates thrust. The simplified engine consists of a "*linearised representation with coefficients that vary as a function of operating condition*". [27] The tail rotor drive train is represented by a set of inertia and gear ratio values. Furthermore, an elaborate flight control system and engine fuel flow controller block diagrams are provided. The work of Howlett [27] is often used because of the wealth of data supplied with this verified engineering model.

CAMRAD II CAMRAD II is a highly sophisticated, high fidelity simulation software package to analyse the aeromechanics of rotorcraft. [32] This commercial tool can be used to evaluate rotorcraft performance, loads and vibrations, as well as helicopter response and stability. It consists of advanced component models incorporating MBD, non-linear FEM, and rotorcraft aerodynamics. For example, the main rotor is modelled with flexible blades built up of non-linear finite elements. Aerodynamic blade modelling is based on second-order lifting line theory. CAMRAD II includes transmission components for the drive train model to account for torque transfer. Examples of CAMRAD II use include the correlation of performance and loads from wind tunnel measurements of a UH-60A main rotor, and the UH-60A in level flight conditions. [54] [65]

These flight simulation software packages offer varying modelling fidelity and capability. The NASA NDARC, FLIGHTLAB, and GenHel tools do not offer the capability to predict loads in the tail rotor drive train of a helicopter. The remaining CAMRAD II tool can be used to model transmission components in the drive train but it is unknown what the tail rotor drive train modelling capabilities of this tool are. Furthermore, CAMRAD is a commercial software package that is not available for this research. Because of this, a flight simulation model has to be constructed that can predict TRDT loads.

2.2.2. Helicopter loads

A helicopter is subjected to static and vibratory loads stemming from control inputs, rotor and fuselage aerodynamics, and structural loads in the drive train. These loads lead to wear and tear of the system. Exceeding limit loads may lead to outright failure of components for instance. Oscillatory loads may lead to fatigue damage whereby parts will fail at stress levels lower than the limit load.

Research to understand and predict helicopter loads has focused on the main rotor which is the primary source of aerodynamic loads having to provide lift, thrust and part of the control. Higher harmonics of rotor loads lead to unexpected and unacceptable vibrations in rotorcraft. This is one of the common and disruptive challenges for rotorcraft development today. [13] Examples of aerodynamic phenomena investigated are dynamic stall, stall flutter, and blade tip effects. [17] [36] These phenomena may lead to large aero-elastic loads and deflections, resulting in large structural rotor hub moments and pitch link control loads. [51] [61]

Part of the vibrations encountered in rotorcraft stems from the drive train with its engines, drive shafts, gearboxes, bearings and couplings. [29] Vibrations are a significant cause of fatigue damage and failure in the drive train. [52] Hence, a lot of attention is given to research into the causes and effects of drive train loading. Examples include the analysis of drive shaft coupling transient overload capacity [3], overload evaluation of bevel gears [4], and condition monitoring of drive shafts. [24] Tail rotor loading differs from that of the main rotor in that at higher forward speed the aerodynamic force on the vertical fin increases so that it provides more anti-torque. Furthermore, the engine power required reduces when transitioning from hover to forward flight. The combination of these two effects result in unloading of the tail rotor for increasing forward speed. [39] Dynamic structural loads occurring in the TRDT are mainly the result of engine torque variation and aerodynamic loads acting on the tail rotor. Deformation of the tail boom subjected to aerodynamic and manoeuvring loads, shaft misalignment and eccentricity, and drive train vibrations are amongst other effects affecting TRDT loads [25]

2.2.3. Component modelling methods

Modelling of the complete UH-60 drive train requires component models of the main rotor, tail rotor, tail rotor drive train, and engines. These components models entail the calculation of structural and aerodynamic loads, as well as engine performance.

Structural modelling For structural models, a distinction can be made between static and dynamic models and small versus large deformations. If low fidelity is required and/or deformation is not considered, rigid models may be used. Static Finite Element Method (FEM) models may be used to obtain high fidelity results for both small and large deformations, for instance with the analysis of local internal stresses and forces in a gearbox. [55] Other examples include modelling of TRDT shafts and hanger bearings. [16] [18]. To model the dynamics of a drive train, it appears that MBD models are well suited. MBD models consists of a system with rigid bodies that are linked to each other with joints to restrict relative motion. The MBD method has been successfully applied in the past to high fidelity drive train modelling of wind turbines. [49] For large deformations the authors highlight the use of FEM models to replace rigid bodies in an MBD model assembly.

Aerodynamic modelling Aerodynamic models are needed to calculate the loads acting on the main and tail rotor during flight and the airframe. Models range from lookup tables, actuator disk theory, and lifting line methods, to full Computational Fluid Dynamics (CFD). [12] [8] CFD modelling is used for high fidelity simulations, for example to obtain more accurate harmonic vibration results. [17] The Flight Performance and Propulsion (FPP) group at TU Delft Aerospace Engineering has an in-house developed MBD UH-60 rotor model based on look-up tables using MATLAB SimMechanics.

Engine modelling To evaluate helicopter engines, performance models are used varying from empirical, state-space, to 0-D models. [20] A zero dimensional (0-D) model computes the average state of the gas at discrete engine stations, based on component maps or equations. These models can quickly analyse the performance of a gas turbine engine with high accuracy. Previous work in the FPP group has led to the development of a high fidelity 0-D Black Hawk T700-GE engine model made with the Gas Turbine Simulation Program (GSP). [59] [60]

2.2.4. Load alleviation and limit protection

Loads can be reduced by means of alleviation control or prevented by means of limit protection control. The development of fly-by-wire and digital control systems has led to AFCSs with functions that can go from basic stabilization to advanced envelope protection schemes and autopilots. [61] [15] Using active control based on the system state, one could potentially utilize the maximum helicopter performance capabilities in a safe manner without exceeding structural limits. [62] Research examples of load alleviation by means of active control include UH-60 hub moment limit protection and pitch link load alleviation. [51] [61] Current use of active control includes main rotor yoke bending alleviation for the Bell-Boeing V-22 Osprey and tail rotor SLA for the Bell 525 Relentless. [35] [34] Here the control laws are adjusted such that a load alleviation objective is taken into account while at the same time satisfying handling qualities.

Instead of applying active control and changing control laws, one could also opt to alter manoeuvres such that limit loads are not exceeded and/or load levels are reduced. Examples include control input limitations during manoeuvres as described in operating manuals, or trajectory optimization. [11] The complexity of helicopter dynamics and control renders the design and validation of load alleviation control systems a difficult task. Control strategies where helicopters manoeuvres are adjusted to reduce loads are less complicated and hence appear better suited for this load alleviation research project.

2.2.5. Handling qualities and requirements

Load alleviation control and limit protection are closely coupled to helicopter Handling Qualities (HQs). Voskuijl et al. [62] state: "*for advanced control systems with load alleviation and flight envelope protection, control tuning is essentially a trade-off between handling qualities and structural loads.*" HQs have been defined by Cooper and Harper [14] as "*those qualities or characteristics of an aircraft that govern the ease and precision with which a plot is able to perform the tasks required in support of an aircraft role*". As such handling qualities are improved since "*envelope protection and load alleviation can reduce the pilot's workload because the structural limits do not have to be monitored any more.*" [62]

The military handling quality requirement Aeronautical Design Standard (ADS)-33 standard has been adapted for all US military rotorcraft. [31] An example is the design and optimization of a new control laws for the UH-60M that have to satisfy Level 1 ADS-33 handling qualities requirements. [58] Whether for new designs or upgrades for existing rotorcraft, one should account for the effect of load alleviation and envelope protection on handling qualities, because of the critical role handling qualities play in the both performance and safety. [44] Quantification of the mutual influence between load (alleviation) and handling qualities is needed to account for both handling requirements and load alleviation/envelope protection. [61] [48] These requirements and considerations must be taken into account during the work here.

2.2.6. Synthesis

This literature review has presented an overview of rotorcraft research and industry practices relevant for load alleviation in the tail rotor drive train. Technology and understanding is still relatively immature compared to fixed wing aircraft because of the fundamental complexity of rotorcraft. Helicopters are expensive to acquire and operate, and many modern helicopters suffer from excessive vibrations. These loads are difficult to model/predict which frequently leads to exceeding load limits. Consequently, the maintenance of rotorcraft is expensive and the accident rate is significantly higher than for fixed wing aircraft.

A large portion of the ongoing research focuses on measuring and modelling helicopter loads, specifically for the main rotor. Active control is investigated for vibration suppression, load alleviation, and improving handling qualities such as required by the military ADS-33 specifications. However, few helicopters are equipped with such systems today. Though load alleviation for the main rotor system has been investigated, little attention is given to load alleviation in the Tail Rotor Drive Train. Increased load levels, and demanding manoeuvres leading to high tail rotor loads, make the TRDT a viable candidate for load alleviation.

There is no current flight simulation tool available that has the capability to predict TRDT loads. Hence a flight simulation model must be constructed that can capture these loads during critical manoeuvres. Various component models and modelling methods have been discussed, including promising MBD models and a high fidelity engine model already available at the FPP group.

This page is intentionally left blank.

3

Scope and objectives

Helicopter drive train modelling for manoeuvre load alleviation is a broad subject which can be approached in many different ways. Clearly, the scope and aim of this project must be defined so that the steps to successfully complete this work can be determined. Section 3.1 details the scope and aim of this thesis. Next, the research objectives and questions are formulated in section 3.2.

3.1. Research scope and aim

Structural Load Alleviation has the potential to reduce maintenance cost and improve helicopter component reliability for both current and new rotorcraft. This is especially relevant for the UH-60 Black Hawk that is currently operated at significantly higher gross weights compared to the original design. While more powerful engines have been installed to supply sufficient power, the Tail Rotor Drive Train (TRDT) has essentially remained the same. [3] As a result the mean torque loading of the TRDT has increased which may degrade component life and lead to exceeding limit loads.

Though load alleviation for helicopter main rotor systems has been investigated, little attention is given to load alleviation in the Tail Rotor Drive Train. This work seeks to address that current research knowledge gap. The aim of this project is to develop load alleviation control strategies for the UH-60 tail rotor drive train based on a flight simulation model that has the ability to predict dynamic TRDT loads. The results may serve as guidelines and highlight possible control options as well as constraints for flight control systems that include TRDT SLA objectives. The novelty of this work lies in the combination of expert interviews to identify critical manoeuvres, and constructing a simulation capability that is not offered by state of the art simulation software.

Past research efforts at the Flight Performance and Propulsion group of the faculty of Aerospace Engineering at Delft University of Technology have focussed on modelling of the UH-60 rotor and engines. [59] This has resulted in a SimMechanics MBD model representative of the UH-60 main rotor and a high fidelity GSP model of the UH-60 T700-GE engine. The current research effort will focus on drive train modelling of the UH-60. An MBD TRDT model will be constructed to calculate dynamic loads in tail rotor drive train. These models will be coupled to construct a flight model representative of the UH-60 Black Hawk.

A number of choices have to be made to keep this project feasible in terms of time and complexity.

1. The MBD TRDT model will be build using ideal gearbox models and single twist DOF drive shafts. Modelling complex phenomena such as out-of-plane shaft flexural motion or gear effects such as backlash is beyond the scope of this thesis. Furthermore, complex structural models will likely have an adverse affect computational effort. As a consequence of this reduced model fidelity, shaft torque loads will be used as an indicator of critical dynamic loads in other parts of the tail rotor drive train.
2. Aerodynamics of non drive train components such as the airframe will not be accounted for because the scope of this investigation is on drive train modelling.

3. Simplified engine and flight control systems will be used to reduce the flight simulation model complexity. Incorporating highly complex flight control laws and engine controller such as found on the actual UH-60 is beyond the scope of this research.
4. Lastly, the complexity of critical manoeuvres to be simulated will be carefully evaluated to reduce the required complexity of the flight simulation model.

3.2. Research objectives and questions

Research objectives

The overall research objective is to reduce critical dynamic loads in the UH-60 Tail Rotor Drive Train (TRDT) by developing a detailed flight simulation model that will be used to identify manoeuvre load alleviation control strategies.

This research project consists of two parts. The groundwork is to construct an UH-60 flight simulation model, which will secondly be used to investigate structural load alleviation in the tail rotor drive train for identified critical manoeuvres. Separate objectives have been drafted for these two parts.

1. The first objective is to develop a simulation model of the UH-60 Black Hawk that can be used to determine dynamic loads in the tail rotor drive train during manoeuvres by constructing and validating a UH-60 TRDT multi-body dynamics model and coupling this to existing rotor, and engine models.
2. The second objective of this research is to reduce critical dynamic loads in the UH-60 TRDT by developing novel load alleviation control strategies

Research questions

The following research questions have been formulated to steer this thesis project:

1. What are relevant model criteria and methods to construct a UH-60 flight simulation model?
   - What are the specifications of the UH-60 and its drive train components?
   - What are the characteristics of critical dynamic loads occurring in the TRDT?
   - What manoeuvres cause critical dynamic loads in the TRDT?
   - What methods can be used to validate the UH-60 flight simulation model and its components?
   - What components and couplings are needed to construct a UH-60 flight model for the simulation of critical manoeuvres?
2. What SLA control strategies can be identified to reduce critical dynamic loads in the UH-60 TRDT?
   - What constraints affect feasible SLA control strategies?
   - What regulations have to be accounted for in the design of load alleviation control strategies?
   - What is the relation between handling qualities and dynamic loads for various levels of aggressiveness during critical manoeuvres?

4

Critical manoeuvres

Part of this research is to construct a flight simulation model representative for the UH-60 Black Hawk. This model will be used to evaluate dynamic loads in the tail rotor drive train during critical manoeuvres. The following research question was posed in chapter 3: "*What manoeuvres cause critical dynamic loads in the Tail Rotor Drive Train (TRDT)?*" This chapter concerns the identification of manoeuvres resulting in critical dynamic loads in the UH-60 tail rotor drive train. First the results of a brief literature survey are presented in section 4.1. Furthermore, a number of pilot interviews have been conducted to learn how helicopters are used in practice and to determine what pilots view as critical manoeuvres for the helicopter. Section 4.2 presents a summary of these interviews. The findings and conclusions of this chapter are presented in the final section 4.3.

4.1. Literature survey

The structural and aerodynamics loads acting on a helicopter depend to a large extent on the type of manoeuvres flown and the demanded level of aggressiveness. Standard manoeuvres for military helicopters are specified in operating manuals and handling quality requirements (e.g. ADS-33, [7]). The literature survey reveals that tail rotor aerodynamic forces are the dominant source of external TRDT loading. The tail rotor is designed either for the critical hover altitude or for the engine critical altitude, where it must provide sufficient torque for directional control and to counter main rotor reaction torque. [40] The UH-60 has a CCW rotating MR (viewed from above) and a top aft rotating Tail Rotor (TR) in tractor configuration which is canted to provide some lift. [22] See Figure 2.1 for an overview of the UH-60. This layout is important because of the interaction between main rotor wake and the tail rotor, tail rotor stall effects due to precession, and the direction of positive main rotor torque. As a result of these interactions, yaw acceleration in the nose left direction requires higher tail rotor torque than in the other direction. [40]

TRDT loads are for a large part caused by tail rotor loads during flight, especially for manoeuvres that require a lot of engine torque for the tail rotor. [40] Critical manoeuvres for tail rotor loads are different from critical manoeuvres for the main rotor. The tail rotor is unloaded at increasing forward speed due to the lift force generated by the vertical fin whereas the main rotor is not. [39] The following manoeuvres resulting in high tail rotor loads have been identified from literature:

- Maximum sideward flight speed at the critical ambient design condition will result in maximum steady tail rotor torque. [40] Lombardo [39] also mentions sideways flight as a demanding manoeuvre.
- Steady sideslip is deemed to be a critical manoeuvre for tail rotor loads as well [39]
- Near zero forward velocity yawing manoeuvres are critical for maximum required tail rotor thrust. [40] Examples of such manoeuvres resulting in high TRDT loads are rapid turns and abrupt turn stops that for instance result from tail rotor pedal reversals. [39]
- Laberge et al. [37] indicate that "*for the UH-60 specifically, right sideward flight and aggressive left turns in a hover can produce high transient torques within the H-60 tail rotor drive train that are well above the maximum continuous power level at which the tail rotor drive system components are qualified.*"

Concerning aggressive left turns it should be noted that pilots rate the UH-60 handling qualities for a hovering turn as "*acceptable but unsatisfactory*". [21][14] This may lead to large and/or aggressive pedal inputs to achieve the desired heading change. Other contributing factors to TRDT loads are deformation of the tail boom subjected to aerodynamic and manoeuvring loads, shaft misalignment, and vibrations. [25] Aggressive manoeuvres and rapid turns are typically encountered in combat. Polanco [50] mentions combat manoeuvres against fixed-wing aggressors which results in apparent higher tail rotor loads, but does not elaborate on these manoeuvres. The author discusses load variability as well: "*loading for the same aircraft and same flight conditions can vary dramatically due to pilot technique, altitude and weight.*"

4.2. Expert interviews

The US Army is the world's largest operator of helicopters and the main operator of the UH-60A Black Hawk utility helicopter. It has explored and implemented the concept of Condition-Based Maintenance (CBM) using Health and Usage Monitoring System (HUMS) in its fleet to extend helicopter life time, operational availability and reliability. This has been done in cooperation with helicopter manufacturers, including Boeing and Sikorsky, and research institutions such as National Aeronautics and Space Administration (NASA) and universities. The University of South Carolina (USC) is involved in CBM research for helicopters of the South Carolina Army National Guard (SCARNG). Their contacts with the SCARNG made it possible to conduct interviews with pilots flying the UH-60A Black Hawk and the AH-64D Apache helicopter. Furthermore, a retired pilot flying the SH-60B Sea Hawk has been interviewed. (The Sea Hawk is the maritime version of the Black Hawk.) The AH-64 and UH-60 have very similar rotor configurations and tail rotor drive train layouts. Furthermore, these military rotorcraft are used in similar operating environments and maintained according to the same standards. This makes the interviews with AH-64 pilots relevant valuable as well. The aim of these interviews was to determine what manoeuvres are most demanding for the helicopter tail rotor drive train, to identify weak and strong parts of the UH-60A and AH-64D helicopters, and to get a better understanding of how these helicopters are used in military service. The findings of these interviews are presented in this section. First the interviews with AH-64D pilots are summarized in subsection 4.2.1, followed by the interviews with H-60 pilots in subsection 4.2.2.

4.2.1. AH-64 pilot interviews

"*We are flying close to a lot of our limits in normal operations because of the weight and everything else dragging on the aircraft*" - Maintenance test pilot E. Hynes

A combined interview with two pilots has been conducted to investigate critical tail rotor drive train manoeuvres for the AH-64 and how the helicopter is used. Two AH-64D pilots from the SCARNG, Eric Hynes and a fellow maintenance test pilot, were willing to answer questions about operational use and maintenance of the Boeing AH-64D Apache helicopter. The content of this section is a summary of that interview. Both test pilots have extensive experience with flying helicopters, Mr. Hynes has flown for more than 30 years logging more than 4000 flights hours in helicopters such as the UH-1 Huey, OH-58 Warrior, and now the AH-64 Apache. As maintenance test pilots, these guard members take the aircraft out for test flights after major maintenance. A helicopter can only return to service after is has passed all checks during a test flight.

Overview AH-64 Apache

The Boeing Attack Helicopter (AH)-64D Apache is operated by a crew of two: a pilot in the back seat and a co-pilot/gunner in the front seat. It carries a rotating gun under its nose, and is able to carry ordnance on hard points that are mounted on stub-wing pylons to either side of the fuselage. See Figure 4.1 for a side view of this helicopter. The aircraft full-fills an anti-armour role and is also used for close combat air support of ground troops. It is powered by two T700-GE-701C turboshaft engines and features a four bladed main rotor and a four bladed x-shaped tail rotor pusher propeller. The tail rotor is driven by a drive train that runs along the top of the tail boom, see Figure 4.2. The Tail Rotor Drive Train is connected to Main Gearbox (MGB) and transfers torque to the TR using a system of shafts interconnected by bearings, shaft couplings, and gearboxes.

Figure 4.1 – Interviewed SCARNG AH-64D maintenance test pilot.

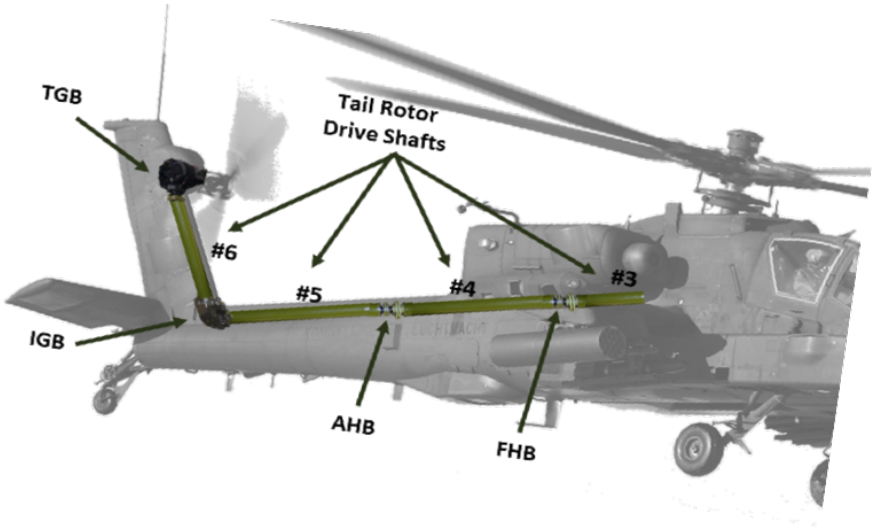

Figure 4.2 – Schematic overview of AH-64 TRDT components including four drive shafts, forward and aft hanger bearings (FHB, AHB), the Intermediate Gearbox (IGB), and the Tail Rotor Gearbox (TGB). - Courtesy of USC CBM

Helicopter operations

The 24 strong AH-64D fleet at the McEntire Joint National Guard Base is part of the South Carolina Army National Guard. Units from this base have been deployed to Kuwait during the initial phase of the second Gulf War. McEntire currently serves as a AH-64D training base where guard pilots from neighbouring states go to for practising night flights over the nearby Fort Jackson military base. On average, the Apache fleet logs about 3000 flight hours a year, with aircraft being launched daily. A regular training flight lasts about two-and-a-half to three hours, in which pilots train on flying low above the tree tops, practice night time (slope) landings, and train on using the night vision system.

Maintenance and hardware

Questions were asked about the reliability of drive train components and the maintenance required to keep the aircraft flying to discover which parts of the helicopter drive train are vulnerable. Apache helicopters are very maintenance intensive, with service intervals set at 25, 50, 125, 250, and 500 hours. During the 500 hour phase overhaul the helicopter is completely taken apart, inspected and serviced, and then put back together again. The pilots indicated that for the complex AH-64D "*it is mostly the electronics that go bad. Mechanically the helicopter is very solid.*"

The weakest parts of the tail rotor drive train in their opinion are the drive links attached to the tail rotor which drive the tail rotor swash plate. (The tail rotor is in turn driven by the output quill shaft from the TGB.) Especially when flying at high altitudes, cracks are known to form in the drive links. The hollow shafts in the tail rotor drive train are very thin and light. See Figure 4.2 for an overview of the TRDT on the AH-64. When the drive train is run up, but before reaching its nominal speed, the shafts will wobble significantly. Anti-flailing sleeves are used to limit drive shaft flexing. Most vibrations in the tail rotor drive train are found at the location of the flexible couplings and hanger bearings which connect the various drive shafts. Bearings are known to fail from time to time, accelerometers are used to monitor the vibrations of shafts at these locations. The drive shafts seldom fail, although scratching of these thin tubes may lead to discarding the component entirely. Furthermore, the IGB and TGB contain quill shafts which connect shafts to gears. These components sometimes fail due to wear and tear, as can the grease seals inside these gearboxes. When the measured level of vibration becomes too high, the gearboxes will be replaced entirely. The engines are very reliable, the only problems are because of ingestion or over-torquing the system.

Critical manoeuvres and conditions

A significant part of the interview was spent on identifying demanding manoeuvres for the Tail Rotor Drive Train which result in high torque loading of the drive shafts. Combat flights are critical because most of the manoeuvres here are done at speed during which a lot of power changes occur. Every time this happens the pilot has to move the pedals which changes the loading of the TRDT system as well. Another effect of pedal inputs is flexing of the vertical fin. This in turn may affect the shaft installed between the IGB and TGB. A particular demanding manoeuvre is the so-called high-g pull up. At the end of a high speed dive, the pilot pulls out and then makes a turn. A turn to the left is worse for the AH-64 than a turn to the right because of the way the main rotor system is loaded. To not over-torque the system, so to not ask too much torque from the engines and transmission, the pilot has to take out power. This in turn requires a pedal input as well.

Secondly, a very steep bank turn to accomplish a 180°heading change is demanding for the entire drive train and in particular the tail rotor. The aircraft is rolled into the turn and then collective is applied to pull the aircraft through the turn. Many pilots use pedal input to turn even faster. This way pilots significantly increase helicopter loading, especially when they whip the tail around. Because of the earlier mentioned crack forming in the drive links of the tail rotor, a note has been added to the operators manual of the AH-64. Aggressive pedal inputs greater than one inch per second are to be avoided during left hand turns because of suspected excessive loads on the drive links.

Third, take-off and hover manoeuvres are also very demanding for the helicopter, especially at high weight, high temperature, and high altitude. There is no translational lift which means that a lot of power must be applied to the MR to generate sufficient thrust. High loads are encountered in the drive shafts because of the high TR thrust level that is needed to counter the MR reaction torque. A lot of stress is put on the TRDT

components, especially in cross or tail winds, and certainly for Out of Ground Effect (OGE) hover conditions. Furthermore, high dynamic loads are present because power changes occur frequently in hover.

Lastly, flying the aircraft out of trim may also result in high loading of the drive train. This happens when inexperienced pilots do not check the trim indicator or do not smoothly fly a demanding manoeuvre by simultaneously applying controls but rather execute the required input sequentially. It can also be difficult to detect if one is flying out of trim when in the back seat of a large helicopter such as the AH-64.

Summary

The AH-64 Apache is a complex helicopter that requires a lot of maintenance. Some components of the drive train such as drive links, hanger bearings, and gearboxes have been known to fail because of wear and tear, but all in all the mechanical part of the AH-64 is reliable. The drive train is loaded severely during combat manoeuvres where aggressive control inputs are applied, or in hover where frequent power changes are required. Pilots must apply pedal inputs whenever this happens which affects the load in the TRDT.

4.2.2. H-60 pilot interviews

"*It is really very rare that a pilot has to yank the helicopter around*" - Retired Navy pilot M. Keaney

Two separate interviews have been conducted with pilots flying aircraft from the Sikorsky H-60 family, the UH-60 Black Hawk and the SH-60B Sea Hawk. The findings from both interviews are summarized here in a single section covering both the UH-60 and SH-60B because of the drive train similarity between these aircraft. Retired aviator Martin Keaney has served in the US Navy for almost 30 years. In his distinguished career he has served from junior naval officer to commanding officer of the amphibious assault ship USS Essex that can carry up to 36 aircraft. During his career he has been a maintenance officer and pilot of the UH-1 Huey, SH-2 Sea Sprite, and the SH-60B Sea Hawk. The second H-60 pilot that has been interviewed is a maintenance and Instructor Pilot (IP) for the UH-60A at the SCARNG, call-sign Dusty. As an Instructor Pilot, he is responsible for the training of new SCARNG pilots, but he has also seen deployment in Afghanistan.

Overview UH-60A Black Hawk and SH-60B Sea Hawk

The UH-60 and SH-60B Sea Hawk helicopters are members of the same family of aircraft. Figure 4.3 gives an impression these helicopters. The UH-60 is already described in chapter 1. This section will highlight the commonality and differences between UH-60 and SH-60 hardware. The SH-60B has been derived from the UH-60A, and as such shares a large number of parts with its land based UH-60 counterpart, e.g. the rotor system and TRDT components. However, the tail boom of the SH-60B is foldable in order to fit on frigates. This required a forward shift of the tail landing gear. Moreover, the floor section of the Sea Hawk has been reinforced to accommodate ship landings with or without help of an arrestor system. Also, the SH-60 carries ordnance and sensor systems attached to this hardened floor section, whereas on the UH-60 this is attached to wing stubs hanging from the upper part of the fuselage. Furthermore, the SH-60B has more powerful navalised T700-GE-401 engines to cope with the larger maximum gross weight of 20,300 lbs compared to around 16,400 for the UH-60A. Lastly, the SH-60B can only seat three people compared to twelve people in the UH-60A because of the large fuel tanks and heavier systems load on-board.

Operational usage and missions

A typical mission for the Utility Helicopter (UH) UH-60A is to transport 10 troops from A to B on flights that usually take around 2 to 3 hours. The helicopter is not equipped with weapons, hence the idea is to keep away from combat manoeuvring. The aircraft will fly either very low or very high, to minimize exposure time in missile envelopes and small arms fire from the ground. UH-60A's stationed at the McEntire Joint National Guard base are deployed as Medevac helicopters to provide (medical) assistance in emergency situations, and as utility transport helicopters.

The SH-60B on the other hand is an Anti-Submarine Warfare (ASW) helicopter deployed from frigates and aircraft carriers. It uses radar, dipping sonar, and a mix of passive and active sonar buoys to track down and attack enemy submarines. The Sea Hawk is equipped with Hellfire missiles and torpedoes to engage the

(a) UH-60 Black Hawk - US Government work

(b) SH-60B Sea Hawk - US Navy - CC0

Figure 4.3 – Overview of **(a)** US Army UH-60 Black Hawk, and **(b)** US Navy SH-60B Sea Hawk.

enemy. A typical mission of the Sea Hawk consists of a flight to the operation area followed by 3.5 to 4 hours of on station time. Operational SH-60B's will log about 25 to 40 flying hours per week on average.

Hardware and maintenance

As detailed in chapter 1, the Black Hawk TRDT transfers engine torque applied at the MGB to the tail rotor by using a system of gearboxes interconnected by hollow drive shafts with Thomas couplings and hanger bearings. The tail rotor is designed to operate at a minimum stress level flying at a 100 knots or more in trimmed flight conditions. On the Sea Hawk, the drive train components which are replaced the most are couplings with bearings on the pitch links of the tail rotor. The reason for this is that the bearings wear out due to dust, sand and other foreign particles there. The UH-60 pilot was not aware of this being an issue on the Black Hawk although tear-down inspections of the UH-60 tail rotor pitch control system is mandatory every 360 flight hours.

Wear also affects the Thomas shaft couplings in the SH-60B. Corrosion was found to be an issue that sometimes resulted in in-flight decoupling of the tail rotor drive shafts and subsequent loss of control. As a temporary fix for all SH-60B aircraft, shaft alignment and rotational slippage checks where made mandatory to ensure structural integrity. The drive shafts are the most flexible part in the H-60 drive train. However, these drive shafts show less flexural motion compared to the drive shafts of the AH-64D. The H-60 drive shafts seldom fail, only when they are shot or during very hard landings may they fail. Overall, both the Sea Hawk and Black Hawk pilot found their helicopters to be reliable and structurally strong.

Critical manoeuvres and conditions

A lot of manoeuvring has to do with power management, where the pilot should take care not to exceed rotor speed limits, or over-torque the system. H-60 aircraft have a torque indicator in the cockpit to warn pilots when the system limit torque is exceeded. This instrument also represents rotor speed limits. When there is a lack of excess engine power, over-torquing the drive train will result in a slowing down of the rotor which may lead to crossing the lower rotor speed limit. On the other hand, torque limits will be exceeded when the rotor speed is too high. A high power setting (and associated high torque loading of the drive train) is required when flying at a high gross weight, for combat manoeuvres with high pitch and roll rates, and for high speed turns. A high amount of anti-torque is required by the tail rotor during these high torque manoeuvres, which in turn loads the TRDT and tail spar. The operators manual of the SH-60B warns pilots to limit high translational torque loading of the tail spar, which for example occurs during high roll rates, to combat manoeuvring only. This also is an issue for the UH-60 where pilots have a hard time to keep vibrations of the rudder box within limits during manoeuvring.

Defensive combat manoeuvres are most demanding manoeuvres for the H-60 drive train. The aim is to get out of the line of fire as soon as possible. High torque situations occurs during high-g, high speed turns, or combat manoeuvres with high pitch, roll, and yaw rates. An example is the high-g pull up, also described for the AH-64 in subsection 4.2.1, but here a right turn is more demanding for the H-60. This puts a tremendous amount of torque on the tail cone, vertical stabilizer, and the main rotor itself. A second critical manoeuvre is yawing the aircraft when requiring a lot of power from the system after rolling. A third example of a severe manoeuvre for the H-60 is a fast approach at low altitude followed by a quick stop manoeuvre. The aircraft approaches at high speed, then it is pitched up to bleed off speed and the collective is quickly dropped to reduce power. The pedals are used to flare the aircraft after which power is reapplied to land smoothly and get the troops out. All these manoeuvres entail power changes which in turn require pedal inputs. This results in high torque loading of the entire drive train and with it the tail rotor drive train.

Both the Sea Hawk and Black Hawk pilot indicate that (defensive) combat manoeuvres rarely occur, maybe less than 1-2% of the time. However, by definition the Army will fly more aggressive manoeuvres with its helicopters than the Navy does because flying over water means you do not have to worry about hitting tree tops or hostile fire from the ground. A recurring theme after questions about demanding manoeuvres for the drive train is pilot experience and flying out of trim. According to the Black Hawk pilot, flying with an indicated "one ball out of trim" above 120 knots results in severe loading of the drive train. This is confirmed by the Sea Hawk pilot who notes that helicopters should be flown smoothly and that inexperienced pilots do not know how to do this well.

Besides pilot input, flight conditions have a significant impact on system performance and drive train loading as well. Helicopter gross weight, wind conditions, flight altitude, and ambient temperature have a significant effect on performance and loading. For instance, UH-60 pilot Dusty mentioned that at high temperature and weights it is not possible to achieve a steady hover condition because the pilot can not apply enough pedal to prevent the aircraft from changing its heading. Another example is his experience with flying in high altitude areas of Afghanistan: it was not possible to hover in OGE conditions simply because there was not enough power available. Both pilots indicated that hover by itself is very demanding for the helicopter, especially with a high mission load. In such cases a running take-off can be done whereby the helicopter overcomes translational lift in ground effect conditions and then gradually climbs away. The trend is to equip helicopters with more powerful engines to cope with the ever increasing weight of helicopters and mission payload. A good example is the successor of the SH-60B. This SH-60R has 25% more engine power for a gross weight increase from 20,700 to 25,300 lbs while the rest of the drive train components are identical to that of the SH-60B. This means that the average load level in the drive train has increased.

Summary

The UH-60A and SH-60B are members of the H-60 family of aircraft sharing a large number of parts and components. Except for the engines and main transmission, the drive train systems of the two helicopters are identical. However, the mission and conditions in which these aircraft fly vary significantly. The Navy uses the SH-60B helicopter at sea in an Anti-Submarine Warfare role, whereas the UH-60A is used mainly as a troop transport helicopter. The gross weight of the Sea Hawk is 4,000 lbs higher than that of the Black Hawk because of a higher structural weight and larger mission load of weapons, fuel, and sensors.

Both former naval officer Keaney and Instructor Pilot Dusty found their aircraft to be very reliable. The most critical parts of the drive train are the pitch link couplings of the tail rotor and the Thomas couplings connecting the drive shafts in Navy helicopters. The operating conditions at sea make the Sea Hawk more susceptible to corrosion problems which affects wear and tear of the Tail Rotor Drive Train. Furthermore, flexing of the vertical stabilizer is an issue for which pilots are warned.

Aggressive defensive combat manoeuvres such as the high-g pull up, banking turn, and combat landing results in severe loading of the entire drive train. However, these manoeuvres are flown less than 1-2% of the time. Hover is also demanding for the aircraft, especially considering the ever increasing operational weight of the helicopter while drive train components have remained the same. (Except for more powerful engines and main transmission.) Aircraft weight and ambient conditions such as air density, temperature, and wind conditions have a marked effect on hover performance.

4.3. Synthesis

This chapter listed the outcome of a short literature survey on manoeuvres that result in high loading of the UH-60 helicopter Tail Rotor Drive Train, the so-called 'critical manoeuvres'. Furthermore, the results of four interviews with AH-64D Apache and H-60 helicopter pilots have been presented. These interviews have been conducted to get a better feeling of how military helicopters are used, what drive train components are susceptible to failure, and what demanding manoeuvres are flown with these helicopters.

The UH-60 and AH-64 are complex helicopters that require a lot of maintenance. However, pilots found the mechanical part of the helicopter very reliable. Critical drive train parts are the Tail Rotor drive links of the AH-64 and TR pitch links of the UH-60. Furthermore, the gearboxes and shaft connections with bearings and flex couplings were found to be susceptible to wear and tear.

A survey of pertinent literature shows that right sidewards flight at maximum speed and critical ambient conditions results in maximum steady tail rotor torque. Furthermore, near zero velocity yawing manoeuvres such as rapid turns and turn stops will result in high TRDT loads. Aggressive left turns in a hover are especially taxing to the UH-60 tail rotor drive train. The interviewed pilots all mentioned that hover is a demanding manoeuvre for helicopters, especially when there is not much excess power available due to ambient condition or helicopter weight. Furthermore, pilots indicated that the entire drive train of a helicopter is severely loaded during combat manoeuvres such as high-g pull ups, steep banking turns, and combat landings. Aggressive pedal inputs during such flights will result in an even higher load level of the tail rotor drive train. However, combat manoeuvres are flown less than 1-2% of the time with both the H-60 and AH-64 helicopters. The literature findings for critical TRDT manoeuvres do not mention these high speed combat manoeuvres. However, both literature and pilots remark on high TRDT loads in hover and near zero forward velocity flight. Aggressive pedal inputs in hover will result in both high average stress levels and high dynamic loads in the tail rotor drive train.

Both combat manoeuvres at high speed with pedal inputs, or hover and near zero forward velocity flight with aggressive left turn yaw commands are critical manoeuvres that result in high TRDT loads. However, the required complexity of a flight model to simulate high speed, 6-DOF combat manoeuvres is outside the scope of this investigation. It is therefore decided to limit the scope of this investigation to the simulation of aggressive left turn manoeuvres in hover. These manoeuvres present a relevant study case for manoeuvre load alleviation, especially considering the fact that pilot Handling Quality Ratings (HQRs) indicate that the handling qualities of the UH-60 for yaw turns in hover are unsatisfactory. [21]

5

Flight simulation model

A flight simulation model representative of the UH-60 has been constructed to calculate structural loads in the TRDT during yaw and heave manoeuvres. A Multi Body Dynamics TRDT model forms the backbone of this flight simulation model to which a MBD Main Rotor model, GSP engine model, and a mathematical Tail Rotor model are coupled. This layout is illustrated in Figure 5.1. The properties of each of these component models will be briefly discussed in the following sections. First, the TRDT model is discussed in section 5.1. The next section 5.2 treats the engine model. The main rotor and tail rotor models are described in section 5.3 and section 5.4 respectively. The last part of this chapter concerns validation of the static and dynamic response of the constructed flight simulation model. This section 5.5 details the validation of flight simulation model for hover and a vertical climb manoeuvre. The reader is referred to Appendix A for more technical details about the flight simulation model and how to run it.

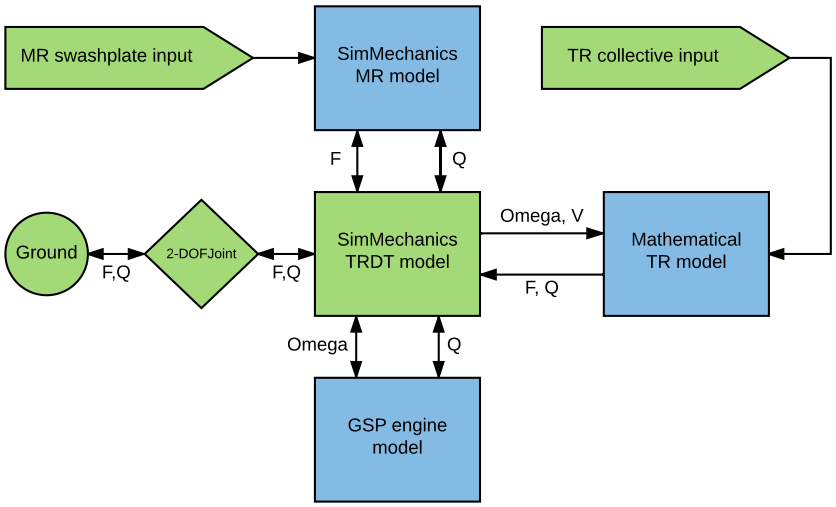

Figure 5.1 – Schematic of flight simulation model layout with components and couplings.

The layout and components of the flight simulation model are illustrated in Figure 5.1. Green indicates new model parts and blue indicates existing models that have been adapted for use in the UH-60 flight simulation model. The arrows indicate what variables are exchanged between the various components. Here F stands for force, Q for torque, V for translational speeds, and *Omega* indicates rotational speeds. The component models are coupled using the SimMechanics V1 environment from MATLAB.[57] More information on the component models may be found in Appendices B, D, E, and C.

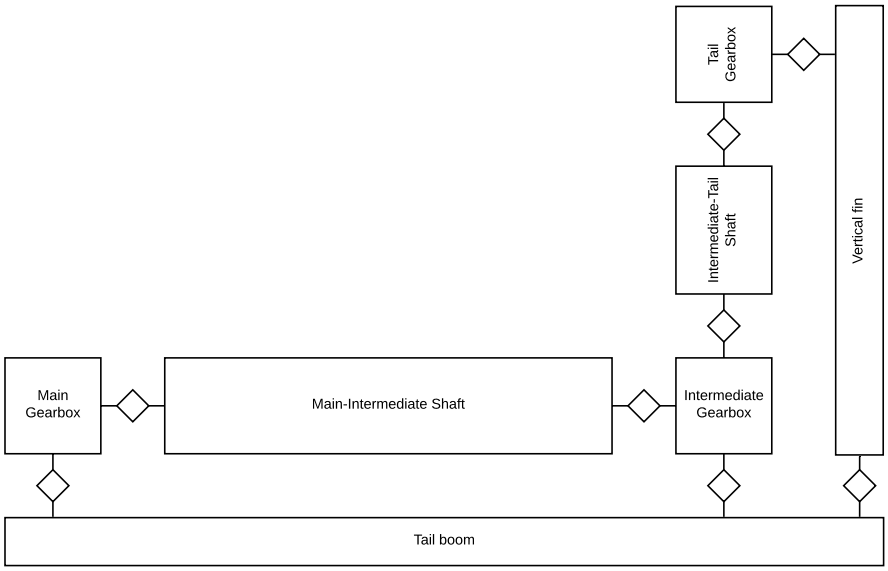

Figure 5.2 – Schematic overview of the UH-60 tail rotor drive train model with components indicated by rectangular blocks and weld connections by diamond shapes. Revolute joints in the gearboxes allow for shaft rotation.

5.1. Tail rotor drive train model

The UH-60 Tail Rotor Drive Train transfers power from the MGB to the tail rotor. See Figure 2.2 for an overview of the components in the UH-60 drive train. The TRDT consists of a system of drive shafts that run along the upper part of the tail boom, flexible couplings, bearings, and gearboxes and an oil cooler. The couplings allow for shaft misalignment, viscous bearings are used to support the shafts along tail boom and vertical fin, and the gearboxes change the angle of rotation as well as shaft Revolutions Per Minute (RPM). A MBD TRDT model is included in the UH-60 flight simulation model to connect the engines to the main and tail rotor models. See Figure 5.2 for a schematic overview of this model and its components. The gearboxes which allow for shaft rotation are attached to the rigid tail boom and vertical fin bodies. The Main-Intermediate (MI) shaft represents the shaft with couplings and bearings between the MGB and IGB. Similarly, the Intermediate-Tail (IT) shaft represent the rotating components between IGB and TGB. A reduced number of shafts has been selected to reduce the complexity of the flight simulation model and associated computational effort required for the simulation of manoeuvres.

Shafts are modelled with single Degree(s) of Freedom to allow for twist, with springs and dampers to account for shaft flexibility and structural damping. The spring constant are determined on the basis of shaft geometry and material. Stiffness proportional damping is estimated to be 0.04% of critical damping for aluminium/steel transmission lines. [1] Dimensions have been determined on the basis of measurements of drive train components and CAD drawings and online available material manuals and reports. [5] [27] Note that losses in the oil cooler, hanger bearings, flex couplings and gearboxes are not accounted for. Determining these losses would require complex structural models and is outside the scope of this thesis. Refer to Appendix B for more information on the tail rotor drive train and components properties.

The TRDT modelling method has been partially validated by means of an experiment conducted at the USC CBM AH-64 tail rotor drive train test stand. Torque measurements have been performed with a strain sensor attached to a drive shaft for various drive train input speeds and torque loads. The results show that the AH-64 TRDT model, which has the same set-up as the UH-60 TRDT model, is able to predict low frequency torque loads in the drive train. This experiment is deemed useful because the tail rotor drive trains of AH-64 and UH-60 are very similar, compare for instance Figure 4.2 and Figure B.1. It is assumed that validation of the similar AH-64 TRDT model means that the UH-60 TRDT model will be able to predict low frequency loads as well. More information on the UH-60 tail rotor drive train model and the experiment may be found in Appendix B.

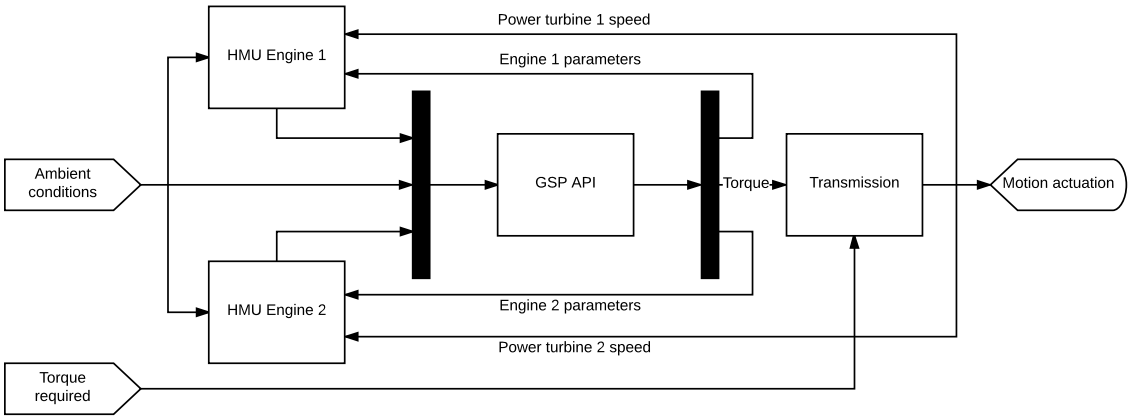

Figure 5.3 – Schematic representation of T700-GE-701 engine model.

5.2. Engine model

The UH-60A Black Hawk is powered by two General Electric T700-GE-701 turboshaft engines rated at 1,560 shaft horsepower each. These engines and a simplified engine transmission system are included in the flight simulation model using a validated Gas Turbine Simulation Program engine model constructed by van Liempt [59]. This high fidelity T700-GE-701 engine model is employed in SimMechanics with help of the GSP MATLAB Application Programming Interface (API). See Figure 5.3 for a schematic overview of the SimMechanics GSP engine model. Model inputs are ambient conditions and torque required. The output of the model is motion actuation (angle, angular velocity, angular acceleration). The Hydro Mechanical Unit (HMU) blocks shown in this figure provide fuel flow control for each engine. See Appendix C for more details on the workings of this fuel flow controller and changes that have been made to the original model by van Liempt [59].

The flight simulation model contains a dummy engine model to provide MGB motion actuation of 258 RPM (≈ 27.02 rad/s) at the start of a simulation run. This prevents the main rotor blades from hitting the hard stops when there is not enough lift generated at low rotational speed Ω. Avoiding this situation significantly reduces the computational effort required. After the GSP engine model has reached the desired output speed the ideal engine is uncoupled and the GSP engine model is used to drive the system instead.

5.3. Main Rotor model

The UH-60 features a four-bladed, articulated Main Rotor with a CCW direction of rotation. This main rotor is modelled using a MBD SimMechanics model created by Dr. Voskuijl that was inspired by the work of Pastorelli et al. [46]. Figure 5.4 shows the resulting SimMechanics model. Dimensions, physical properties and

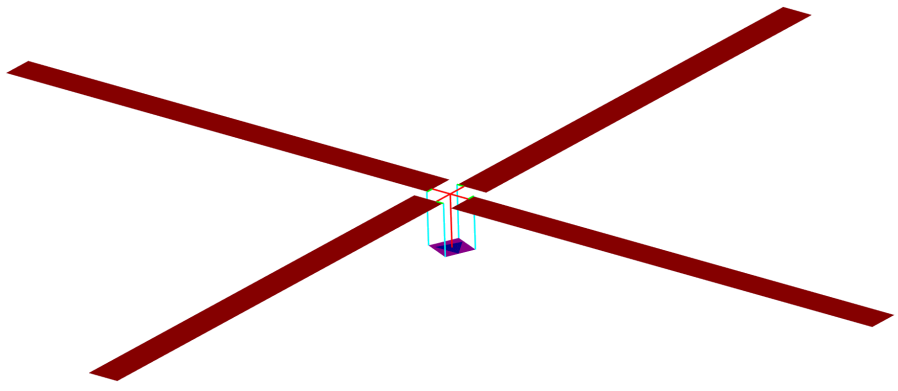

Figure 5.4 – Visualization of SimMechanics main rotor model.

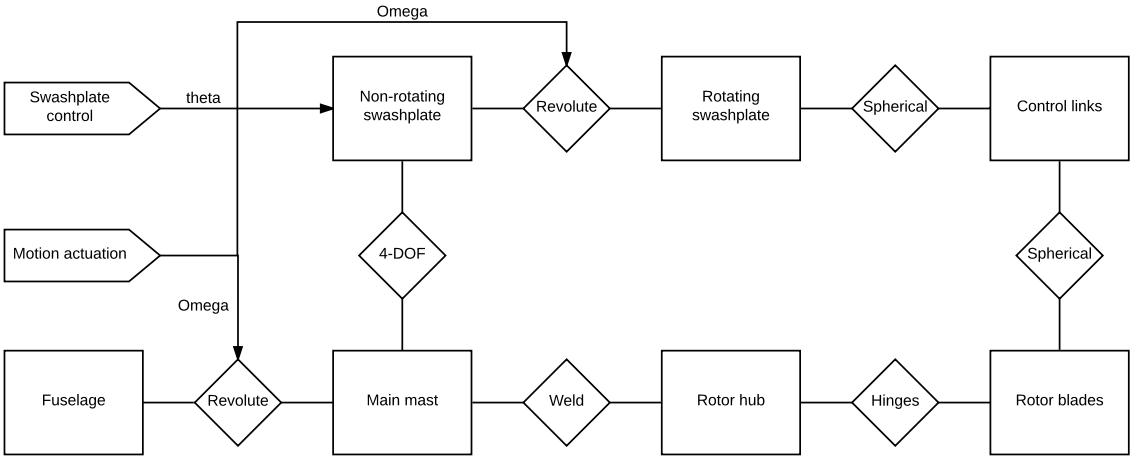

Figure 5.5 – Schematic of main rotor model components.

aerodynamic data of the UH-60 MR have been obtained from the FGR model. [19] See Appendix D for more details on the MBD model as well as changes with respect to the original model by Dr. Voskuijl.

Figure 5.5 provides a schematic overview of the main rotor model components (rectangular blocks) and joints (diamond shaped blocks). The main mast can rotate with respect to the fuselage using a revolute joint. The rotor hub that is attached to the main mast holds the four rotor blades using two hinges which allow for flap and pitch motion. The blade pitch angle is controlled by control links that move when the rotating swashplate moves. The rotating swashplate is in turn actuated by the non-rotating swashplate.

As can be seen, both the main mast and the rotating swashplate are motion actuated using the engine model output. This is different from the actual UH-60 helicopter where torque scissors attached to the main mast are used to drive the rotating swashplate. [46] The main rotor model could be simplified significantly by eliminating this drive system and directly actuating the rotating swashplate. Main rotor forces and moments are transferred from the main mast to the other parts of the helicopter. The rotor blades are modelled as single element rigid bodies with ten aerodynamic calculation points per blade. Using lookup tables the blade forces and moments are calculated and applied to the blade, and then transferred to the main rotor hub which attaches the blades to the main mast.

A PI controller has been created to trim the helicopter before the start of a manoeuvre simulation. Collective control is calculated based on the difference between measured vertical rate and desired vertical rate (0) and the trim collective angle. This controller governs the main rotor collective pitch such that the vertical rate of the helicopter is reduced to zero. See Figure 5.6 for a schematic overview of this hover trim controller. For more information on the controller gains or main rotor components, please refer to Appendix D.

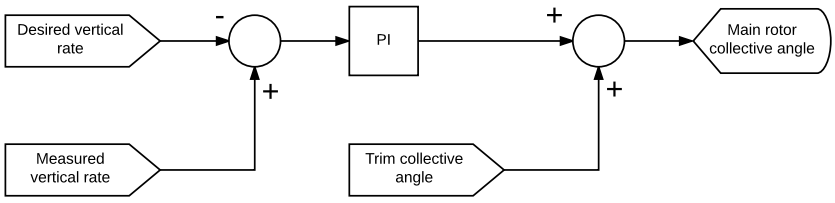

Figure 5.6 – Schematic of main rotor trim collective controller.

5.4. Tail rotor model

The Tail Rotor is represented by a mathematical model from Hilbert [26], which in turn is based on the work done by Talbot et al. [56]. The model consists of a set of quasi-static load equations similar to a Bailey tail rotor model. [8] In contrast to a Bailey rotor model, the mathematical model also yields rotor torque and in-plane rotor forces next to thrust. A mathematical tail rotor has been implemented because using a scaled down version of the MBD main rotor in the simulation model resulted in high computational cost and made the

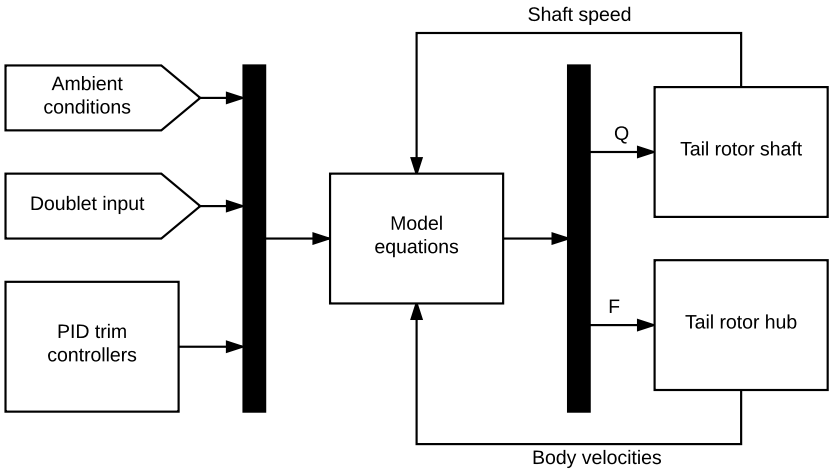

Figure 5.7 – Schematic of tail rotor model implementation.

model susceptible to tail rotor inflow instability. This was visible in the form of an exponentially increasing main and tail rotor blade flapping motion.

Figure 5.7 presents a schematic overview of the TR model and its connections to the complete drive train. The inputs to the mathematical model are ambient conditions, collective inputs from either the PI trim controller or manual settings (Doublet input), tail rotor shaft speed, and helicopter body velocities. The calculated tail rotor reaction torque is applied to the rotating tail rotor shaft and the tail rotor forces (defined with respect to the helicopter body) are applied to the non-rotating tail rotor hub.

A tail rotor collective controller is used to trim the helicopter at a steady heading angle by eliminating yaw rate, see Figure 5.8. This controller works in the same way as the MR trim controller discussed in section 5.3. However, two separate sets of PI gains are used to trim the helicopter. The first set of gains is used at the start of new simulation runs when the heave DOF is activated and an ideal helicopter engine model is used with constant speed. The second set of gains is used after the simulation of a TR doublet input.

Hilbert [26] describes how the effect of main rotor downwash on the tail rotor can be included. That effect is not implemented in the current flight simulation model because it is not within the scope of this research. As a result, the predicted TR torque and pitch angle for a given rotor thrust T will differ from the tail rotor model by Hilbert [26]. The tail rotor torque in hover without main rotor downwash will be lower than for the original model because the inflow from the direction of the tail fin through the tail rotor is neglected.

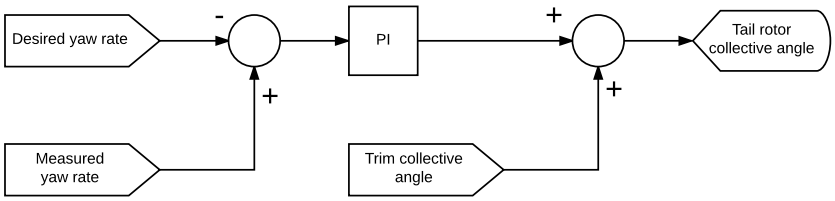

Figure 5.8 – Schematic of tail rotor collective controller for yaw rate trim.

5.5. Model validation

A flight model of the UH-60 helicopter has been constructed to investigate Tail Rotor Drive Train load alleviation during yaw manoeuvres. This model must first be validated before any substantive conclusions can be drawn based on simulation results. To this end, the performance predicted by the flight simulation model will be checked for both a trimmed hover condition and a vertical climb following a main rotor collective pitch step input. First the calculated performance in hover will be compared to FLIGHTLAB results in subsection 5.5.1. Second, compliance of the model dynamic response during a climb is checked with the ADS-33 collective response requirement in subsection 5.5.2.

5.5.1. Hover performance and control

It is important to first verify the flight simulation model results for steady conditions. This will provide a sound basis to further investigate the response of the UH-60 flight simulation model during dynamic manoeuvres. The constructed model only includes yaw and heave Degree(s) of Freedom. For this reason a trimmed hover manoeuvre has been selected to verify results of the simulation model in steady flight conditions. The well-known FLIGHTLAB simulation software is used to generate reference hover performance data. Response and control data have been obtained for a restricted 2-DOF FLIGHTLAB Generic Rotorcraft model, such as the flight simulation model constructed here, and a free flying 6-DOF FGR model for completeness. [19] The results are compared in Table 5.1 and Table 5.2.

Table 5.1 – Comparison of trimmed hover simulation control inputs with FLIGHTLAB. Hover altitude h = 27.4m, helicopter mass W = 7439kg. FLIGHTLAB models are a free flying 6-DOF model and a restricted 2-DOF model with heave and yaw freedom. Both FLIGHTLAB models feature a uniform Glauert inflow model, main rotor without lead-lag hinge, a simple engine model, and account for the ground effect.

Control variable	*Symbol*	**FGR 6DOF**	**FGR 2DOF**	**Model**
MR collective pitch [rad]	θ_0	0.3017	0.3019	0.3008
MR lateral cyclic pitch [rad]	θ_{1c}	-0.0145	0.0003	0.0003
MR longitudinal cyclic pitch [rad]	θ_{1s}	0.0040	-0.0011	-0.0011
TR collective pitch [rad]	$\theta_{0_{tr}}$	0.3480	0.3574	0.4585

The following observations can be made when comparing the control variables listed in Table 5.1:

- The main rotor collective pitch $\theta_{0_{mr}}$ of the flight simulation model is similar to that of the FGR models.
- The cyclic pitch angles θ_{1c} and θ_{1s} of the FGR models are governed by a Stability Augmentation System (SAS) and hence cannot be set to a desired value. For the 2-DOF FGR and flight simulation model these have been reduced to almost zero to discard cyclic pitch effects on main rotor loads.
- The tail rotor collective pitch $\theta_{0_{tr}}$ of the flight simulation model is significantly higher than that of the two FGR models. This is because the effect of main rotor downwash on the tail rotor is neglected, see section 5.4. A higher collective pitch angle is needed to generate the required trim thrust compared to the original TR model by Hilbert [26].

Table 5.2 – Comparison of hover simulation results with FLIGHTLAB for control variables listed in Table 5.1.

Response variable	*Symbol*	**FGR 6-DOF**	**FGR 2-DOF**	**Model**
Fuselage pitch angle [rad]	θ_{fus}	0.0531	0	0
Fuselage roll angle [rad]	ϕ_{fus}	-0.0445	0	0
MR rotational speed [rad/s]	Ω	27.00	27.00	27.065
MR thrust coefficient [−]	C_T	0.0055	0.0055	0.00568
MR inflow ratio [−]	λ	0.052	0.052	0.0534
MR coning angle [rad]	β_0	0.0490	0.0490	0.0435
MR lateral flapping angle [rad]	β_{1c}	-0.0151	0.0021	0.0033
MR longitudinal flap angle [rad]	β_{1s}	-0.0025	0.0003	0.00063
MR hub z-force [N]	F_z	66354	66461	65825
MR hub z-moment [N m]	M_z	-40148	-40566	-41239
TR hub z-force [N]	$F_{z_{tr}}$	4635	4889	4609
TR hub z-moment [N m]	$M_{z_{tr}}$	-948	-1015	-631

The simulation results for the control values shown in Table 5.1 are listed in Table 5.2. Please note that the flight simulation model does not account for the ground effect. A hover altitude of 27.4m has been selected for this comparison so that the resulting small ground effect contribution to the FLIGHTLAB results can be neglected. The following observations can be made:

- The main rotor rotational speed in the simulation is slightly higher than the FGR speed. This is caused by the behaviour of the simplified engine fuel flow controller discussed in section 5.2.

- Main rotor thrust coefficient and inflow ratio values are very similar, which is as expected for a fixed helicopter weight of 7439 kg.
- Blade flapping angles differ significantly between the 6-DOF FGR model and the other two models. This is caused by the difference in cyclic pitch control inputs that have been set to almost zero for the 2-DOF FGR and flight simulation model. Hence the resulting lateral and longitudinal flap angles for both the 2-DOF FGR and flight simulation model are almost zero.
- Main rotor hub loads M_z and F_z calculated using the flight simulation model do not differ more than 5% from the FGR results.
- The tail rotor hub force $F_{z_{tr}}$ of the flight simulation model does not differ more than 6% from the 2-DOF FGR model and is almost identical to that of the 6-DOF FGR model.
- The tail rotor hub moment $M_{z_{tr}}$ predicted by the FGR Bailey tail rotor model is significantly higher than the hub moment predicted by the flight simulation model.

The main cause for the tail rotor torque difference and higher required collective pitch input compared to FLIGHTLAB is that the flight simulation model does not account for the interaction between main rotor downwash and the tail rotor. If main rotor downwash is neglected one would expect the effective tail rotor blade angle to decrease because there is no flow component from the tail fin through the tail rotor. As a result a higher collective pitch angle is needed to generate the required amount of tail rotor thrust. Furthermore, the neglected downwash results in lower in-plane velocity of the tail rotor disk part that would otherwise be exposed to the main rotor downwash. Hence a lower torque is required to overcome the lower drag of the tail rotor blades in this condition. Both these effects are visible for the mathematical TR model that does not include MR downwash. Based on these findings it is assumed that the variation of thrust and torque with collective pitch angle $\theta_{0_{tr}}$ in the mathematical model is representative for the Black Hawk tail rotor.

The comparison between the flight simulation model results and FLIGHTLAB shows that only tail rotor results differ significantly. However, the flight simulation model is expected to yield a torque and thrust variation with tail rotor collective pitch that is representative for the Black Hawk tail rotor. Hence it is concluded that the constructed flight simulation model yields adequate results for steady state hover conditions. The next step is to check the validity of flight simulation model results for dynamic manoeuvres.

5.5.2. Response to collective controller

Section 3.3.10 of ADS-33 [7] outlines the hover and low speed response requirements for a collective step input. These are relevant for validating the flight simulation model, since the yaw manoeuvres to be investigated is in the hover and low speed (up to 45 knots) regime. The UH-60A Black Hawk has been shown to exhibit Level 1 handling qualities for the ADS-33 vertical manoeuvre where a collective input is used to assess the heave axis controllability, see Fletcher et al. [21, pp. 24]. Hence the UH-60 flight simulation model response to a collective step input should also be within the Level 1 handling quality requirements. The flight simulation model will be checked for both height and torque response to a collective step input.

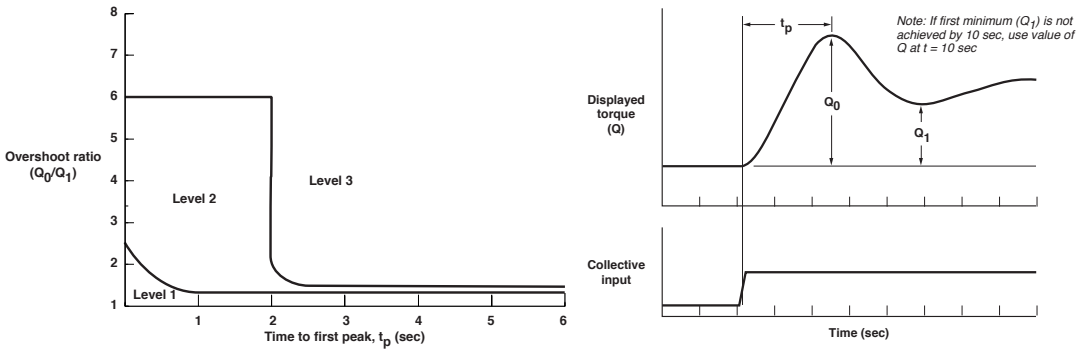

(a) Torque dynamics requirements

(b) Overshoot definition for collective step

Figure 5.9 – ADS-33 displayed torque response requirement. [7, pp. 82] Note that the time to first peak will be indicated as t_{pk} in this report instead of t_p.

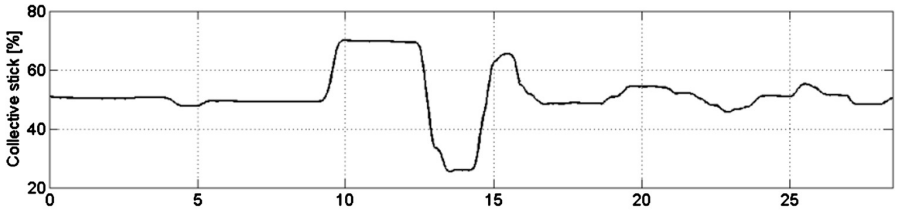

Figure 5.10 – Example collective input for a high aggression bob-up manoeuvre. Voskuijl et al. [62, pp. 330]

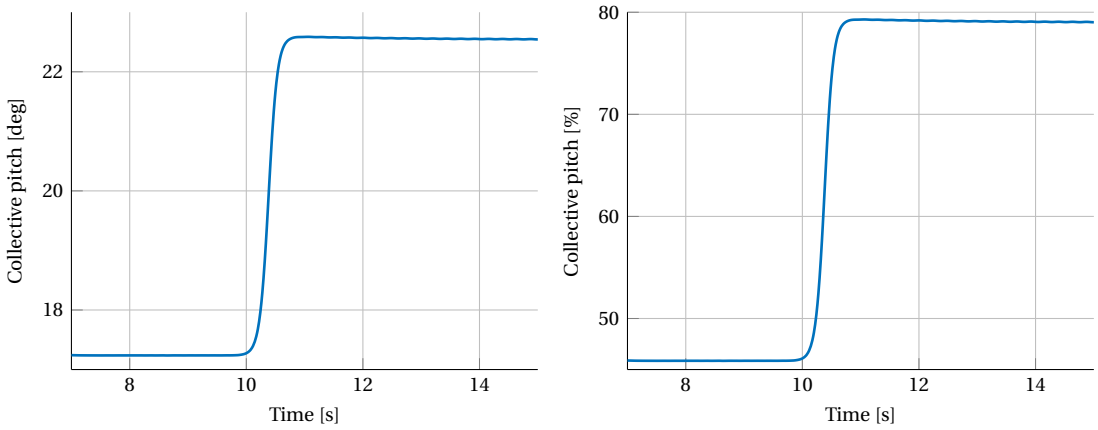

(a) Angle **(b)** Percentage

Figure 5.11 – Step input after 10s for validation of collective controller response. Step steepness constant $K = 6.5$. Model has reached stable hover condition after run-in from 0 to 10 seconds of simulation.

Figure 5.9b shows the general shape of the required collective step input but does not give information on the step input slope. Voskuijl et al. [62, pp. 330] contains information on a piloted collective step input for a high aggression bob-up to quickly reach a higher altitude. The authors show that a 20% collective step increase is realized in around one second for the Bell 412 helicopter. Furthermore the collective input rate of change is smooth at the start and end of the step input, see the collective input signal around 10 seconds displayed in Figure 5.10. To mimic pilot behaviour and to prevent required torque oscillations, an approximate, smooth step input signal has been selected to verify the collective controller response. Equation 5.1 describes the unit shape used for this collective pitch input, where K is the step steepness constant.

$$y(t) = \frac{1}{1 + e^{-2Kt}} \tag{5.1}$$

A collective step input of about 5° has been selected to validate the collective controller response. This blade pitch signal is shown in Figure 5.11 together with the same step input represented as the percentage of maximum collective pitch.

Height response

ADS-33 stipulates in section 3.3.10.1 that the vertical rate response following a collective step input must have a qualitative first order appearance for at least five seconds. During this time, pitch, roll and yaw excursions must be maintained "*essentially constant*". [7] The first order appearance of the vertical rate response has to be verified by using a time domain fitting of the following form:

$$\dot{h}_{est}(t) = K\left[1 - \exp\left(\frac{-(t - \tau_{\dot{h}_{eq}})}{T_{\dot{h}_{eq}}}\right)\right] \tag{5.2}$$

The maximum Level 1 and 2 limits for the curve fit parameters from Equation 5.2 are shown in Table 5.3.

Table 5.3 – Maximum and found values for height response parameters - hover and low speed.

Parameter	**Level 1**	**Level 2**	**Model**
$T_{\dot{h}_{eq}}$ [s]	5.0	∞	2.5
$\tau_{\dot{h}_{eq}}$ [s]	0.20	0.30	0.185
K [-]	N.A.	N.A.	20.5

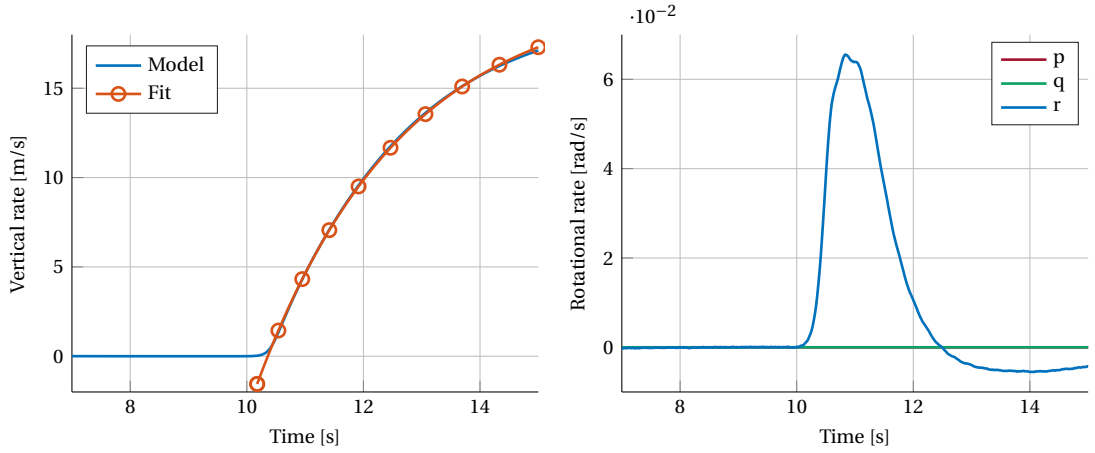

(a) Rate of climb

(b) Rotational rates

Figure 5.12 – (a) Vertical rate response with curve fit, (b) rotational body rates following collective step input at 10s. Fit coefficient of determination r^2 = 1.0011 for height response parameter values as shown in last column of Table 5.3.

The goodness of the fit can then be verified with the coefficient of determination r^2 which must have a value between 0.97 and 1.03 to comply with the height response requirement:

$$r^2 = \frac{\sum_{i=1}^{n}\left[\dot{h}_{est} - \dot{h}_m\right]^2}{\sum_{i=1}^{n}\left[\dot{h} - \dot{h}_m\right]^2}, \text{ with } \dot{h}_m = \sum_{i=1}^{n}\frac{\dot{h}}{n} \tag{5.3}$$

The vertical rate response $\dot{h}$ to the collective step input is shown in Figure 5.12a together with a curve fit of the form prescribed by Equation 5.2. The coefficient of determination r^2 equals 1.0011 for the curve fit parameters shown in the last column of Table 5.3. The r^2 and curve fit parameters all satisfy the Level 1 handling quality requirements limits. Furthermore, Figure 5.12b shows that the maximum yaw rate is small which satisfies the requirement that yaw response should be "*essentially constant*". [7]

Hence it can be concluded that the height response of the UH-60 flight simulation model satisfies Level 1 handling quality requirements as outlined in section 3.3.10.1 of ADS-33.

Torque response

The response to a collective input can also be checked by considering the torque response of the helicopter (or any other measure of maximum allowable power). Section 3.3.10.2 of ADS-33 requires "*torque, or any other parameter displayed to the pilot as a measure of maximum allowable power that can be commanded without exceeding engine or transmission limits, shall have dynamic response characteristics that fall within the limits specified*". These limits are shown in Figure 5.9. For Level 1 handling qualities, the torque overshoot ratio should be lower than 1.5 for a time to first peak value, here indicated by t_{pk} instead of t_p, larger than one second or lower than 1.5 - 2.5 for smaller t_{pk} values.

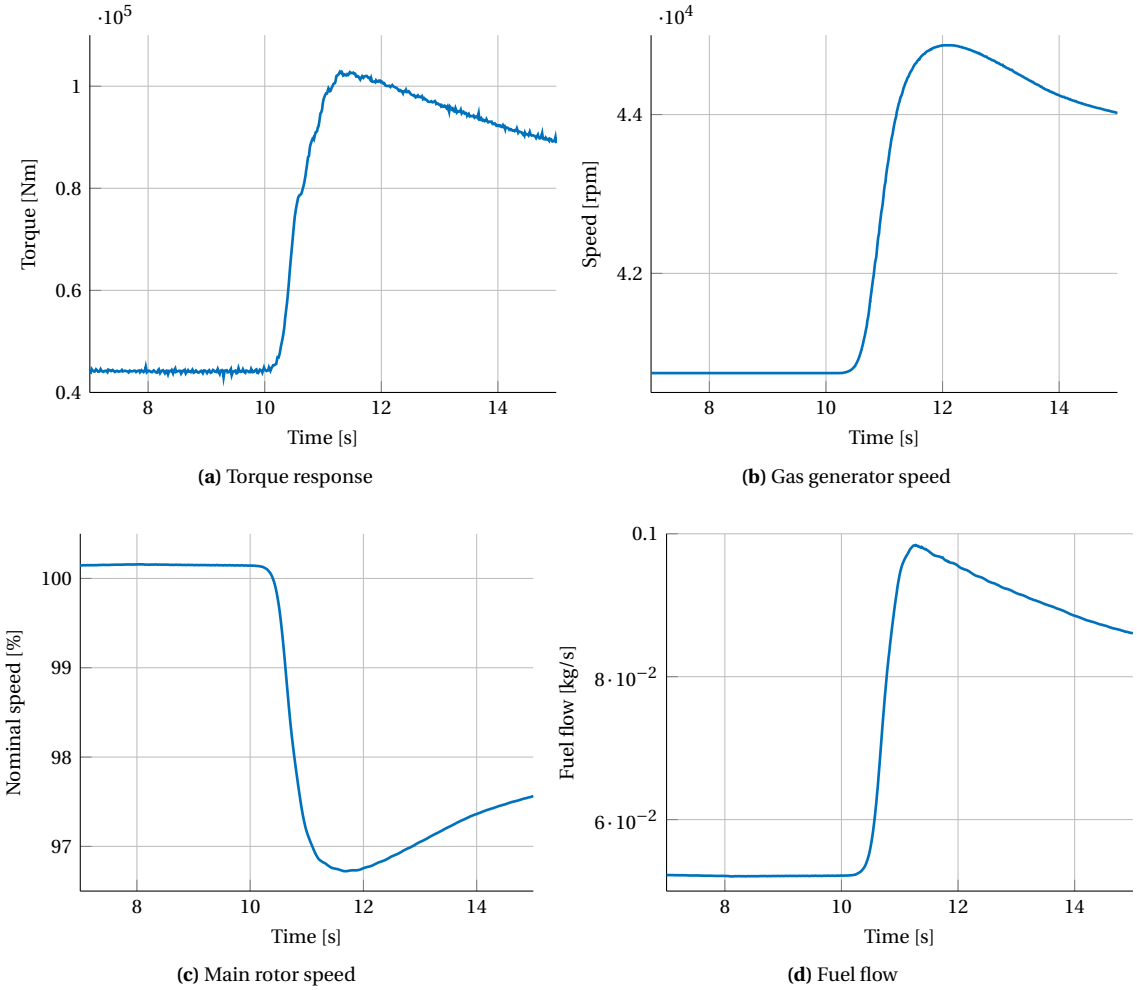

(a) Torque response

(b) Gas generator speed

(c) Main rotor speed

(d) Fuel flow

Figure 5.13 – **(a)** Total required engine torque, **(b)** GSP gas generator speed, **(c)** main shaft speed, and **(d)** fuel flow per engine following a collective step input at 10s after run-in time from 0 to 10s.

Figure 5.13a displays the torque response of the UH-60 flight model following a step collective input at 10 seconds. The main rotor shaft speed and fuel flow per engine are shown in Figures 5.13c and 5.13d. It was found that the flight simulation model is quite sensitive to a collective step input. A steeper step input will result in engine torque oscillations. These oscillations are caused by the interaction between the dynamics of the MR (which acts as a large damping mass), the required TR torque, and the variation in engine torque governed by the fuel flow controller. By selecting a realistic step input, as described in subsection 5.5.2, the torque required does not show large oscillations. However, in case the torque signal shows significant oscillations, the gas generator speed as shown in Figure 5.13b can be used as a power measure instead. A similar course has been selected by van Liempt [59] because "*Even though the gas generator spool speed does not influence the torque output directly, it does contain information on the ability of the engine to deliver torque.*"

Both the torque response and the gas generator speed visualized in Figure 5.13 do not show any significant overshoot. The peak time t_{pk} is defined with respect to the time halfway during the step input, here from $t = 10.8$s. As can be seen in Figures 5.13a and 5.13b the peak times for both parameters are smaller than one second. These responses satisfy the ADS-33 torque response requirements.

Hence it can be concluded that the model presented here torque response satisfies Level 1 ADS-33 handling qualities. This is in line with the UH-60A handling qualities for a vertical manoeuvre which were shown to be Level 1. [21, pp. 24].

This page is intentionally left blank.

6

Load alleviation experiments

The previous chapters saw the identification of manoeuvres resulting in critical loads of the UH-60 TRDT, and the construction of a flight simulation model to simulate these manoeuvres and capture the resulting loads in the tail rotor drive train. This chapter outlines the constraints and set-up of experiments to investigate load alleviation control strategies. First the Handling Quality requirements that apply to the UH-60 during yaw manoeuvres are detailed in section 6.1. Second, a load metric is defined in section 6.2 that can be used to quantify the relation between the variation of Tail Rotor Drive Train loads and handling qualities for varying levels of yaw manoeuvre aggressiveness. The concluding section 6.3 outlines the set-up and input variables of the experiments.

6.1. Handling qualities requirements

Military US Army rotorcraft are subject to the Handling Quality specifications outlined in Aeronautical Design Standard (ADS)-33 and the MIL-DTL-9490E military aircraft specification. [7] [6] Applicable regulations from the ADS-33 specifications will be used here as a framework for load alleviation research in the UH-60 TRDT during critical manoeuvres as identified in chapter 4. The Black Hawk is a utility helicopter for which less aggressive manoeuvring is expected and lower agility is required than for scout or attack helicopters like the AH-64 Apache. Handling quality requirements are specified for good and degraded visibility environments. The scope of TRDT load alleviation is limited to HQ requirements for good visibility environments.

ADS-33 defines Predicted and Assigned handling quality levels to assess the quantitative HQ criteria and required Mission Task Element (MTE) agility. "*Predicted Levels are obtained by comparing the rotorcraft's flying qualities parameters with the boundaries appropriate to the rotorcraft's operational requirements. Assigned Levels are obtained from test pilots performing the designated MTEs.*" [7] The Cooper-Harper scale is used to establish assigned HQ levels. Level 1 to 3 HQs correspond to the 1-3, 4-6, and 7-8 Cooper-Harper scale range respectively.[14] [7] Flying qualities in the operational flight envelope must be Level 1.

The Tail Rotor is the dominant source of Tail Rotor Drive Train loading, especially at low forward speed where the vertical fin does not generate lift to unload the tail rotor. In chapter 4 it was found that near zero velocity yawing manoeuvres and tail rotor pedal reversal are among the critical manoeuvres for the TR in terms of loading. ADS-33 contains a section on hover and low speed (V<45kn) requirements that are applicable to these flight conditions. Sections 3.3.5, 3.3.6, and 3.3.8 list handling quality requirements for small-, moderate- and large-amplitude heading changes respectively, see Anonymous, US Army AMCOM [7, pp. 10–15]. The selected critical yaw manoeuvres will result in moderate- to large-amplitude heading changes. Therefore ADS-33 section 3.3.5 does not apply here. Furthermore, the scope of this investigation is limited to moderate-amplitude heading changes. This is done because the requirements for these manoeuvres provide more guidelines for the load alleviation research than the single requirement on angular rate for large-amplitude changes as listed in section 3.3.8 of ADS-33. [7]

Section 3.3.6 of the ADS-33 specifications concern HQ requirements for moderate-amplitude heading changes, also termed attitude quickness. The ratio of peak yaw rate to change in heading, $r_{pk}/\Delta\psi_{pk}$ must meet the

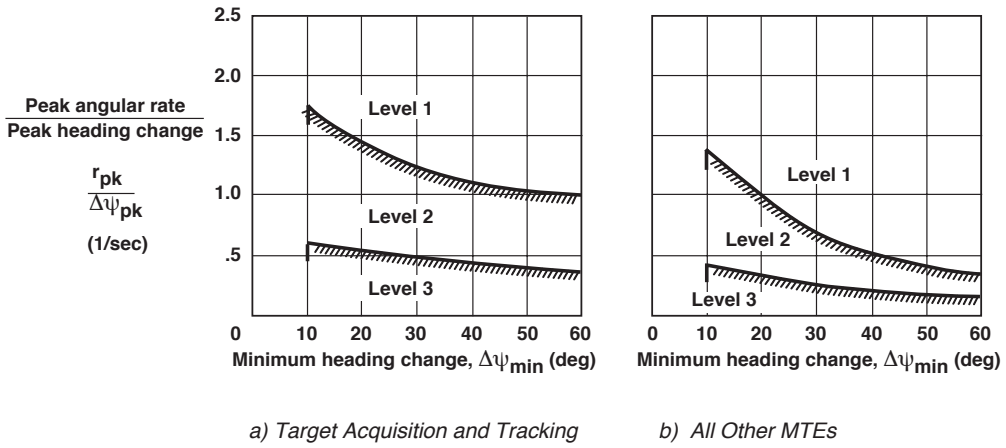

Figure 6.1 – Handling qualities requirements for moderate-amplitude heading changes in hover and low speed. [7]

limits specified in Figure 6.1. Target Acquisition and Tracking agility is not required for the Black Hawk Utility Helicopter, hence Figure 6.1b applies here. Furthermore, a supplement requirement is that "*the minimum heading change $\Delta\psi_{min}$ must be made as rapidly as possible without significant reversals in the sign of the cockpit control input relative to the trim position.*" [7]

6.2. Load metric

The ADS-33 requirements for moderate amplitude heading changes will be used as a framework for this load alleviation research. A load metric is needed to quantify the relation between TRDT load variation and yaw manoeuvre aggressiveness in conjunction with ADS-33 handling quality requirements. First a brief overview of load types and load quantification concepts is given followed by the definition of a load metric for TRDT load alleviation research. The approach taken here is based on the work by Voskuijl et al. [61].

6.2.1. Load types

Static and dynamic loads in the tail rotor drive train will vary considerably during hover yaw manoeuvres with tail rotor collective inputs. If loads in the drive train become too high this may lead to failure of drive train components. As a rule of thumb, components should be able to withstand the ultimate load for at least three seconds. [61] Ultimate load is defined as the limit load times a prescribed factor of safety. (For aerospace applications usually n = 1.5). The limit load is equal to the maximum load expected in service. Federal Aviation Requirements (FAR) and Joint Aviation Requirements (JAR) prescribe the maximum static load a component should be able to withstand. [61]

However, components may also fail at stress states far lower than the ultimate load because of called fatigue damage. When a component is subjected to oscillatory loads over its lifetime, damage will accumulate which may eventually lead to failure. The fatigue tolerance of a component can be visualized using $S-N$ curves which summarize after how many cycles the component will fail when subjected to a certain mean stress level and at a certain oscillatory load with a given stress amplitude. Figure 6.2 gives examples of such $S-N$ curves. The curves will shift upward for a higher mean average stress level. The ultimate load is represented by the stress amplitude at $N = 1$. This means that components fail after one load cycle. If the $S-N$ curve has a horizontal asymptote this is what is called the fatigue or endurance limit. The component will not fail due to fatigue for any amount of load cycles N when loaded below this stress amplitude.

6.2.2. Load severity and amplification factor

The load alleviation study in this thesis project will be conducted with a UH-60 flight simulation model that can predict dynamic loads in the Tail Rotor Drive Train. Torque loads in the drive shafts will be used as an indicator of critical static and dynamic loads in the entire drive train. Now a load metric is needed to quantify

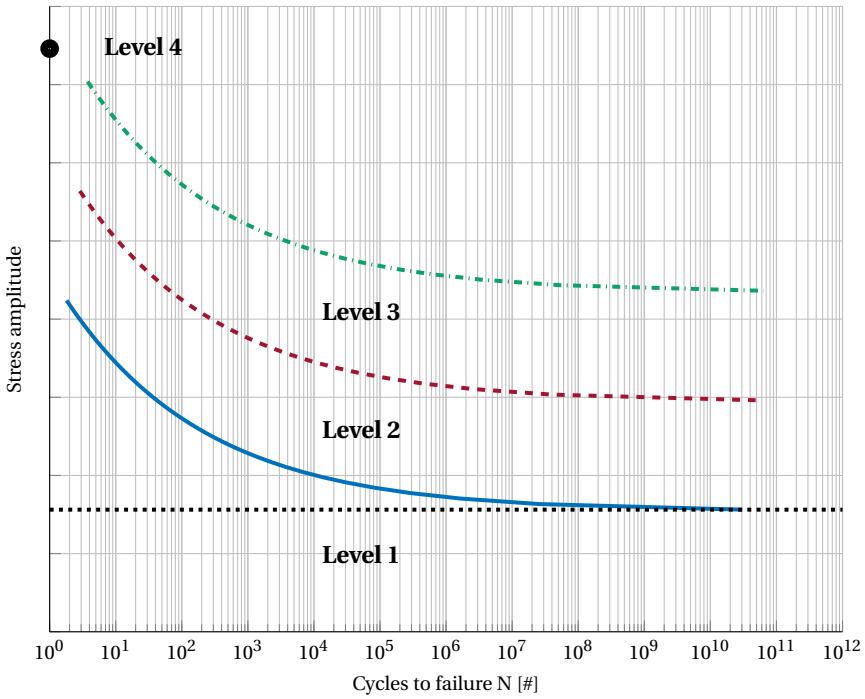

Figure 6.2 – Example load severity levels.

the relation between TRDT load variation and yaw manoeuvre aggressiveness. Voskuijl et al. [61] propose a structural load severity scale based on $S-N$ curves that can be used in a similar fashion as the ADS-33 HQ requirements. The authors define four load severity levels:

- Level 1: Stress level < fatigue limit
- Level 2: High cycle fatigue loading ($N > 10^5$)
- Level 3: Low cycle fatigue loading ($N < 10^4 - 10^5$)
- Level 4: Stress level > ultimate load

An example of these load severity levels is shown in Figure 6.2. The fatigue damage accumulated in the drive train components must be quantified to use this concept of load severity levels for SLA purposes. This requires $S-N$ curves of TRDT components, but unfortunately these are not available. Voskuijl et al. [61] recognize this limitation and therefore introduce a concept which can be applied to more general structural loads. The authors propose the so-called Load Amplification Factor (LAF) which is "*the factor with which the steady state oscillatory load $S_{a,ss}$ at the beginning of the manoeuvre is multiplied during the manoeuvre*". [61] The LAF provides a measure of the load severity experienced by structural components:

$$LAF = \frac{S_{a,max}}{S_{a,ss}} \tag{6.1}$$

6.2.3. Load quickness metric

In order to use the LAF concept for load alleviation during manoeuvres, the Load Amplification Factor must be related to the handling qualities requirements that apply during manoeuvres flown with the rotorcraft. Pavel and Padfield [47] have proposed a vibratory load quickness metric that can be used together with handling quality metrics for high speed longitudinal manoeuvres:

$$Q_l \hat{=} \frac{n_{z,pk}^{vib}}{\Delta\gamma} \tag{6.2}$$

where Q_l is the vibratory load quickness, $n_{z,pk}^{vib}$ represents the peak load factor in vibratory loads, and $\Delta\gamma$ is the change in flight path angle. Voskuijl et al. [61] make use of a modified version of Q_l to evaluate the vibratory

loads in MR pitch links during high speed pull up manoeuvres and integrate the previously defined LAF for pitch link loads to obtain:

$$Q_{l,\gamma} = \frac{F_{pk}}{F_{ss} \cdot \Delta\gamma} = \frac{LAF}{\Delta\gamma} \tag{6.3}$$

where F_{pk} is the peak oscillatory load during a manoeuvre and F_{ss} is the steady state load. The LAF can be employed to define various structural load levels. In combination with load quickness $Q_{l,\gamma}$ this yields a design parameter for structural load alleviation purposes during manoeuvres. The load quickness metric can be adapted for load alleviation research in the tail rotor drive train, simply by replacing pitch link loads with shaft torque and flight path angle γ with heading angle ψ. The result is a load quickness metric for drive shaft torque during yaw manoeuvres:

$$Q_{l,\psi} = \frac{Q_{pk}}{Q_{ss} \cdot \Delta\psi} = \frac{LAF}{\Delta\psi} \tag{6.4}$$

where Q_{pk} is the peak oscillatory shaft torque load during the manoeuvre and Q_{ss} is the steady state torque at the start. Note that the load metric $Q_{l,\psi}$ has the dimension [1/deg]. This allows comparing LAFs during manoeuvres for different helicopters.

6.2.4. Load quickness application

High frequency oscillatory loads may occur in the tail rotor drive train shafts because of shaft flexure and imbalance, as well as external forcing from the main and tail rotor. The MBD tail rotor drive train model in its current form cannot capture these high frequency torque variations because of torque peaks that are likely caused by the combination of the SimMechanics `ode23s` solver used and motion actuation instead of torque. See Appendix A for more information. However the doublet tail rotor collective input required to perform a heading change can in itself be regarded as a single oscillation, see Figure 6.4. Hence the torque acting on the drive shafts during a tail rotor doublet collective input will show a similar variation. Furthermore, from the pilot interviews in chapter 4 it became apparent that pilots apply pedal inputs whenever power changes are made. The induced oscillatory loads can be classified as low cycle fatigue loading of the drive shafts, Level 3 load severity in Figure 6.2, to which the load quickness metric $Q_{l,\psi}$ can be applied.

Constant Load Amplification Factor contours can be calculated using Equation 6.4. This is visualized in Figure 6.3. Note that these lines have similar shapes as the previously discussed ADS-33 handling qualities requirements for heading changes as visualized in Figure 6.1. Simulations will be done for various levels of yaw manoeuvre aggressiveness. The resulting attitude quickness levels and requirements can then be compared to the load quickness in a figure that also contains the LAF contours. This comparison will show how loads in shafts are amplified for various levels of heading change aggressiveness and enable the identification of SLA control strategies. Furthermore, these result may aid in the design of flight control systems that incorporate SLA capabilities for the tail rotor drive train.

6.3. Experiment set-up

Simulations will conducted to determine the variation of handling qualities and dynamic loads with various levels of yaw manoeuvre aggressiveness. Doublet TR collective inputs are applied to simulate left-turn heading changes starting from a trimmed hover condition. The doublet signals are constructed using the smooth step defined by Equation 5.1. Left-hand turns will be simulated because these are more critical in terms of handling qualities than right-hand turns owing to the puller configuration of the tail rotor. A significant amount of left pedal tail rotor collective input is needed to trim the helicopter in hover. This leaves a limited amount of pedal travel to turn left. A TR collective controller is activated to stabilise the helicopter at a new heading angle ψ after the doublet has been completed, see Figure 5.8 for a schematic of this controller.

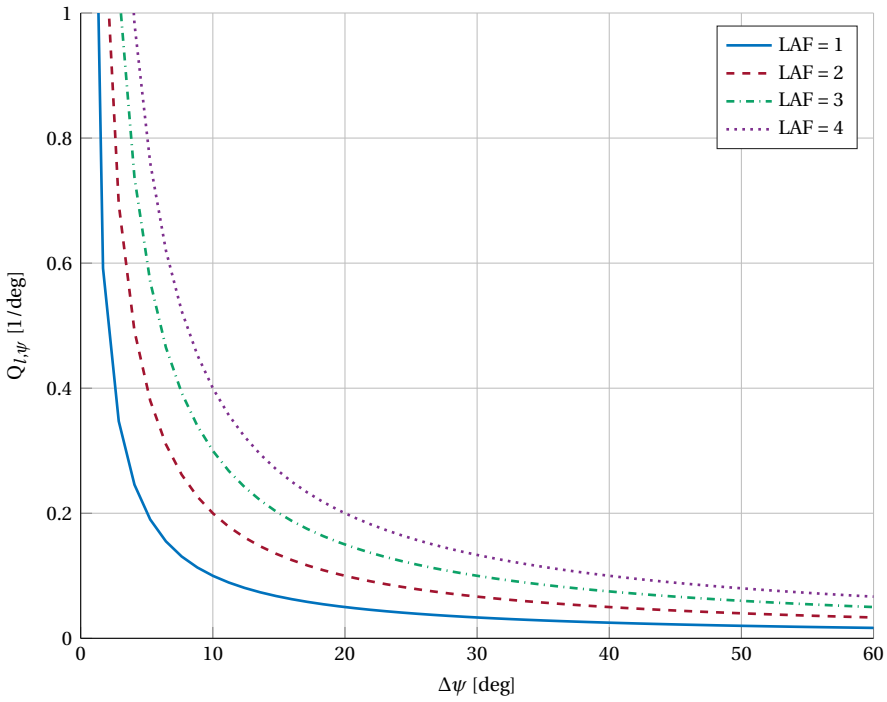

Figure 6.3 – Contours of load amplification factors, adapted from [61]

6.3.1. Control limits

The TR collective control limits listed in Table E.1 will determine the maximum doublet collective step-size in conjunction with the trim collective value. Note that these collective limits differ from the actual UH-60 control limits as given by Howlett [27]. The reason for this discrepancy is that larger $\theta_{0_{tr}}$ values are needed to reach the same tail rotor thrust when the MR inflow effect is ignored. See subsection 5.5.1 for more details on this issue.

ADS-33 requires that attitude changes should be accomplished as fast as possible. The slope of the doublet step is determined by how fast the pilot can move the pedals. Very steep tail rotor collective pitch inputs do not reflect reality and will also lead to engine torque oscillations in the flight simulation model. Care must be taken to avoid unrealistic pedal inputs. Ballin [9, pp. 71] describes flight test data for the UH-60 helicopter where a total pedal travel of 1 inch is achieved in ± 0.75 s The corresponding collective rate of change $\Delta\theta_{0_{tr}} \approx 6$ deg/s. However, a larger rate of collective change occurs halfway during the input. For this reason it was decided to limit the tail rotor collective rate of change at 10 deg/s. The doublet step steepness K is chosen such that this limit is satisfied at the doublet start and end steps.

6.3.2. Experiment variables

Experiments will be conducted to investigate the effect of manoeuvre aggressiveness and duration, helicopter weight, and Centre of Gravity (CG) station on handling qualities and load variation during left-hand yaw turns. The lower and upper limits of these variables are listed in Table 6.1.

Manoeuvre aggressiveness is defined here as the percentage of maximum tail rotor collective pitch. This parameter has been selected as experiment variable because larger collective inputs will likely result in larger yaw rates and affect the resulting attitude quickness handling quality. Longer duration of doublet collective inputs will result in larger values of minimum achieved heading change $\Delta\psi_{\text{min}}$. Yaw rate and heading change directly influence the attitude quickness handling qualities requirements, see Figure 6.1. See Figure 6.4 for examples of TR collective doublet inputs that have been constructed using Equation 5.1.

Furthermore, the effect of helicopter CG position will be investigated. As described in chapter 5, the helicopter rotates around its CG during the simulated yaw manoeuvres. A shift in CG location changes the tail

Table 6.1 – Overview of load alleviation experiment variables.

Parameter	Symbol	Lower limit	Upper limit
Doublet step [% max. $\theta_{0_{tr}}$]	$\%\Delta\theta_{0_{tr}}$	85	100
Doublet duration [s]	$t_{\Delta\theta_0}$	1.5	3.5
Helicopter weight [kg]	W	7439	8709
CG station [m]	STA_{cg}	8.7808	9.1491

Table 6.2 – Helicopter weight, CG location and yaw inertia from Howlett [27], and tail rotor trim collective angle.

Configuration	Weight	CG station	Yaw inertia	Trim $\theta_{0_{tr}}$
Forward CG, design weight	7439 kg	8.7808 m	52 575 kg m^2	25.95°
Nominal CG, design weight	7439 kg	9.0932 m	50 012 kg m^2	26.23°
Aft CG, design weight	7439 kg	9.1491 m	48 891 kg m^2	26.29°
Nominal CG, extended range	8709 kg	8.9535 m	52 178 kg m^2	28.14°

rotor anti-torque arm and helicopter yaw inertia. This in turn affects the required tail rotor thrust and loads in the TRDT as well as the yaw rate that can be achieved. The forward limit, nominal position, and aft CG limit will be used as three separate conditions in the experiment.

Helicopter weight is the fourth variable in the experiment. This parameter has been selected because pilots indicated that weight has a significant effect on handling qualities and loads in the drive train, see chapter 4. Simulations will be done for two different helicopter weights: a design weight of 7439 kg and an extended range mission weight of 8709 kg. An overview of CG position, weight and yaw inertia is given in Table 6.2.

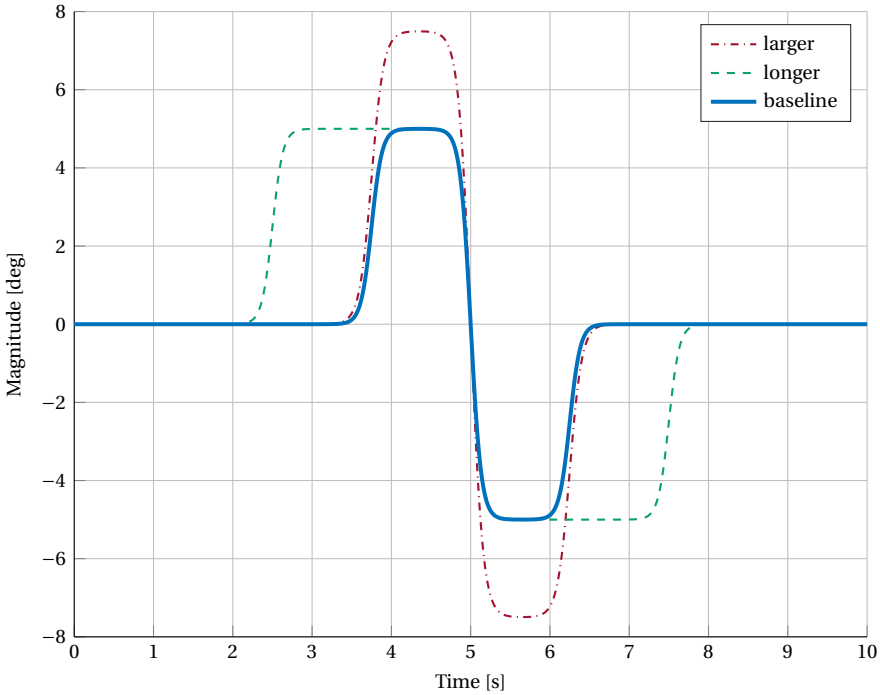

Figure 6.4 – Example TR collective $\theta_{0_{tr}}$ doublet inputs, where the *larger* doublet will mainly result in a bigger r_{pk} and the *longer* doublet will mainly result in a larger $\Delta\psi_{\text{min}}$ value compared to the *baseline* doublet.

7

Simulation results

Experiments have been devised to investigate the relation between handling qualities and structural loads in the UH-60 TRDT. This chapter presents the outcome of these simulations and a discussion of the results. First, the model control and response results for a left hand moderate heading change manoeuvre are discussed in section 7.1. This is done to provide a better understanding of what happens during a turn by applying tail rotor collective. The effect of varying yaw manoeuvre aggressiveness and duration, aircraft weight, and longitudinal CG position are presented in sections 7.2, 7.3 and 7.4 respectively. A discussion of the results is presented in section 7.5. Next, simulation findings will be used to devise a SLA control strategy in section 7.6. This chapter concludes with a synthesis of simulation findings and notes on the validity of results in section 7.7.

7.1. Moderate-amplitude heading change

This section details the model input and responses for the simulation of a left turn moderate-amplitude heading change starting from a hover condition. Yaw manoeuvres are simulated by applying a doublet input to the tail rotor collective $\theta_{0_{tr}}$. A yaw controller is activated at the doublet end to trim the helicopter at a new heading angle. Main rotor collective commands are regulated by a PI controller that acts to eliminate the helicopter vertical rate. These control inputs are visualized in Figure 7.1. The resulting helicopter motion and load responses are shown in Figure 7.2 and Figure 7.3 respectively. A number of observations can be made about the control, motion response, and load response.

Collective input As shown in Figure 7.1 the tail rotor collective $\theta_{0_{tr}}$ is first increased (and hence tail rotor thrust) to turn left and then decreased again. This is as expected because the tail rotor is a puller propeller that provides thrust to counteract torque from the CCW rotating main rotor. The collective peak around $t = 12$ s is caused by the TR trim controller that acts to stop the yawing motion by eliminating yaw rate. Meanwhile a MR collective PI controller acts to eliminate the body vertical rate. The main rotor collective pitch $\theta_{0_{mr}}$ is decreased at the start of the manoeuvre to compensate for the higher tail rotor thrust that contributes to lift because of tail rotor canting.

Motion response Note that the motion responses shown in Figure 7.2 are referenced with respect to the helicopter body axis system with the z-axis pointing downward. The heading change response shown some overshoot of the final heading angle after which the helicopter is stabilized by the TR collective trim controller. This also shows in the yaw rate response visualized in Figure 7.2b that is successfully reduced to zero. Furthermore, it can be seen that the helicopter loses altitude during the first half of the tail rotor collective doublet input, although this effect is small. The corresponding vertical rate shows an initial downward positive value and a negative value (hence positive rate of climb) after pedal reversal. The MR collective controller is successful in eliminating the vertical rate after the doublet input.

Load response The flight simulation model load response and engine speed are shown in Figure 7.3. Tail rotor thrust varies in a manner similar to TR collective input. However, thrust decreases when the yaw rate decreases and vice versa. This is as expected because a negative yaw rate (when turning left) will result in a

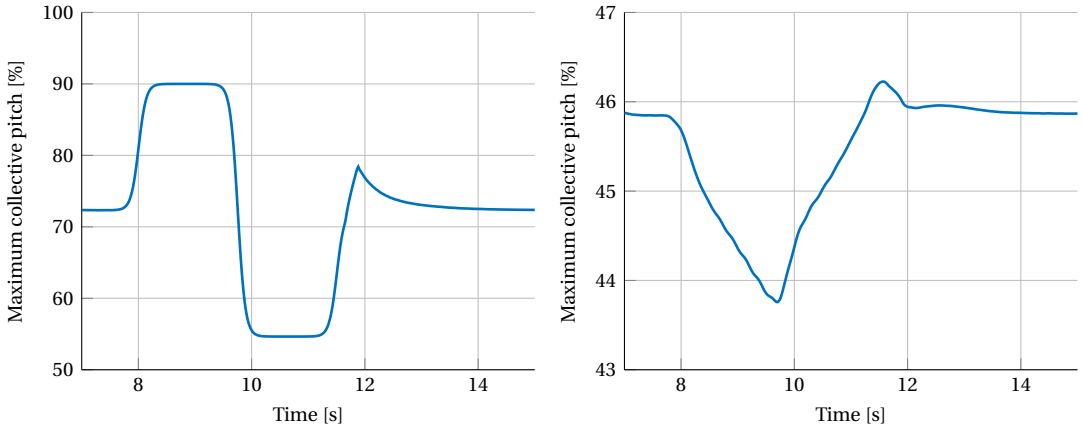

(a) Tail rotor **(b)** Main rotor

Figure 7.1 – **(a)** Tail rotor collective input, **(b)** main rotor collective control for a doublet input on the tail rotor collective $\theta_{0_{tr}}$ around 8 seconds after run-in. Helicopter weight W = 7439 kg, nominal CG position at STA_{cg} = 9.0932 m, trim $\theta_{0_{tr}}$ = 26.23°, trim $\theta_{0_{mr}}$ = 17.24°.

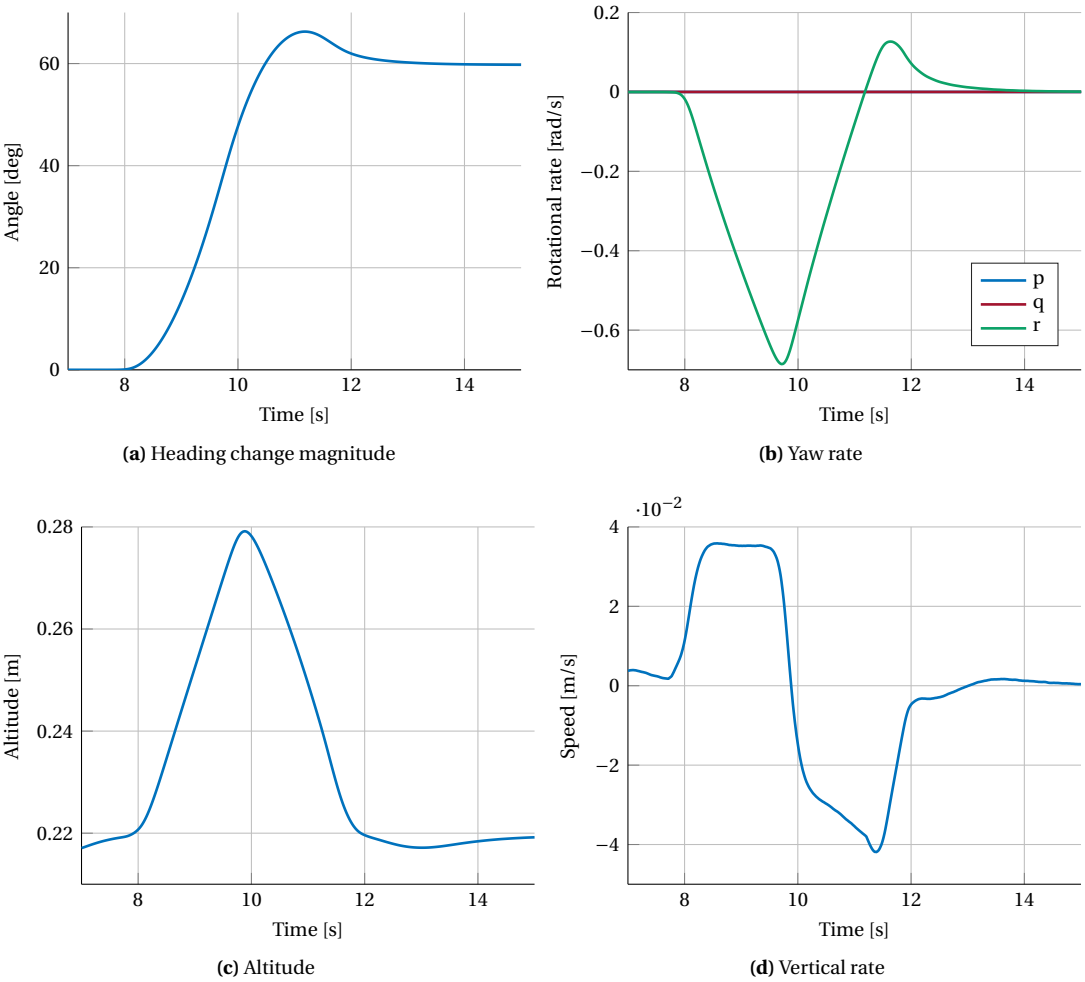

(a) Heading change magnitude **(b)** Yaw rate

(c) Altitude **(d)** Vertical rate

Figure 7.2 – **(a)** Heading change, **(b)** yaw rate, **(c)** altitude, **(d)** rate of climb for collective inputs from Figure 7.1.

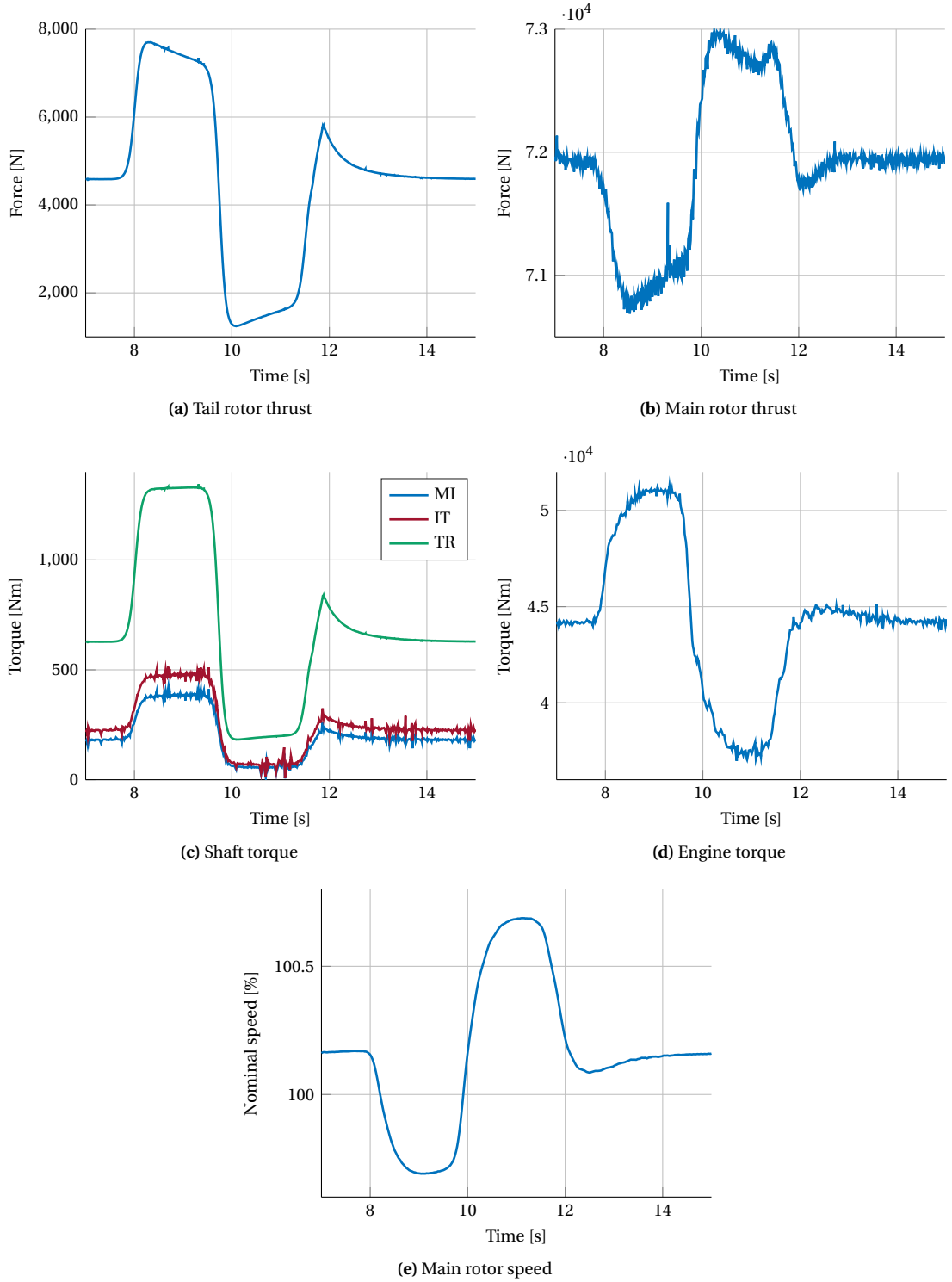

(a) Tail rotor thrust

(b) Main rotor thrust

(c) Shaft torque

(d) Engine torque

(e) Main rotor speed

Figure 7.3 – **(a)** Tail rotor thrust, **(b)** main rotor thrust, **(c)** drive shaft torque, **(d)** required engine torque, **(e)** main rotor speed for collective inputs shown in Figure 7.1.

tail rotor inflow similar to a positive rate of climb. Such inflow reduces the blade angle of attack and hence reduces thrust. [22]

The main rotor thrust is mainly affected by the reduction in main rotor speed, although the main rotor collective angle does of course also influence the generated main rotor thrust. See for instance the thrust peak around $t = 11.5$ seconds in Figure 7.3b and the corresponding peak in main rotor collective $\theta_{0_{mr}}$ in Figure 7.1b. The MR thrust peak around $t = 9.5$ seconds is an artefact caused by the `ode23s` solver used in the simulation. Load artefacts also show in the shaft torque plot of Figure 7.3c and the engine torque variation visualized in Figure 7.3d. Smoothing is applied here to filter out erroneous torque peaks, see Appendix A.

Figure 7.3c shows that the required tail rotor torque is more or less constant for a constant collective control input. Furthermore, it can be seen that shaft IT (between the IGB and TGB) is subjected to a higher torque load than shaft MI (between the MGB and IGB). This is as expected because shaft IT rotates at a lower speed than shaft MI while having to transfer (almost) the same amount of power to the tail rotor. As a result the torque level of shaft IT must increase which is indeed visible here.

The engine torque response rapidly follows the tail rotor collective input. Figure 7.3d shows that more power is required during the first half of the TR doublet input and less power after pedal reversal. The increased tail rotor power demand to turn left offsets the reduced main rotor power. This results in an initial increase of engine torque and subsequent decrease after pedal reversal (while the engine speed varies about 1%) The main rotor speed is directly proportional to the engine speed through the MGB gear reduction ratio. The main rotor slows down when more power is demanded from the engines and increases again after pedal reversal. Figures 7.3d and 7.3e show that the main rotor speed trend is the inverse of engine torque variation. This is because of the engine coupling in the flight simulation model where engine output speed (and thus main rotor speed) are calculated using the drive train rotational inertia and excess torque.

7.2. Effect of manoeuvre aggressiveness and duration

First the effect of manoeuvre aggressiveness and duration is investigated for a helicopter at its design weight of 7439 kg and nominal cg position at $\text{STA}_{\text{cg}} = 9.0932$ m. Various levels of manoeuvre aggressiveness have been simulated with $\theta_{0_{tr}}$ doublet step sizes ranging from 85% to 100% maximum $\theta_{0_{tr}}$ (upper limit is 36.27°). Note that a collective value of 26.23° is needed to trim the helicopter before the start of the manoeuvre. The doublet duration is varied from 1.5 to 3.5 seconds in steps of 0.5 s. An increase of doublet duration shows as an increase in heading change ψ_{min}. A total of 18 simulation have been performed: five runs for 85% and 90% $\theta_{0_{tr}}$ each with a doublet duration from 1.5 to 3.5 s, and four simulations for 95% and 100% maximum $\theta_{0_{tr}}$ with doublet duration from 1.5 to 3 s. The resulting handling qualities are shown in Figure 7.4a and the accompanying variation in load metric $Q_{l,\psi}$ is shown in Figure 7.4b. The following is observed:

- A tail rotor collective of ±72% max. $\theta_{0_{tr}}$ is needed to trim the helicopter in hover which leaves a limited amount of pedal travel to turn. High $\theta_{0_{tr}}$ values are required to achieve Level 1 HQs for left turns.
- The highest values of attitude quickness $r_{pk}/\Delta\psi_{pk}$ occur for the smallest doublet duration.
- Attitude quickness lines in Figure 7.7a move to the right and slightly downward for larger collective inputs. Similar $r_{pk}/\Delta\psi_{pk}$ values are reached for each doublet duration but this occurs at larger ψ_{min} values for increasing $\theta_{0_{tr}}$ which benefits the achieved HQs level.
- Inputs of 95 and 100% maximum $\theta_{0_{tr}}$ result in Level 1 HQs irrespectively of doublet duration.
- Load metric curves in Figure 7.4b shift downward and to the right for increasing doublet step size.
- The shape of the $Q_{l,\psi}$ lines is similar to those of constant LAF. This means that shaft torque is more or less constant with increasing manoeuvre duration (and resulting increase of $\Delta\psi_{\text{min}}$).
- Shaft torque is amplified by a factor of ±1.8 for the smallest doublet step size up to LAF = ±3 for maximum tail rotor collective.

One can see that the handling qualities requirements for small $\Delta\psi_{\text{min}}$ values are more critical than those at larger heading change values. Larger collective step sizes which increase LAFs are needed to achieve Level 1 handling quality requirements. For example, a collective input of more than 90% maximum $\theta_{0_{tr}}$ is needed to achieve Level 1 performance for $\Delta\psi_{\text{min}} < 15°$. This results in a torque amplification factor ≥ 2.5. However, for larger heading changes the resulting LAF for Level 1 performance is ≥ 2. The best Level 1 attitude quickness is achieved for maximum collective deflection. However, a 95% theta deflection will already result in Level 1 performance while the load amplification factor reduces with 0.5 to 2.5 compared to maximum $\theta_{0_{tr}}$.

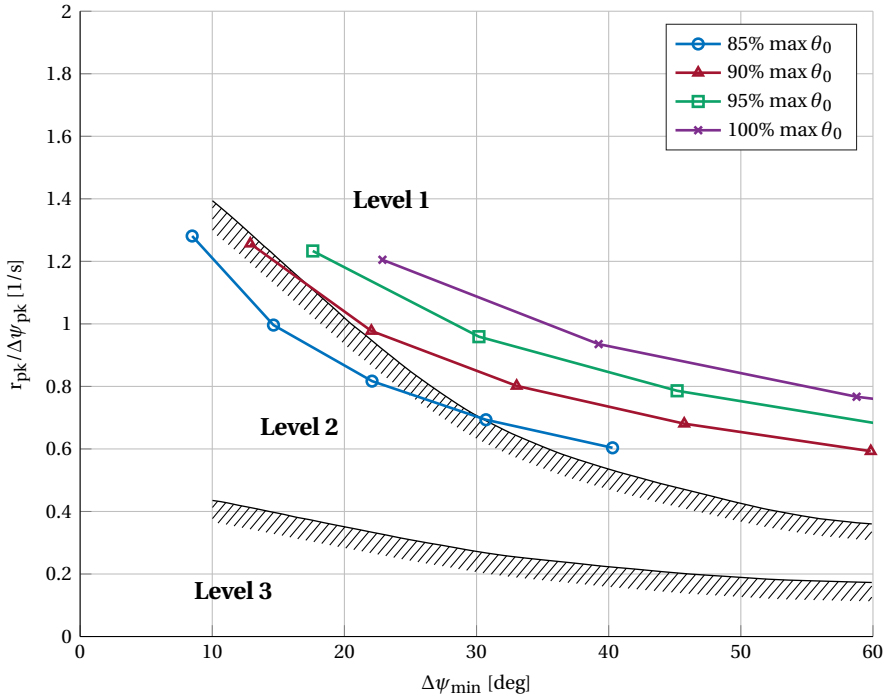

(a) Handling qualities

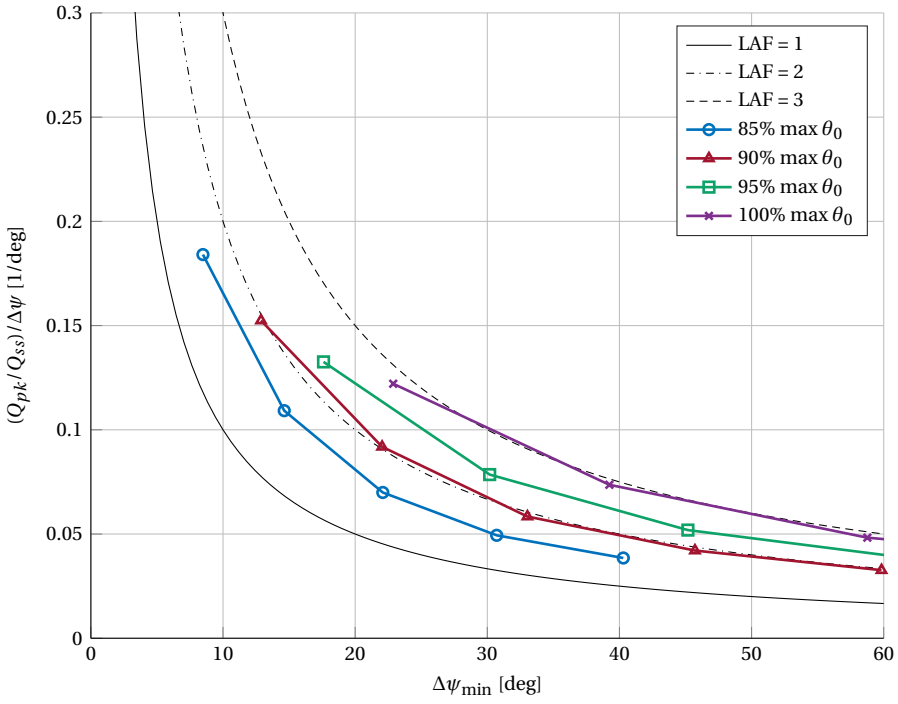

(b) Load metric

Figure 7.4 – (**a**)Variation of handling qualities, (**b**) variation of vertical shaft load metric with manoeuvre aggressiveness. Helicopter at design weight with nominal CG station. Flight altitude $h = 27.43$ m, upper limit $\theta_{0_{tr}} = 36.27°$.

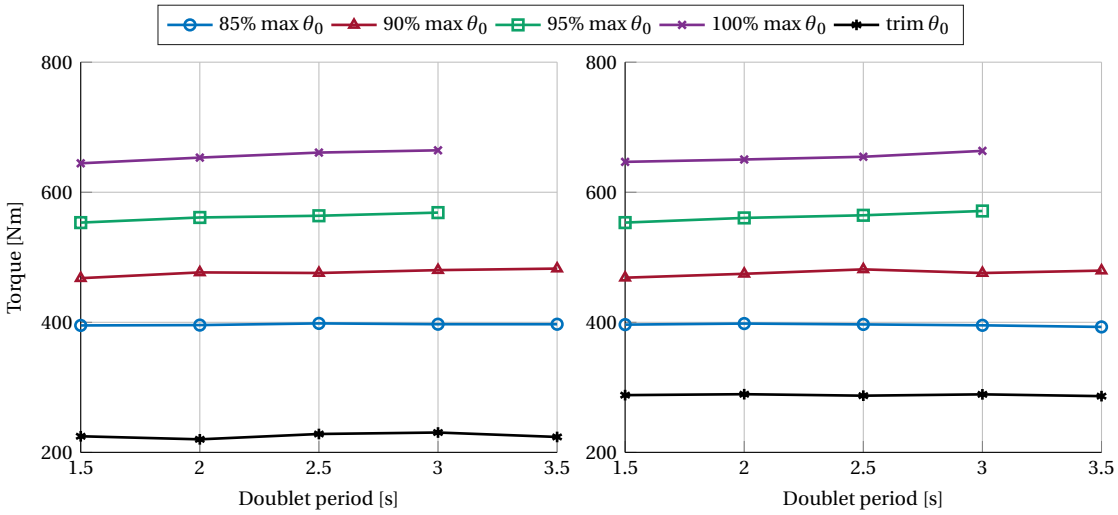

(a) Design weight **(b)** Extended range

Figure 7.5 – Variation of vertical shaft maximum torque with manoeuvre duration at various $\theta_{0_{tr}}$ step sizes for (**a**) helicopter at design weight and nominal CG station, (**b**) extended range mission and nominal CG station. Flight altitude $h = 27.43$ m, upper limit $\theta_{0_{tr}} = 36.27°$.

7.3. Effect of helicopter weight

The effect of helicopter weight on handling qualities and load quickness is investigated next. Yaw manoeuvres have been simulated for an extended range mission weight of 8709 kg. The outcome of these simulations are then compared to the simulation results for a helicopter weight of 7439 kg from the previous section 7.2. Table 6.1 shows that for this increased helicopter weight there also is a slight forward shift of nominal CG position and an increase of yaw inertia increases by ±4%. The same doublet percentages and relative collective step sizes will be used as for the previous experiment. However, now a larger TR trim collective (28.14° instead of 26.25°) is needed to counteract the increase in main rotor torque that follows from the higher thrust demand. As a result, the absolute step sizes $\left|\Delta\theta_{0_{tr}}\right|$ will be lower compared to the previous experiment. Figure 7.5 displays the variation of shaft torque with doublet duration for both the design weight and extended range mission weight. Handling qualities and load quickness variation are shown in Figures 7.6a and 7.6b. The following observations can be made:

- From Figures 7.4 and 7.6 it can be seen that HQs deteriorate with an increase in weight. Attitude quickness lines have shifted left compared to the simulations for a lower design weight. Heavier aircraft require a larger trim collective input which leaves a smaller amount of pedal travel to perform a yaw turn. This leads to smaller achieved heading changes for similar values of $r_{pk}/\Delta\psi_{pk}$.
- Again the domain of small $\Delta\psi_{\min}$ values is critical for the handling qualities that can be achieved. Now only a 100% of maximum $\theta_{0_{tr}}$ always results in Level 1 handling qualities. Deflections to 85 and 90% of maximum $\theta_{0_{tr}}$ results in Level 2 handling qualities except for $\psi_{\min} > 30°$.
- Interestingly, the load quickness metric variation shows that LAF values decrease with increasing aircraft weight. A larger $\theta_{0_{tr}}$ trim angle is required for heavier aircraft which in turn leads to a higher shaft torque load. However, the maximum torque value in the drive train for a pre-set tail rotor collective angle does not vary with aircraft weight. This is shown in Figure 7.5. As a result, the LAF decreases.
- Figure 7.5 shows that the torque difference for various collective inputs $\theta_{0_{tr}}$ does not vary with doublet period. Furthermore, this torque differences is almost constant for every 5°% of $\theta_{0_{tr}}$ increase. Hence the tail rotor model appears to exhibit a linear relation between increasing tail rotor collective pitch θ_0 and torque for this region of $\theta_{0_{tr}}$.

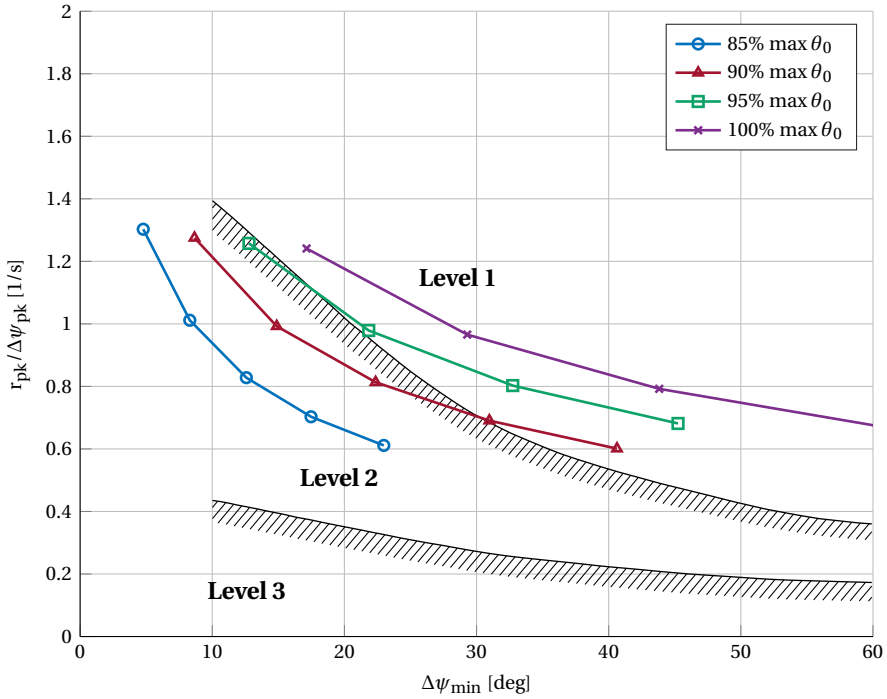

(a) Handling qualities

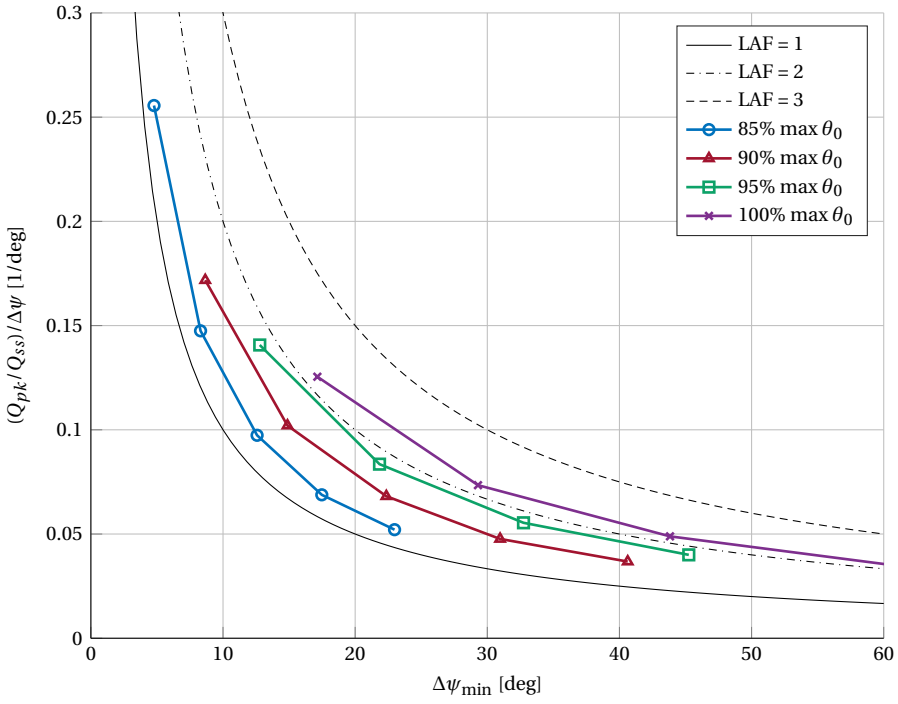

(b) Load metric

Figure 7.6 – (**a**)Variation of handling qualities, (**b**) variation of vertical shaft load metric with manoeuvre aggressiveness. Helicopter at extended range weight and nominal CG station. Flight altitude $h = 27.43$ m, upper limit $\theta_{0_{tr}} = 36.27°$.

7.4. Effect of centre of gravity location

Lastly, the effect of a shift in CG position has been investigated for a tail rotor collective step input of 95% maximum $\theta_{0_{tr}}$. The CG station is varied between forward, nominal, and aft position of a UH-60 at its design weight. Refer to Table 6.2 for values of CG stations and yaw inertia as well as applicable tail rotor trim collective angles. The nominal and aft CG position lie within 6 cm from each other, but the forward CG position lies more than 30 cm in front of the nominal CG station. A shift in CG station alters the tail rotor thrust arm with respect to the CG. Hence the collective trim value varies slightly between the three CG positions. The simulation results for this experiment are presented in Figure 7.7. The following may be observed:

- A TR collective change to 90% of maximum $\theta_{0_{tr}}$ results in Level 1 HQs for all three CG positions.
- There is little variation of handling qualities with CG position although simulation results for the forward CG position show slightly higher $\Delta\psi_{\min}$ values compared to the other two CG stations. This is caused by the increase in moment arm for the forward CG station. However, the margin of attitude quickness $r_{pk}/\Delta\psi_{pk}$ with respect to the Level 1 HQ border does not change. Apparently, the influence of tail rotor thrust arm is offset by changes in yaw inertia.
- The differences in CG station result in a higher shaft torque value for the forward CG position compared to the nominal and aft CG stations. Consequently, the LAF for a forward CG position is higher than for the nominal and aft positions which yield identical load quickness values. (Shaft torque for a pre-set collective angle does not vary with CG position or aircraft weight.)

7.5. Discussion of results

The previous sections presented the results of simulations that were done to investigate the relation between handling qualities and structural loads in the UH-60 TRDT for left-hand yaw manoeuvres. It was found that manoeuvre aggressiveness has a marked effect on yaw quickness and torque loads. Larger tail rotor collective inputs results in similar attitude quickness albeit at larger values of minimum heading change $\Delta\psi_{\min}$. This benefits the resulting handling qualities. Furthermore, weight significantly affects Handling Quality (HQ), but shifts in CG location only have a small effect on handling qualities. The lower domain of the minimum heading change $\Delta\psi_{\min}$ axis forms the critical region for moderate-amplitude heading change requirements. For example, near maximum collective inputs (95%-100% of maximum tail rotor collective pitch) are required to achieve Level 1 handling qualities for $\Delta\psi_{\min} < 20°$ at the helicopter design weight. For increasing weight it is apparent that only maximum $\theta_{0_{tr}}$ may result in Level 1 performance.

The variation of load quickness metric $Q_{l,\psi}$ with manoeuvre aggressiveness shows that the Load Amplification Factor increases linearly with collective step size $\Delta\theta_{0_{tr}}$ at a given weight and CG position. Hence, an increase of handling qualities is achieved at the expense of an increase in LAF. Furthermore, a larger weight means that a larger shaft torque is present for trimmed hover conditions. Maximum torque load in the drive train occurs when maximum tail rotor collective is applied, this is independent of aircraft weight and CG position. LAFs therefore decreases with increasing weight (for same collective step and duration). Hence, the load metric $Q_{l,\psi}$ can be used to compare loads for a given weight and CG position, but not to compare results for different weights or various rotorcraft.

7.6. Control strategies

The simulation findings can be used to answer the second research question posed in chapter 3:
"*What SLA control strategies can be identified to reduce critical dynamic loads in the UH-60 TRDT?*" The goal is to reduce LAFs while still satisfying Level 1 handling quality requirements. Use can be made of the fact that tail rotor torque loading is proportional to tail rotor collective angle. Hence, lower shaft torque loading can be achieved by selecting appropriate collective angles and input duration leading to the desired heading change with as low as possible $\theta_{0_{tr}}$ values while still satisfying Level 1 handling qualities.

To demonstrate this method, a control strategy has been devised and tested for a UH-60 at its design weight and nominal CG position. The collective control inputs are listed in Table 7.1, and the resulting handling quality requirements and load metric variation are shown in Figure 7.8. Figure 7.8a shows that Level 1 handling quality requirements are met. The attitude quickness variation has a similar shape as the Level 1 handling

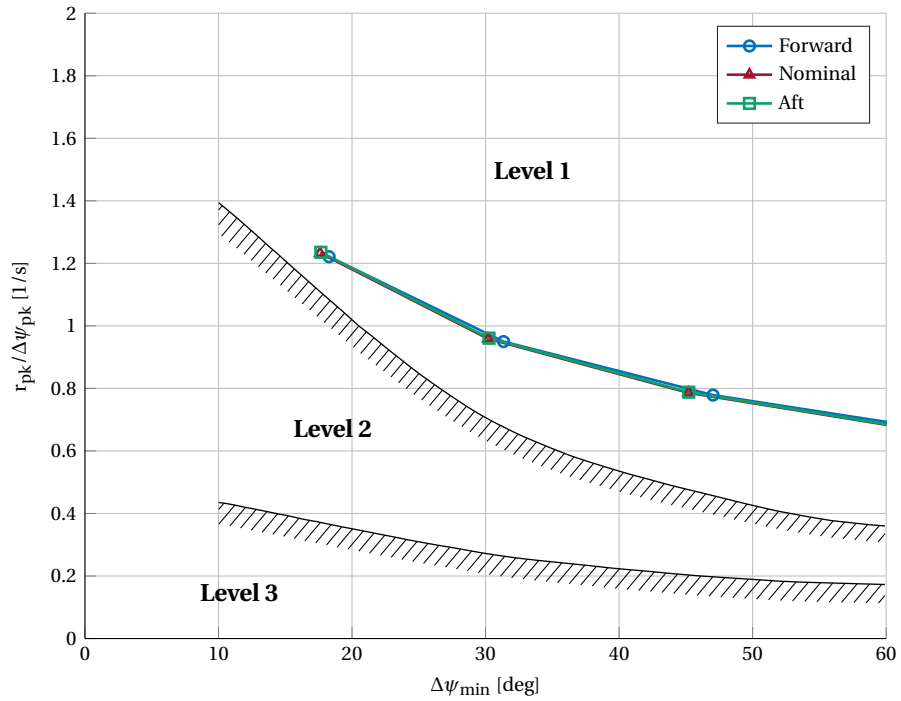

(a) Handling qualities

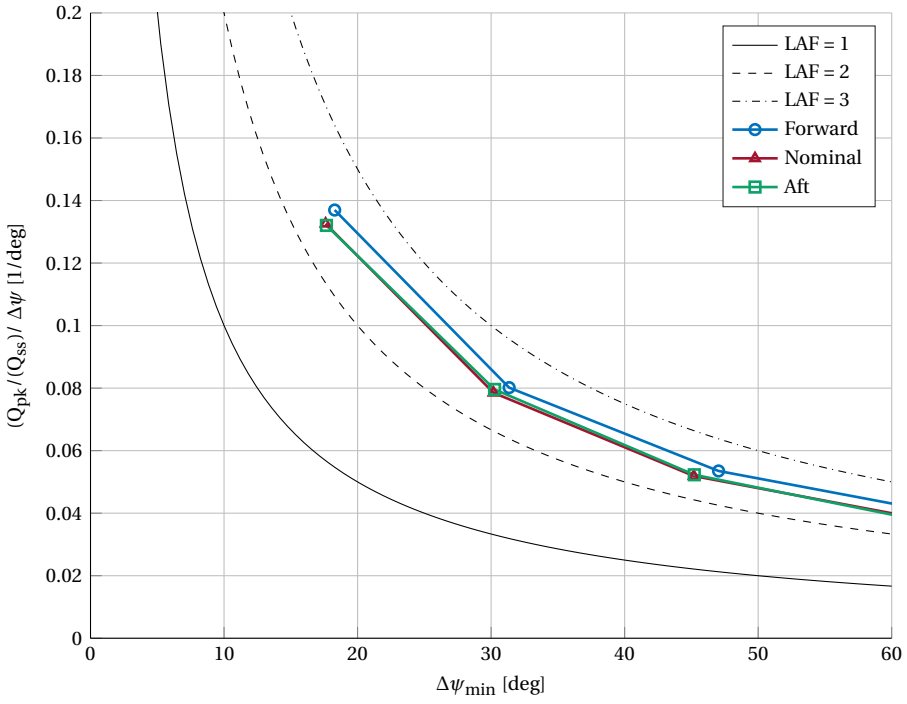

(b) Load metric

Figure 7.7 – (**a**)Variation of handling qualities, (**b**) variation of load metrics with centre of gravity position for 90% of maximum $\theta_{0_{tr}}$. Upper limit $\theta_{0_{tr}} = 36.27°$. Helicopter at design weight with varying CG stations as listed in Table 6.2. Flight altitude $h = 27.43$ m.

Table 7.1 – Tail rotor collective input for SLA control strategy.

Variable	Turn 1	Turn 2	Turn 3	Turn 4	Turn 5	Turn 6
Doublet duration [s]	1	1.5	2	2.5	3.5	4
Doublet step [% max. $\theta_{0_{tr}}$]	95	95	92.5	89	85	84

quality border and there still is some margin before this boundary is crossed. Figure 7.8b shows that the Load Amplification Factor varies from 2.4 at small $\Delta\psi_{\min}$ to 1.7 at larger heading changes. This is a $\sim$ 30% reduction of LAF over the $\Delta\psi_{\min}$ domain. For lower heading change angles larger collective inputs are required which limits a reduction of collective pitch in this area and hence the load reduction that can be achieved. Based on these findings it can be said that the SLA control strategy is successful in reducing dynamic loads in the tail rotor drive train while satisfying Level 1 HQ requirements.

7.7. Synthesis

This chapter presented simulations results for different left-turn yaw manoeuvre aggressiveness, helicopter weight, and CG station. The results show that all these variables except CG position have a significant influence on handling qualities and torque loads in the TRDT. High tail rotor collective angles are needed to perform left yaw turns as fast as possible in hover while still satisfying Handling Quality (HQ) requirements. It was found that tail rotor torque varies in a linear fashion with tail rotor collective angle. This has been used in the design of a SLA control strategy intended to reduce the load amplification during yaw manoeuvres while still satisfying ADS-33 Level 1 handling quality requirements. The devised control strategy was successfully applied to a UH-60 at its design weight and nominal CG position. Load amplification factors were reduced up to by 30% for larger values of $\Delta\psi_{\min}$ while handling qualities still satisfied ADS-33 Level 1 requirements for moderate-amplitude heading changes.

Based on these results, it appears that the Black Hawk satisfies Level 1 handling quality requirements for left turn yaw manoeuvres. However, pilots rate the UH-60 handling qualities for a Black Hawk as 4.5 on the Cooper-Harper HQR scale. [21] This means that actual UH-60A yaw manoeuvre performance is "*acceptable but unsatisfactory*" [14] and results in Level 2 handling qualities. The difference between the Level 1 handling qualities found by simulations and the Level 2 handling qualities indicated by pilots can be explained by examining the effect of modelling assumptions and restrictions on the determined handling qualities. The following three model limitations affect handling qualities:

1. The flight simulation model does not account for fuselage and airframe aerodynamics. If included in the model, airframe drag will generate a moment that counteracts the yaw motion during heading change manoeuvres. This leads to a decrease in achievable yaw rate and hence lowers the attitude quickness handling qualities.
2. The flight simulation model has two degrees of freedom for yaw and heave motion. Only main and tail rotor collective control is applied to simulate yaw manoeuvres and the position with respect to the ground is limited by the 2-DOF joint to vertical translation only. A heading change for the actual UH-60 will also require longitudinal and cyclic pitch inputs to "*limit excursions in the other axes.*" [7] This will result in power changes that adversely affect the yaw response and increase pilot workload.
3. ADS-33 stipulates rotation around the pilot station when evaluating attitude quickness for large aircraft like the UH-60. The results presented in this chapter entail rotation about the helicopter CG instead. Rotating with respect to the pilot position means that the aircraft CG will experience lateral and longitudinal motion as well. The power required to achieve these CG translations may adversely affect yaw manoeuvre handling qualities.

These limitations will affect the found handling qualities and SLA control strategy results. However, the flight simulation model does provide valuable insight in the variation of handling qualities and dynamic loads for various manoeuvre aggressiveness, even though handling qualities are over-predicted. This insight is relevant for the design of flight control laws that incorporate SLA capabilities for the tail rotor drive train. For instance, the results of the SLA control strategy may be used to quickly determine what the reduction in loads is when limiting manoeuvre aggressiveness while still satisfying ADS-33 Level 1 Handling Quality requirements for moderate-amplitude heading change requirements.

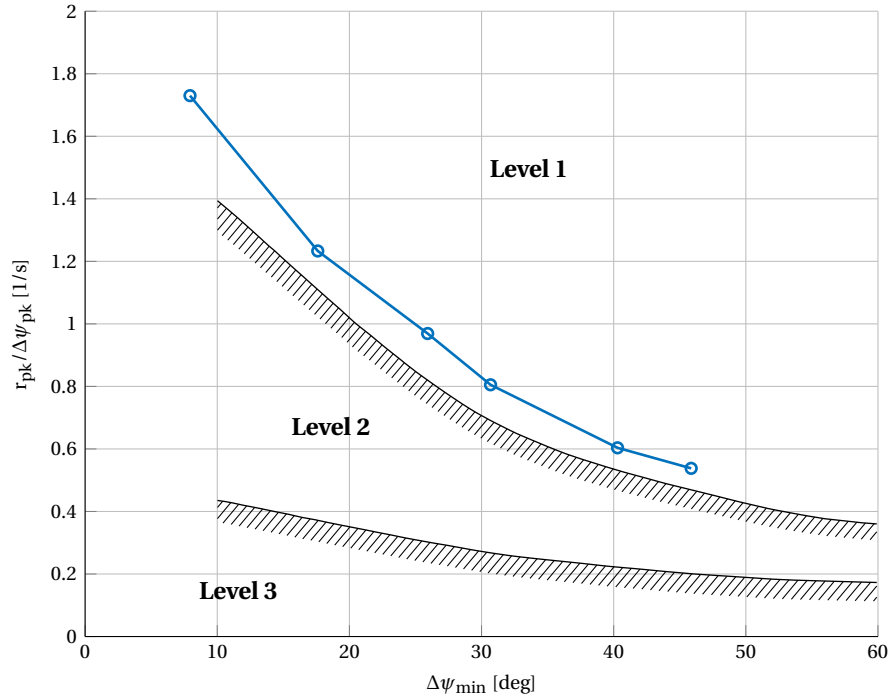

(a) Handling qualities

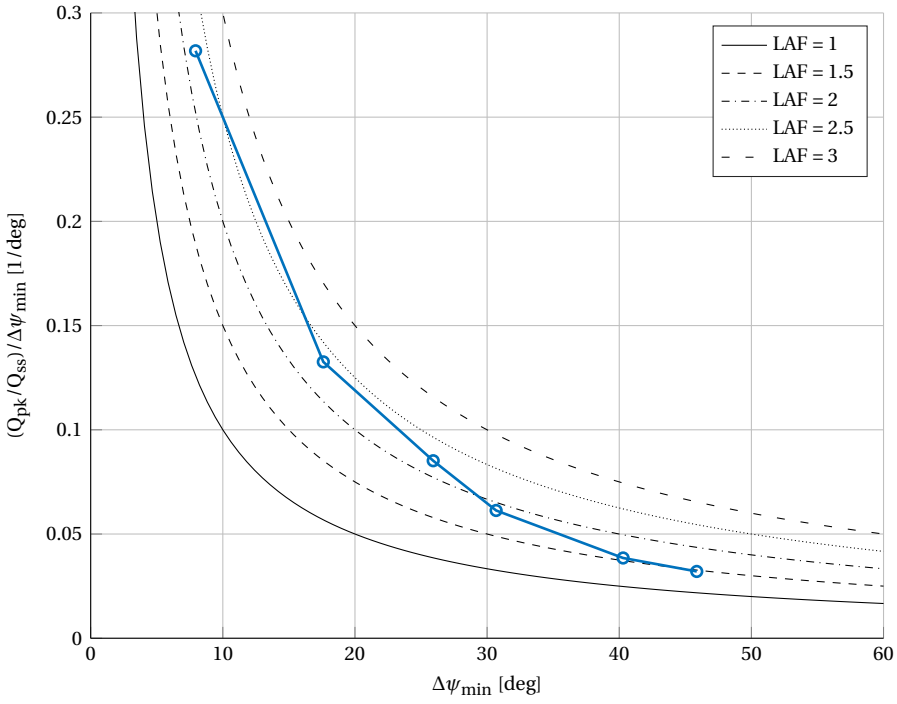

(b) Load metric

Figure 7.8 – (**a**)Variation of handling qualities, (**b**) variation of load quickness for heading change manoeuvres using a SLA control strategy. UH-60 Black Hawk at design weight with nominal CG station as listed in Table 6.2. Flight altitude $h = 27.43$ m.

This page is intentionally left blank.

8

Conclusions and recommendations

A study has been performed on structural load alleviation in the tail rotor drive train of the UH-60 Black Hawk. The aim is to reduce critical dynamic loads in the drive train which lower component damage accumulation and reduce maintenance cost. The following research objective has been defined:

> The overall research objective is to reduce critical dynamic loads in the UH-60 Tail Rotor Drive Train (TRDT) by developing a detailed flight simulation model that will be used to identify manoeuvre load alleviation control strategies.

This research project consisted of two parts. The groundwork was to construct an UH-60 flight simulation model, which could then be used to investigate structural load alleviation in the tail rotor drive train for identified critical manoeuvres. Separate objectives have been defined for these two parts:

> The first objective is to develop a simulation model of the UH-60 Black Hawk that can be used to determine dynamic loads in the tail rotor drive train during manoeuvres by constructing and validating a UH-60 TRDT multi-body dynamics model and coupling this to existing rotor, and engine models.
>
> The second objective of this research is to reduce critical dynamic loads in the UH-60 TRDT by developing novel load alleviation control strategies

This chapter first presents conclusions about the research that has been done and then discusses recommendations for future work.

8.1. Conclusions

A UH-60 flight simulation has been developed with the novel capability to determine dynamic loads in the Tail Rotor Drive Train during critical manoeuvres. A survey of pertinent literature and pilot interviews indicates that high power settings in hover are demanding for the drive train of any helicopter. Left-hand heading changes in hover are selected as critical manoeuvres for dynamic loads in the UH-60 drive train for which Structural Load Alleviation will be investigated. High transient loads occur during these manoeuvres.

The constructed flight simulation model consists of four components: a Multi Body Dynamics (MBD) main rotor model, a mathematical tail rotor model, a high fidelity Gas Turbine Simulation Program (GSP) engine model, and a MBD Tail Rotor Drive Train (TRDT) model. The flight model incorporates yaw and heave Degree(s) of Freedom for the simulation of yaw and heave manoeuvres. A simplified flight control system is included that consists of a Main Rotor (MR) collective pitch controller to eliminate vertical rates, and a Tail Rotor (TR) collective pitch controller to stabilize the helicopter yaw attitude.

The TRDT model forms the backbone of the flight simulation model. Structural properties and physical dimensions of UH-60 TRDT components have been determined using component measurements and CAD drawings available at the Condition-Based Maintenance (CBM) centre of the University of South Carolina (USC), and technical resources from NASA. The constructed MBD TRDT model is a limited fidelity model

with single Degree(s) of Freedom shafts and ideal gearboxes. The MBD modelling has been validated by an experiment at the USC CBM test stand where a strain sensor was attached to a shaft of the AH-64 TRDT. Results show that the AH-64 tail rotor drive train model, which is similar to the UH-60 TRDT, accurately predicts low frequency torque loads.

The main rotor model is an adapted version of a MBD rotor model by Dr. Voskuijl with properties from the FLIGHTLAB Generic Rotorcraft. The main changes are an updated inflow model that accounts for vertical speed during climb and descent, and a redesign of the rotor blade layout. For the tail rotor, a mathematical model providing a set of force and torque expressions similar to a Bailey rotor has been used. An in-house GSP engine model available at the FPP group represents the two GE-T700 engines. Minor updates to this model include new engine fuel flow controller gains and an updated main transmission ratio.

The static response of the UH-60 flight simulation model has been validated for hover conditions and the dynamic response has been validated for a main rotor collective step input. Comparison with FLIGHTLAB shows that the model yields adequate results for trimmed hover conditions, although the tail rotor torque and required tail rotor collective pitch differ significantly because of omitting the effect of main rotor downwash at the tail rotor. Calculated height and torque results for the response to a collective input have been compared to ADS-33 HQ requirements. Results show that a Level 1 response is achieved which is in line with pilot handling quality ratings found in literature.

Computation time is a major constraint for the usefulness of the model. Hence the complexity of the model has been reduced to limit computational expense. For this reason a simplified TRDT model with fewer bodies has been implemented, a mathematical tail rotor model has been used instead of a scaled down version of the main rotor model, and motion instead of torque actuation is employed. The combination of the `ode23s` solver and motion actuation resulted in erroneous torque peaks encountered in the drive shafts. Torque smoothing was applied to remove these artefacts. As a result, high frequency loads in the order of [1/rev] cannot be captured by the model. Given the limited fidelity of the model it was decided to use torque as an indicator of critical loads in components of the TRDT. Furthermore, omitting airframe aerodynamics and cyclic pitch inputs lead to an over prediction of handling qualities. However, the flight simulation model gives an indication of the relation between dynamic loads and turn performance. As such it can be used to investigate SLA for UH-60 TRDT components during critical manoeuvres.

The second part of this research concerns the development of load alleviation control strategies using the constructed flight simulation model. In this research, the ADS-33 requirements for moderate-amplitude heading changes have been used as a framework for feasible control options. Experiments have been conducted to determine the relation between handling qualities and drive train load amplification for various levels of manoeuvre aggressiveness, manoeuvre duration, aircraft weight, and Centre of Gravity position. A load quickness metric was defined to relate the Load Amplification Factor to the handling qualities requirements that apply during the manoeuvres flown.

The results show that aircraft weight and manoeuvre aggressiveness have a significant influence on handling qualities and torque loads in the TRDT, but that the influence of CG position is negligible. High tail rotor collective angles are needed to perform left-hand heading turns in hover as fast as possible while still satisfying HQ requirements. Tail rotor torque varies in a linear fashion with tail rotor collective angle but attitude quickness performance does not. This has been used in the design of a SLA control strategy intended to reduce load amplification factors during yaw manoeuvres while still satisfying ADS-33 Level 1 handling quality requirements. The devised control strategy is successfully applied to a UH-60 at its design weight and nominal CG position. Load amplification factors are reduced up to by 30% for larger values of $\psi_{\min}$. The control strategy indicates what reduction in load can be achieved when still satisfying level 1 handling qualities. As such it highlights areas of turning performance where SLA flight control systems may be employed in a beneficial way.

8.2. Recommendations

It has been demonstrated that the constructed UH-60 flight simulation can be used to investigate loads in the tail rotor drive train during manoeuvres. If used for further research, model improvements could be made in two areas: model computational effort and model fidelity.

Before discussing model fidelity it is important to consider the computational effort required to simulate manoeuvres with the current flight simulation model. If this issue is not addressed it may limit the suitability of the model for future use. It proved difficult to construct a functional flight simulation model that did not require excessive run time. For instance, simulation of a 15 second flight takes 12 minutes at best using the SimMechanics `ode23s` solver in *Accelerator* mode. Selecting any other solver increases the run time to over 1.5 hours at least (2.7 GHz Intel Core i5 - 8GB RAM) or the simulation may not even start at all. A number of options can be considered to speed up the model:

- Integrate an engine model that does not make use of an external program like GSP, for instance use the simplified T700 engine model as proposed by Duyar et al. [20]. Callbacks to external programs increase the computation time and their presence excludes the use of the SimMechanics *Rapid Accelerator* mode which is expected to reduce the computation time.
- Eliminate model run-in time by importing saved model states for a trimmed hover condition before the start of a new manoeuvre simulation. However, this is only possible when external models that cannot be initialized at a desired state are absent.
- Remove redundant gearbox carrier constrains in the TRDT model that adversely affect model complexity and lead to an increase in computation time.

The current flight simulation model includes simplified representations of a number of components. The model fidelity can be increased when these limitations are addressed:

- Replace the simplified engine fuel flow controller with a control system that is representative of the fuel flow control system found on the actual UH-60 Black Hawk. The engine fuel flow controller has a profound effect on loads in the drive train and system performance as a whole. This has already been indicated by van Liempt [59]: "*a small error in fuel flow schedule has a large effect on surge margin and engine response*" and also became clear during initial simulations. Howlett [27] and Mihaloew et al. [41] provide readily available UH-60 engine fuel flow controller schematics and gains.
- Switch to drive train torque actuation instead of motion actuation in the SimMechanics model. Torque actuation is representative of the actual situation and will likely remove the erroneous torque peaks that requires the use of torque smoothing. Eliminating this phenomenon will increase the model fidelity and enable analysis of higher frequency loads that are now filtered out. However, incorporating torque actuation will likely slow the model down and requires modification of the MR rotating swashplate.
- Update the tail rotor model so that it better predicts the magnitude of tail rotor torque and forces. This can either be done by including the effect of main rotor downwash at the tail rotor, or switching to another rotor model such as the FLIGHTLAB Bailey tail rotor.

A last recommendation is to investigate Structural Load Alleviation for tail rotor pitch and/or drive links. Pilots of the AH-64 and UH-60 indicated that these parts form one of the weakest links in the tail rotor drive train system. SLA research at this location would require a rotor model with the capability to determine loads in the drive/pitch links. A scaled down version of the main rotor could be used for this purpose.

This page is intentionally left blank.

Bibliography

[1] V. Adams and A. Askenazi. *Building Better Products with Finite Element Analysis*. OnWord Press, 1999. ISBN 9781566901604.

[2] E. W. Aiken, R. A. Ormiston, and L. A. Young. Future Directions in Rotorcraft Technology at Ames Research Center. In *Annual Forum Proceedings of the American Helicopter Society*, volume 56. American Helicopter Society, 2000.

[3] E. C. Ames and C. A. Parker. H-60 tail rotor drive shaft thomas coupling transient overload capacity. In *Annual Forum Proceedings of the American Helicopter Society*, volume 65, pages 970–976. American Helicopter Society, 2009.

[4] E. C. Ames and R. V. Pulikollu. Overload evaluation of rotorcraft tail rotor drive spiral bevel gears. In *Annual Forum Proceedings of the American Helicopter Society*, volume 69. American Helicopter Society, 2013.

[5] Anonymous. *UH-60A Student Handout - UH-60A Powertrain/ Rotor System*. United States Army Aviation Warfighting Center, Fort Rucker, Alabama, 2008. 4745-3.

[6] Anonymous, Department of Defence. Flight Control Systems - Design, Installation and Test of Piloted Aircraft, General Specification MIL-DTL-9490E, 2008.

[7] Anonymous, US Army AMCOM. Aeronautical Design Standard Performance Specification Handling Qualities Requirements for Military Rotorcrraft, ADS-33-PRF, 2000.

[8] F. J. Bailey. A simplified theoretical method of determining the characteristics of a lifting rotor in forward flight. Technical Report Report 716, NACA, 1941.

[9] M. G. Ballin. Valiation of a real-time engineering simulation of the UH-60A helicopter. Technical Report NASA-TM-88360, NASA, 1987.

[10] M. G. Ballin. A High Fidelity Real-Time Simulation of a Small Turboshaft Engine. Technical Report NASA-TM-100991, NASA Ames Research Center, 1988.

[11] C. L. Bottasso and A. Croce. Optimization of Critical Trajectories for Rotorcraft Vehicles. *Journal of the American Helicopter Society*, 60(February):165–177, 2005.

[12] W. G. Bousman, C. Young, F. Toulmay, N. E. Gilbert, R. C. Strawn, J. V. Miller, T. H. Maier, M. Costes, and P. Beaumier. A Comparison of Lifting-Line and CFD Methods with Flight Test Data from a Research Puma Helicopter. Technical Report NASA-TM-110421, NASA, 1996.

[13] G. M. Byham. The future of rotorcraft. *Aeronautical Journal*, 107(1072):377–388, 2003.

[14] G. E. Cooper and R. P. Harper. The use of pilot rating in the evaluation of aircraft handling qualities. Technical Report NASA TN-D-5153, North Atlantic Treaty Organisation, 1969.

[15] H. C. Curtiss. Rotorcraft Stability and Control : Past , Present , and Future. *Journal of the American Helicopter Society*, 48(1):3–11, 2003. ISSN 00028711.

[16] M. S. Darlow and J. Creonte. Optimal Design of Composite Helicopter Power Transmission Shafts with Axially Varying Fiber Layup. *Journal of the American Helicopter Society*, 40(2):50, 1995.

[17] A. Datta, J. Sitaraman, I. Chopra, and J. D. Baeder. CFD/CSD Prediction of Rotor Vibratory Loads in High-Speed Flight. *Journal of Aircraft*, 43(6):1698–1709, 2006. ISSN 0021-8669. doi: 10.2514/1.18915.

[18] H. A. DeSmidt, K. W. Wang, and E. C. Smith. Active vibration control of rotorcraft driveshaft-airframe dynamics. In *Annual Forum Proceedings of the American Helicopter Society*, volume 54, pages 472–488. American Helicopter Society, 1998.

[19] R. W. DuVal. A real-time multi-body dynamics architecture for rotorcraft simulation. In *The Challenge of Realistic Rotorcraft Simulation: Proceedings*, volume 1, 2001.

[20] A. Duyar, Z. Gu, and J. S. Litt. A Simplified Dynamic Model of the T700 Turboshaft Engine. *Journal of the American Helicopter Society*, 40(4):62–70, 1995. ISSN 1098-6596.

[21] J. W. Fletcher, J. Lusardi, M. H. Mansur, D. E. Robinson, D. R. Arterburn, I. Cherepinsky, J. Driscoll, C. S. Morse, and K. F. Kalinowksi. UH-60M Upgrade Fly-By-Wire Flight Control Risk Reduction using the RASCAL JUH-60A In-Flight Simulator. In *American Helicopter Society 63rd Annual Forum*, page 856, 2007. ISBN 1552-2938.

[22] J. Gordon Leishman. *Principles of Helicopter Aerodynamics*. Cambridge University Press, 2nd edition, 2006. ISBN 9780521858601.

[23] D. Gransden. *Aeroservoelasticity of articulated rotor hubs*. Phd dissertation, Carleton University, 2011.

[24] M. Hassan, J. Tarbutton, A. Bayoumi, and Y. J. Shin. Condition Monitoring of Helicopter Drive Shafts Using Quadratic-Nonlinearity Metric Based on Cross-Bispectrum. *Transactions on aerospace and electronic systems*, 50(4):2819–2829, 2014.

[25] P. L. Hetherington, R. F. Kraus, and M. S. Darlow. Demonstration of a Supercritical Composite Helicopter Power Transmission Shaft. *Journal of the American Helicopter Society*, 35(1):23–28, 1990. ISSN 00028711.

[26] K. B. Hilbert. A Mathematical Model of the UH-60 Helicopter. Technical Report NASA-TM-85890, Aeromechanics Laboratory, U.S. Army Research and Technology Laboratories-AVSCOM, Moffett Field, California, 1984.

[27] J. J. Howlett. UH-60A Black Hawk engineering simulation program. Volume 1: Mathematical model. Technical Report NASA-CR-166310, NASA, 1981.

[28] C. Hoyle. In a spin: the US Army's Top 10 helicopter types, 2015. URL https://www.flightglobal.com/news/articles/in-a-spin-the-us-armys-top-10-helicopter-types-410852/. Last accessed on August 7, 2017.

[29] E. M. Huff and I. Y. Tumer. An Analysis of Maneuvering Effects on Transmission Vibrations in an AH-1 Cobra Helicopter. *Journal of the American Helicopter Society*, 47(1):42–49, 2002. ISSN 00028711. doi: 10.4050/JAHS.47.42.

[30] Jane's All The World's Aircraft. Sikorsky S-70A, 2014. URL https://www.ihs.com. Retrieved from Jane's All The World's Aircraft.

[31] M. P. Jarvis and P. Sleight. Report on the accident to Aerospatiale (Eurocopter) AS332 L2 Super Puma, registration G-REDL 11 nm NE of Peterhead, Scotland on 1 April 2009, 2011. URL https://assets.digital.cabinet-office.gov.uk/media/5422f86aed915d13710006cb/2-2011_G-REDL.pdf. Last accessed on March 11, 2016.

[32] W Johnson. CAMRAD II: Comprehensive Analytical Model of Rotorcraft Aerodynamics and Dynamics. *Palo Alto, CA*, 2005.

[33] W. Johnson. NDARC-NASA Design and Analysis of Rotorcraft Theoretical Basis and Architecture. In *AHS Aeromechanics Specialists' Conference*. American Helicopter Society, 2010. URL http://ntrs.nasa.gov/archive/nasa/casi.ntrs.nasa.gov/20100021986{_}2010023275.pdf.

[34] S. Kim, M. Bothwell, and R. Fortenbaugh. The Bell 525 Relentless, The World's First "Next Generation" Fly-by-Wire Commercial Helicopter. In *Annual Forum Proceedings of the American Helicopter Society*, volume 70. American Helicopter Society, 2014.

[35] D. W. King, C. Dabundo, R. L. Kisor, and A. Agnihotri. V-22 load limiting control law development. In *Annual Forum Proceedings of the American Helicopter Society*, volume 49, pages 211–224, 1993.

[36] R. M. Kufeld and W. G. Bousman. High Load Conditions Measured on a UH-60A in Maneuvering Flight. In *Annual Forum Proceedings of the American Helicopter Society*, volume 51. American Helicopter Society, 1995.

[37] K. E. Laberge, E. C. Ames, and B. D. Dykas. Detection of Naturally Occurring Gear and Bearing Faults in a Helicopter Drivetrain. Technical Report ARL-TR-6795, Army Research Laboratory, 2014.

[38] J. Land and C. Weitzman. How HUMS systems have the potential of significantly reducing the direct operating cost for modern helicopters through monitoring. In *Annual Forum Proceedings of the American Helicopter Society*, volume 51, pages 744–757. American Helicopter Society, 1995. ISBN 0733-4249.

[39] D. C. Lombardo. Helicopter Structures - A Review of Loads, Fatigue Design Techiques and Usage Monitoring. Technical Report ARL-TR-15, Defence Science and Technology Organisation - Aeronautical Research Laboratory, Melbourne, 1993.

[40] R. R. Lynn, F. D. Robinson, N. N. Batra, and J. M. Duhon. Rotor Design Part I: Aerodynamics. *Journal of the American Helicopter Society*, 15(4):2–15, 1970.

[41] J. R. Mihaloew, M. G. Ballin, and D. G. C. Ruttledge. Rotorcraft flight-propulsion control integration. Technical Report N88-16643, NASA, 1988.

[42] National Aerospace Laboratory NLR. *GSP API*. National Aerospace Laboratory NLR, 2017. URL https://www.gspteam.com.

[43] F. Orban. Damping of materials and members in structures. *Journal of Physics: Conference Series*, 268 (1):1–15, 2011. ISSN 1742-6596. doi: 10.1088/1742-6596/268/1/012022.

[44] G. D. Padfield. The making of helicopter flying qualities: A requirements perspective. *Aeronautical Journal*, 102(1018):409–437, 1998.

[45] G. D. Padfield and M. D. White. Flight simulation in academia HELIFLIGHT in its first year of operation at the University of Liverpool. *Aeronautical Journal*, 107(1075):529–538, 2003.

[46] S. Pastorelli, A. Battezzato, and G. Mattiazzo. Fly-By-Wire Control of a Helicopter : Multibody Main Rotor Model. *26th International Congress of the Aeronautical Sciences*, pages 1–10, 2008.

[47] M. D. Pavel and G. D. Padfield. Defining Consistent ADS-33 – Metrics for Agility Enhancement and Structural Loads Alleviation. In *Annual Forum Proceedings of the American Helicopter Society*, volume 58. American Helicopter Society, 2002.

[48] M. D. Pavel and G. D. Padfield. The Extension of ADS-33—Metrics for Agility Enhancement and Structural Load Alleviation. *Journal of the American Helicopter Society*, 51(4):319–330, 2006.

[49] J. Peeters, D. Vandepitte, and P. Sas. Analysis of internal drive train dynamics in a wind turbine. *Wind Energy*, 9(1-2):141–161, 2006. ISSN 10954244. doi: 10.1002/we.173.

[50] F. G. Polanco. Estimation of structural component loads in helicopters : A review of current methodologies. Technical Report DSTO-TN-0239, Airframes and Engines Division, Aeronautical and Maritime Research Laboratory, Melbourne, 1999.

[51] N. A. Sahani, J. F. Horn, G. J. J. Jeram, and J. V. R. Prasad. Hub moment limit protection using neural network prediction. *Journal of the American Helicopter Society*, 51(4):331–340, 2006.

[52] P. D. Samuel and D. J. Pines. A review of vibration-based techniques for helicopter transmission diagnostics. *Journal of sound and vibration*, 282(1):475–508, 2005.

[53] D. Saranga. Sikorsky UH-60 BlackHawk, 2017. URL http://www.the-blueprints.com/blueprints/helicopters/sikorsky/22996/view/sikorsky_uh_60_blackhawk/. Last accessed on August 7, 2017.

[54] P. M. Shinoda, H. Yeo, and T. R. Norman. Rotor Performance of a UH-60 Rotor System in the NASA Ames 80- by 120-Foot Wind Tunnel. *Journal of the American Helicopter Society*, 49(4):401–413, 2004.

[55] D. B. Stringer, P. N. Sheth, and P. E. Allaire. A new helicopter transmission model for condition-based maintenance technologies using first principles. Technical Report ARL-TR-4984, Army Research Laboratory, Cleveland, Ohio, 2009.

[56] P. D. Talbot, B. E. Tinling, W. A. Decker, and R. T. N. Chen. A Mathematical Model of a Single Main Rotor Helicopter for Piloted Simulation. Technical Report NASA-TM-84281, NASA, 1982.

[57] The MathWorks Inc. *MATLAB Version 8.6 x86 (R2015b)*. The MathWorks Inc., Natick, Massachusetts, 2015. URL http://www.mathworks.com.

[58] M. B. Tischler, C. M. Ivler, M. H. Mansur, K. K. Cheung, T. Berger, and M. Berrios. Handling-Qualities Optimization and Trade-offs in Rotorcraft Flight Control Design. *AHS Specialists Meeting on Rotorcraft Handling-Qualities*, pages 1–40, 2008.

[59] M. van Liempt. Modeling of Engine Dynamics for Flight Mechanics Applications. Master's thesis, Delft University of Technology, 2014.

[60] W. P. J. Visser, O. Kogenhop, and M. Oostveen. A Generic Approach for Gas Turbine Adaptive Modeling. *Journal of Engineering for Gas Turbines and Power*, 128(1):13, 2006. ISSN 07424795. doi: 10.1115/1.1995770.

[61] M. Voskuijl, D. J. Walker, and B. J. Manimala. Helicopter load alleviation using active control. *Aeronautical Journal*, 112(1137):663–672, 2008.

[62] M. Voskuijl, M. J. L. van Tooren, and D. J. Walker. Condition-based flight control for helicopters: an extension to condition-based maintenance. *Aerospace Science and Technology*, 42:322–333, 2015. ISSN 12709638. doi: 10.1016/j.ast.2015.01.026.

[63] G. J. Weden and J. J. Coy. Summary of Drive-Train Component Technology in Helicopters. Technical report, NASA, 1984.

[64] W.A. Welsh, E. Eller, and R.K. Goodman. Gearbox mounted force generator, 9 2005. URL http://www.google.com/patents/US7118328. Sikorsky Aircraft Corporation.

[65] H. Yeo, W. G. Bousman, and W. Johnson. Performance Analysis of a Utility Helicopter with Standard and Advanced Rotors. *Journal of the American Helicopter Society*, 49(3):250, 2004. ISSN 00028711. doi: 10.4050/JAHS.49.250.

A

Flight simulation model

This appendix provides technical details on the UH-60 flight simulation model and instructions on how to use it

A top level view of the SimMechanics UH-60 flight simulation model is presented in Figure A.1. This figure shows how the various components have been merged to form a single flight simulation model. The main rotor inflow model is located in the *Inflow model MR* block, and an International Standard Atmosphere (ISA) model is contained in the *Atmosphere block*. All model output is collected in the *Outputs*. All measured simulation variables will be written to the MATLAB workspace after the simulation run is complete.

This model contains a simplified Flight Control System that consists of a MR collective pitch and a TR collective pitch controller. The aim of these controllers is to eliminate vertical rate and yaw rate respectively. Care must be taken to select appropriate trim constants, otherwise the control system will not be able to stabilize the helicopter. The controllers are located in the *Swashplate input MR* and *TR Collective* blocks respectively.

A custom 2-DOF joint allows for yaw and heave degrees of freedom. These DOF are activated at the start of the simulation. As a result there will be an initial downward velocity of the helicopter body as well as a non-zero yaw rate. A dummy engine model is used to supply motion actuation before the GSP engine model has reached the desired output speed. A switch is employed to simultaneously gradually phase out the dummy engine and include the GSP engine output.

Mass and inertia data, as well as physical dimensions are loaded into the model workspace using `load_model_workspace.m`. This function loads the data from separate load functions for every component model. Component model data is contained structures AC (aircraft), MR (main rotor), TR (tail rotor), and TRDT (tail rotor drive train). Please do not forget to re-initialize the model workspace once changes have been made to the variables in these structures.

Running the model requires a 32 bit MATLAB version because this is a requirement for the current version of the GSP API. It was found that the `ode23s` solver in combination with the *Accelerator* mode resulted in the lowest computation time. To simulate 15s of flight a computation time of 12 minutes is needed. A variable time step is used during the simulations, it is not possible to use a fixed time step because of errors with the over-constrained gearbox carriers. The maximum value of the time step is limited by the main rotor aerodynamic model to ensure a minimum disk rotation between each time step and obtain viable aerodynamic results.

Torque smoothing is used in this model to eliminate erroneous torque peaks in the engine torque required signal as well as other torque measurements such as for the drive shafts. The torque peaks likely result from the combination of motion actuation (where an virtually unlimited amount of torque can be applied to achieve the desired motion) and the `ode23s` solver. Using another solver might reduce the torque peaks but results in a large increase of computation time. Torque smoothing is implemented with the following filter with τ set to values below 0.1:

$$F(s) = \frac{1}{\tau^2 s^2 + \tau s + 1} \tag{A.1}$$

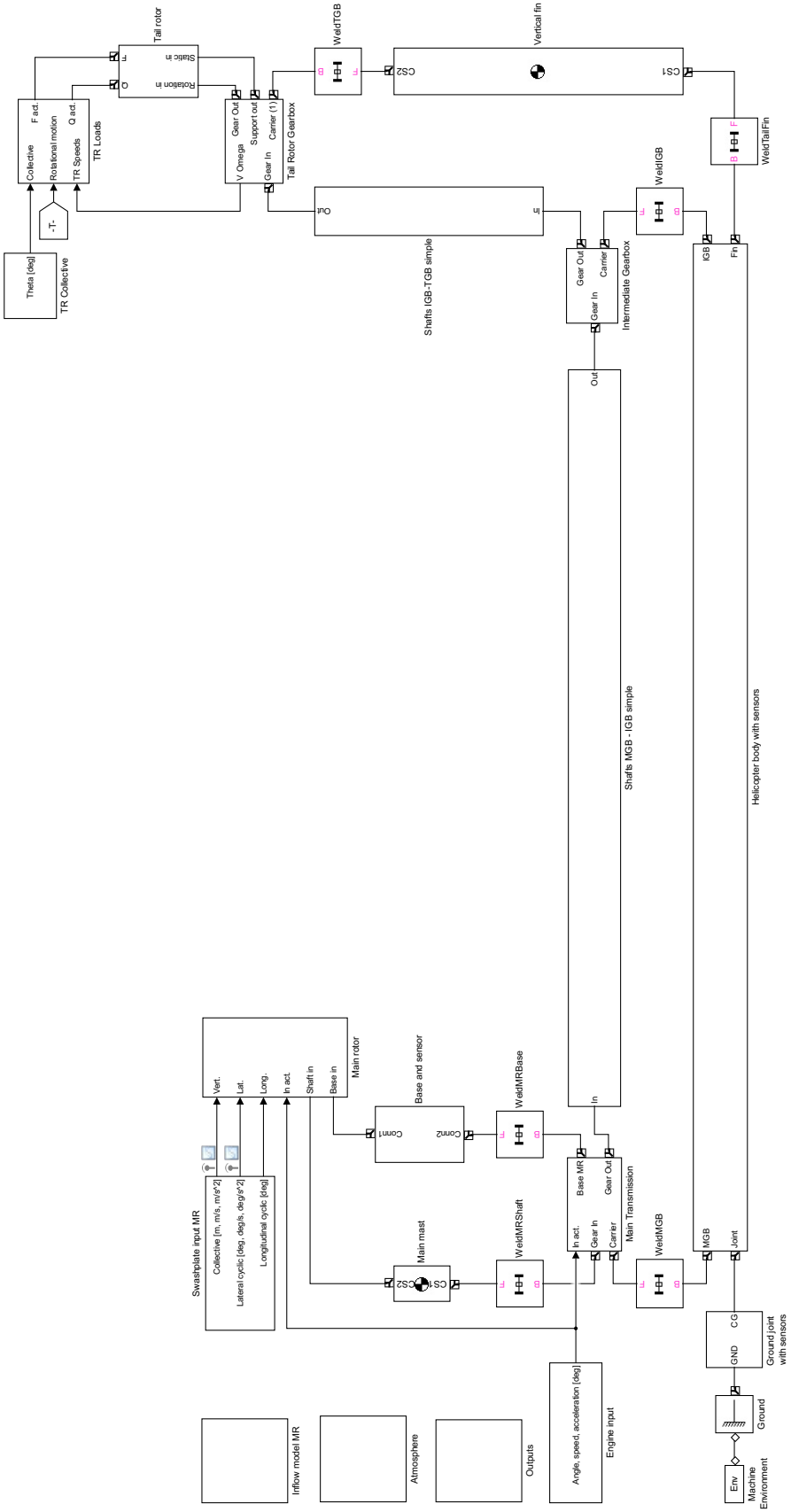

Figure A.1 – Top level SimMechanics UH-60 flight simulation model.

B

Tail rotor drive train model

This appendix provides background information on the MBD TRDT model that is included in the UH-60 flight simulation model. First the properties of the drive train model will be discussed in B.1 and second the experiment that has been conducted to validate the drive train model will be discussed in B.2.

B.1. Properties

The UH-60 Tail Rotor Drive Train consists of a system of drive shafts that run along the upper part of the tail boom, flexible couplings, bearings, and gearboxes and an oil cooler. The couplings allow for shaft misalignment, viscous bearings are used to support the shafts along tail boom and vertical fin, and the gearboxes change the angle of rotation as well as shaft RPM. See Figure B.1 for an overview of the TRDT.

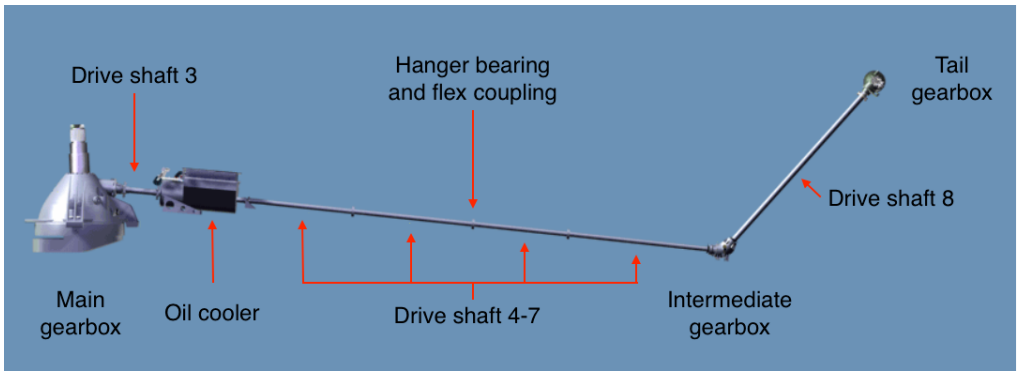

Figure B.1 – Overview of the UH-60 tail rotor drive train. [5]

Table B.1 summarizes the main characteristics of the UH-60 drive train, for more detailed information please refer to the data in `load_UH60_TRDT_data.m`. TRDT component mass and inertia have been determined using CAD drawings that where available at USC CBM or created specifically for this purpose. See Figure B.2 for an example CAD drawing of the UH-60 TGB input gear and connection flange.

The MBD TRDT incorporates rigid bodies for gears, the tail boom, and the vertical tail. Shafts are modelled with single Degree(s) of Freedom to allow for twist, with springs and dampers to account for shaft flexibility and structural damping. A system of shaft elements is interconnected by springs and dampers, see Figure B.3. Here four elements are shown to discretize the shaft, but the implemented model only includes two elements per shaft. Furthermore, the MBD TRDT contains two shafts instead of six as shown in **??**: shaft MI between the MGB and IGB, and shaft IT between the IGB and TGB. This simplification has been made to speed up the flight simulation model.

The following section outlines how the shaft spring and damping constants can be determined.

Table B.1 – Component properties UH-60 tail rotor drive train.

Parameter	Symbol	Value
MGB gear ratio [-]	MGB N_{in}/N_{out}	4119/258
IGB gear mesh ratio [-]	IGB N_{in}/N_{out}	25/31
TGB gear mesh ratio [-]	TGB N_{in}/N_{out}	19/53
MGB drive change angle [°]	θ_{MGB}	101.5
IGB drive change angle [°]	θ_{IGB}	58
TGB drive change angle [°]	θ_{TGB}	110[a]
Gear material	-	steel[b]
Gear shear modulus [GPa]	G_{gear}	70.0
Gear density [kg/m^3]	ρ_{gear}	7860
Shaft material	-	aluminium[b]
Shaft shear modulus [GPa]	G_{shaft}	26.91
Shaft density [kg/m^3]	ρ_{shaft}	2810
Shaft 3-7 inner radius [in]	r_{3-7}	1.75
Shaft 3-7 thickness [in]	t_{3-7}	0.13
Shaft 3-7 speed [rpm]	$\text{RPM}_{3\text{-}7}$	4116
Shaft 8 outer radius [in]	r_8	2.595
Shaft 8 thickness [in]	t_8	0.13
Shaft 8 speed [rpm]	RPM_8	3319

[a] 90 degrees sideward and 20 degrees upward
[b] assumed material type

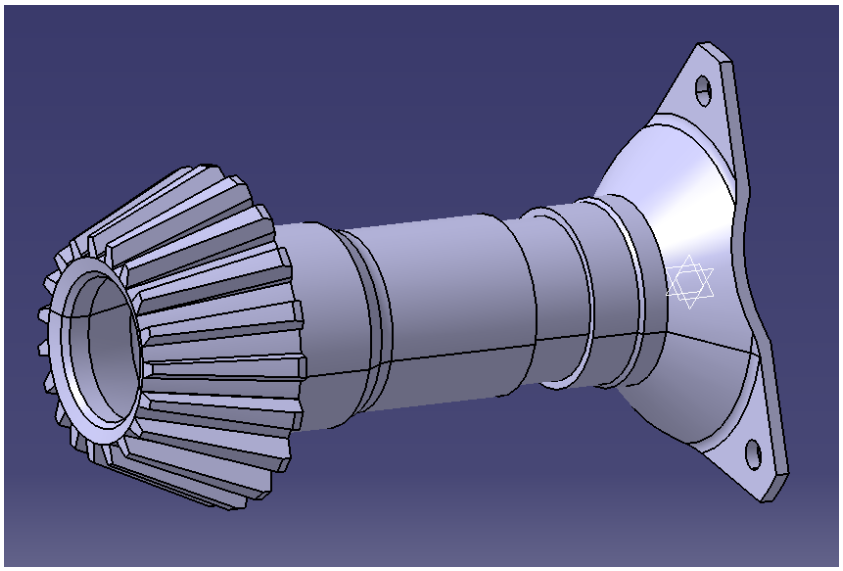

Figure B.2 – CAD drawing of UH-60 TGB input gear and flange.

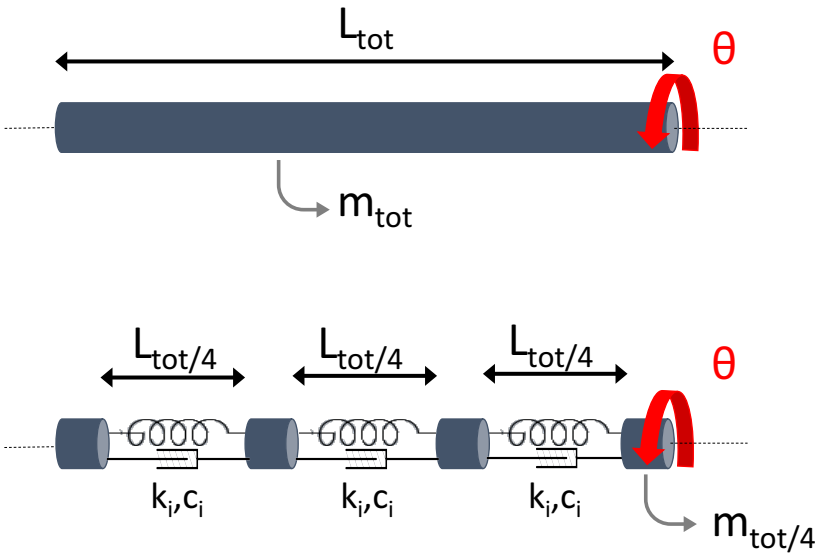

Figure B.3 – Multi-body dynamics shaft discretization.

Stiffness and damping

Drive shaft components that are operated in the linear-elastic material range exhibit a certain torsional stiffness: the extent to which torsion is resisted.The amount of torque needed to achieve a certain twist angle θ depends on the torsional stiffness k:

$$T = k \cdot \theta \tag{B.1}$$

The torsional stiffness k of a rotating shaft depends on its geometric and material properties:

$$k = \frac{GJ}{L} \tag{B.2}$$

Here, G is the shear modulus of the shaft material, J is the shaft polar moment of inertia, and L is the shaft length. The polar moment of inertia for a non-tapered shaft depends on the cross section inner and outer radii r_1 and r_2:

$$J = \frac{\pi}{2}\left(r_2^4 - r_1^4\right) \tag{B.3}$$

If the shaft is tapered, the equivalent polar moment of inertia can be determined by integrating the polar moment of inertia as a function of x, $J(x)$, along the shaft and dividing by the shaft length L:

$$J_{\text{eq}} = \frac{\int_0^L J(x)\,dx}{L} \tag{B.4}$$

The estimated drive train efficiency of modern helicopters is between 97% to 99%. [63] Part of the losses can be attributed to structural (material) damping, another cause is friction damping at the connections of the system. [43] A commonly used damping type is viscous damping, where damping is proportional to the (rotational) speed of a system:

$$m\ddot{u} + c\dot{u} + ku = F \tag{B.5}$$

where m is mass, c is the damping constant, and k is the stiffness constant. Looking at material damping only, the damping factor c depends on the type of material used and other structural properties:

$$c = \xi_n \cdot c_{cr} \tag{B.6}$$

where ξ_n is the fraction of critical damping of structural mode n, and c_{cr} is the critical damping ratio. According to Adams and Askenazi [1], ξ_n has a value of 0.04% for aluminium or steel drive shafts. The critical damping ratio depends on the mass and stiffness of the system:

$$c_{cr} = 2\sqrt{mk} \tag{B.7}$$

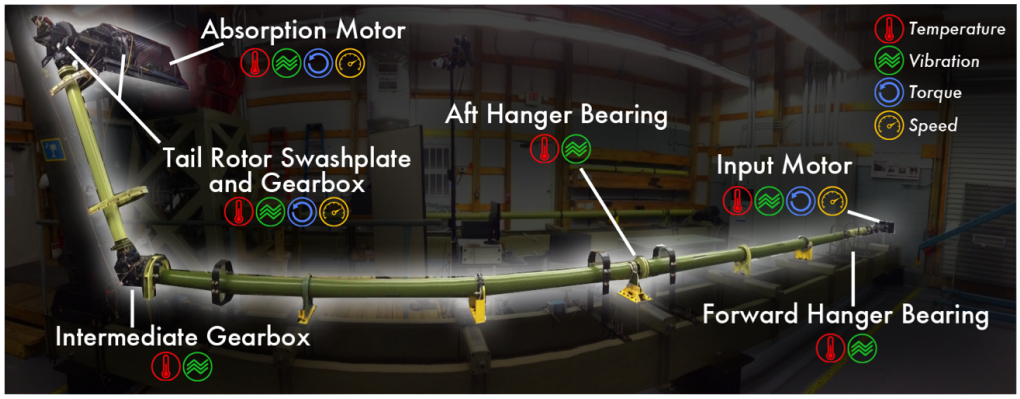

Figure B.4 – Overview of the AH-64 tail rotor drive train test stand at the Condition-Based Maintenance center of the University of South Carolina.

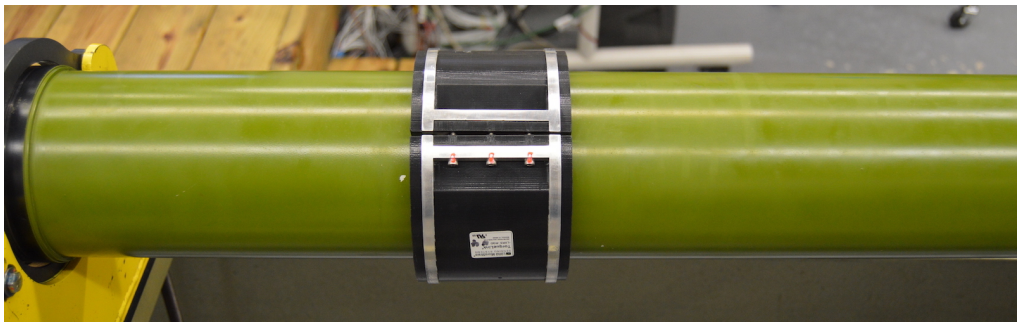

Figure B.5 – TorqueLink sensor installation with custom collar on the AH-64 tail rotor drive train test stand

The above mentioned methods are used to determine the spring stiffness and damping constants of the two shafts (MI and IT) in the MBD TRDT model. The equivalent properties of these two shaft are determined by accounting for the separate stiffness and damping constants of various parts that are contained within. Equivalent stiffness k_{eq} and damping c_{eq} constants are determined in the following way:

$$\frac{1}{k_{eq}} = \sum_{i=1}^{n} \frac{1}{k_i} \qquad c_{eq} = \sum_{i=1}^{n} c_i \tag{B.8}$$

B.2. Validation experiment

The TRDT modelling method has been partially validated by means of an experiment conducted at the USC CBM AH-64 tail rotor drive train test stand. This test stand is used by USC to investigate incipient failure of various drive train components. An overview of the test stand in presented in Figure B.4. This figure shows the various components of the test stand and the embedded sensing capability.

An experiment was devised to validate the MBD tail rotor drive train modelling method by comparing calculated drive shaft torque values to measured torque values on the AH-64 TRDT test stand. Measurements have been performed with a LORD corporation TorqueLink strain sensor attached to a drive shaft for various input speeds and loads. The strain gauge and wireless telemetry system were fitted in a custom collar and installed on the horizontal drive shaft #5 located in front of the IGB. This set-up is shown in Figure B.5.

The experiment inputs had to account for test stand limitations. First of all, the controllers of the drive and absorption motor only allow a maximum torque and speed signal input frequency of 2Hz. Furthermore, the maximum allowable variation in speed is 50 rpm/s and the variation in absorption load is 10 ft lb/s. The maximum allowable speed is 4863 rpm and the maximum load supposedly 1900 ft lb. With these limits in mind, experiment inputs were defined for various loading conditions, including RPM and torque sweeps to capture relevant drive train system dynamics as well as doublet and step inputs. A single input file was created for the various loading conditions, this is visualized in Figure B.6a.

Experiments were performed using the previously discussed RPM and load input. The TorqueLink sensor was used to measure shaft torque and speed sensors at the input and absorption motor were used to measure actual drive train RPM.

Unfortunately, the resulting torque measurements showed excessive noise, see Figure B.6b. This is in part caused by an erroneous setting for maximum torque at the absorption motor: the maximum allowable load should be 1500 instead of 1900 ft lb. This input error resulted in excessive noise in torque measurements for combinations of maximum speed (4863 rpm) and torque demand above the limit value. Clearly filtering is needed to extract useful information from these experiment results. It was found that a moving average filter could be used to retrieve the approximate speed signal and that a low-pass Infinite impulse response (IIR) Cheby2 filter from MATLAB's `designfilt` with a passband frequency of 0.3Hz could be used to retrieve the torque output signal. This very severe low-pass filter eliminates torque signal peaks with a frequency higher than 0.3Hz. The result is shown in Figure B.7. Comparison of Figure B.6a and Figure B.7 shows that the desired experiment input has not always been achieved.

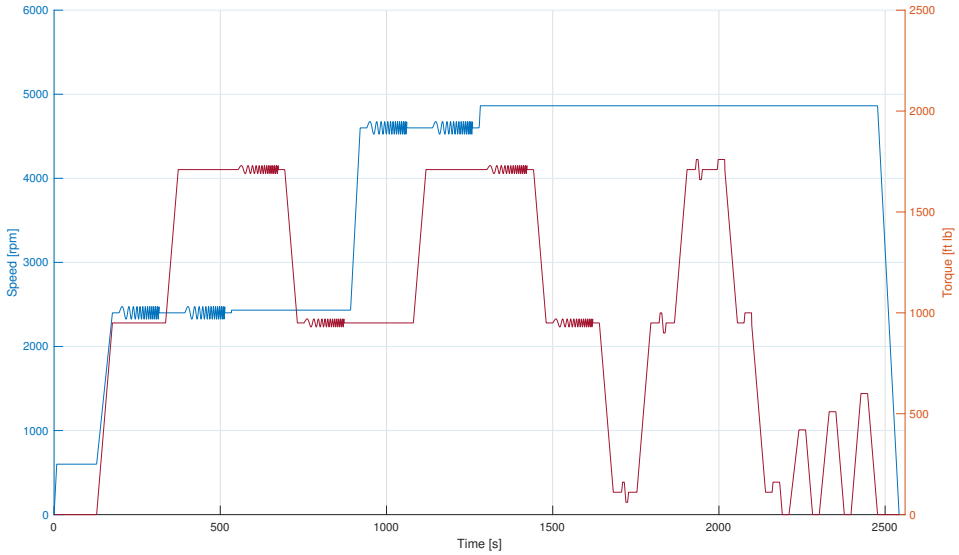

(a) Desired input

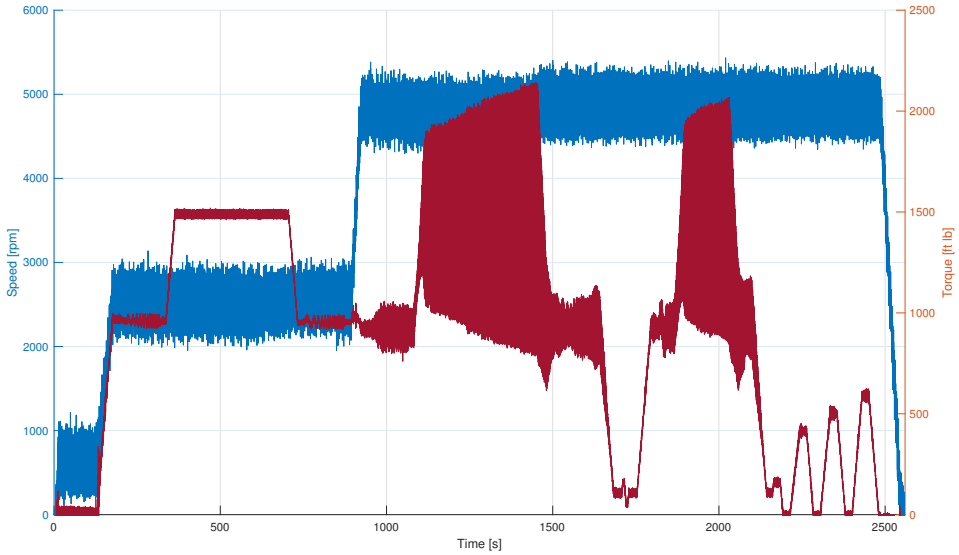

(b) Measured output

Figure B.6 – Tail rotor drive train test stand experiment (**a**) desired input torque and speed, (**b**) measured output torque and speed. Input frequency 2Hz, torque sampling frequency ~860Hz, speed sampling frequency 1000Hz.

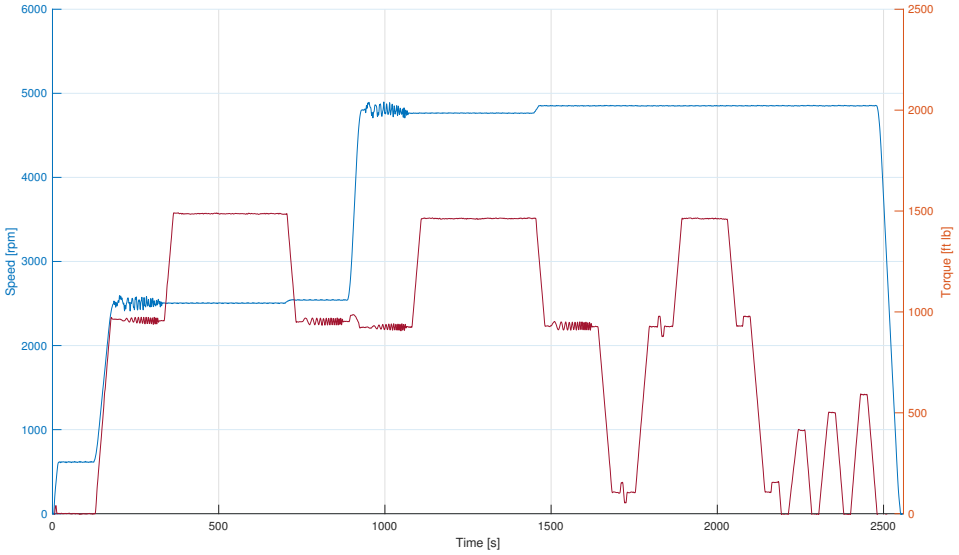

Figure B.7 – Filtered output of tail rotor drive train test stand experiment. Speed signal smoothing with moving average filter with span of 5. Torque signal filtering with lowpass IIR Cheby2 filter, passband frequency 0.3Hz, stopband frequency 0.4Hz, passband ripple 0.025 dB, stopband attenuation 60 dB.

The next and final step is to compare experiment results to the torque calculations of the AH-64 TRDT model. This is shown here for the torque doublet input at medium torque level (910 ft lb) and high speed (4863 rpm) shown in Figure B.7 around 1800s, but the results are the same for any other torque feature tested in the experiment. Input for the MBD tail rotor drive train model is measured (and filtered) torque input and speed at the absorption motor of the tail rotor drive train test stand. The model input, output, and TorqueLink measurements are visualized in Figure B.8.

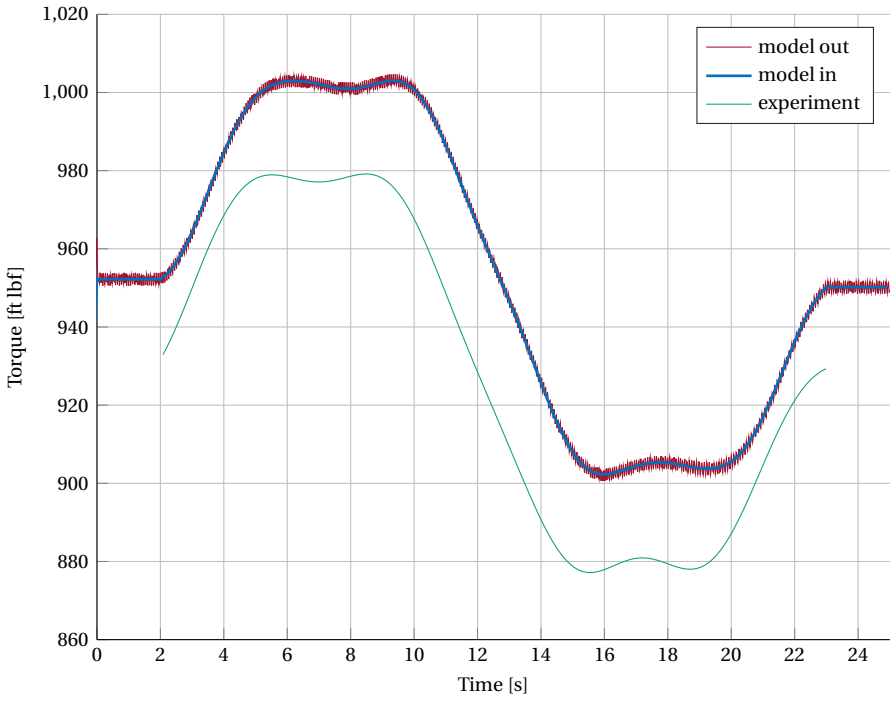

Figure B.8 – Comparison of TorqueLink experiment and MBD model results for torque doublet around 1800s.

Figure B.8 shows that the calculated torque (model out) has a similar overall trend as the model input (filtered from measured tail rotor drive train torque input) although small torque oscillations are visible. The measured and filtered TorqueLink output (experiment) has the same shape as the measured model input and output, although the curve has shifted down and somewhat to the left. This is mainly caused by uncertainties in post-processing of the measurement data: TorqueLink sampling was not started at exactly the same moment as sampling of the applied torque value at the absorption motor. The main observations here are that the model input and output are almost the same (which is as expected for a model with ideal gearboxes and 0.03% damping) and that input and output show the same trend as the TorqueLink measurements for which very similar torque values are found. Based on these observations it is concluded that the AH-64 TRDT model is able to predict low frequency torque loads in the drive train.

However, one should keep in mind that the model has only been validated for low frequency torque variation. Low-pass filtering of measurement data and low frequency experiment inputs exclude the validation of higher frequency load variation.

This page is intentionally left blank.

C

T700-GE-701 engine model

This appendix provides technical details on the engine model that is used in the UH-60 flight simulation model. It highlights what changes have been made with respect to the original model developed by van Liempt [59].

C.1. Model adjustments

Two General Electric T700-GE-701 turboshaft engines power the UH-60 Black Hawk. van Liempt [59] has created a high fidelity model of these engines that can be used in the SimMechanics environment using the GSP API. [42] GSP is a simulation software package that can be used to calculate gas turbine engine performance using the so-called 0-D method. [42] "*Zero dimensional (0-D) models compute the average state of the working fluid at discrete stations in the engine. The performance of the components can either be described by a set of equations or by component maps.*" [59] The static and transient response of this GSP engine has been validated using data from Ballin [10]. Note that a 32-bit MATLAB version is needed to use this API but that MATLAB versions from *R2016a* on are 64-bit only. The simulations in this research project have been carried out in MATLAB *R2015b*. [57]

The engine model includes a high fidelity GSP component, a simplified fuel flow control system, and a main transmission reduction block to calculate the MGB motion actuation output. Minor changes have been made to the fuel flow control system and transmission. These changes and the consequences thereof will be discussed next.

C.1.1. Transmission

The GSP API engine output torque and the total torque required are fed into the main transmission where the excess torque at the main shaft is calculated. The shaft acceleration can then be computed based on this excess torque and the total drive train rotational inertia with respect to the main shaft rotational speed I_{tot}. The rotational acceleration can in turn be integrated to determine shaft speed and angular position. Updated values for the engine transmission ratio and new drive train inertia are listed in Table C.1.

C.1.2. Fuel flow controller

The fuel flow to the UH-60 engines is controlled by means of the Hydro Mechanical Unit (HMU). This component aims to keep the engine output speed at a constant value of 20,900 RPM. [27] Fuel flow is scheduled based on the aircraft and engine state as well as pilot control input. The GSP engine model incorporates a simplified fuel flow Proportional-Integral-Derivative (PID) controller, see Figure C.1 for an overview of this controller.

A PID controller acts on the difference between desired and actual rotor speed. The resulting error correction signal is added to the control signal from a P controller that acts to protect the gas generator speed. The added

Table C.1 – Parameters of the T700-GE-701 engine model.

Parameter	Symbol	Value
HMU P control gain [kg/Pa]	P_{HMU}	6.0e-12
HMU I control gain [kg/Pa]	I_{HMU}	6.5e-12
HMU D control gain [kg/Pa]	D_{HMU}	5.0e-12
Gas generator P control gain [m s/$\sqrt{\text{K}}$]	P_{gg}	2.5e-7
Total drive train rotational inertia [kg m^2]	I_{tot}	12213
Desired main shaft speed [rad/s]	Ω_{des}	27.02
Engine transmission ratio [-]	$\Omega_{\text{eng}}/\Omega_{\text{des}}$	20900/258

controller signals are then fed into a fuel flow scheduler that accounts for the minimum and maximum fuel flow rate that can be supplied to the engine. The outcome is multiplied with engine inlet pressure P3 to obtain the desired engine fuel flow.

The controller gains in the HMU have been tuned to provide an adequate fuel flow control response for main rotor collective step inputs such as required by the ADS-33 handling qualities requirements. [7] However, the original gains did not provide an adequate collective response for the updated main rotor model that requires more torque than the original model and higher drive train inertia due to the added tail rotor drive train inertia. New gain values that provided a satisfactory engine speed response have been determined by hand. The new values of these gains are listed in Table C.1.

As became apparent from simulation results, the torque response is to a large extent influenced by the propulsion system characteristics, specifically the engine fuel flow schedule. van Liempt [59] mentions that: "*A small error in the fuel flow schedule has a large effect upon the surge margin and the response of the engine.*" This is in line with findings by amongst others Ballin [10] and Mihaloew et al. [41] that the engine dynamic response has a significant effect on handling qualities. For higher fidelity one should implement a representative fuel control system such as outlined by Howlett [27] or Ballin [10] These authors provide data and schematics required for building a fuel flow control schedule similar to that on the actual UH-60 helicopter. However, the implementation of such an elaborate controller is outside the scope of this thesis.

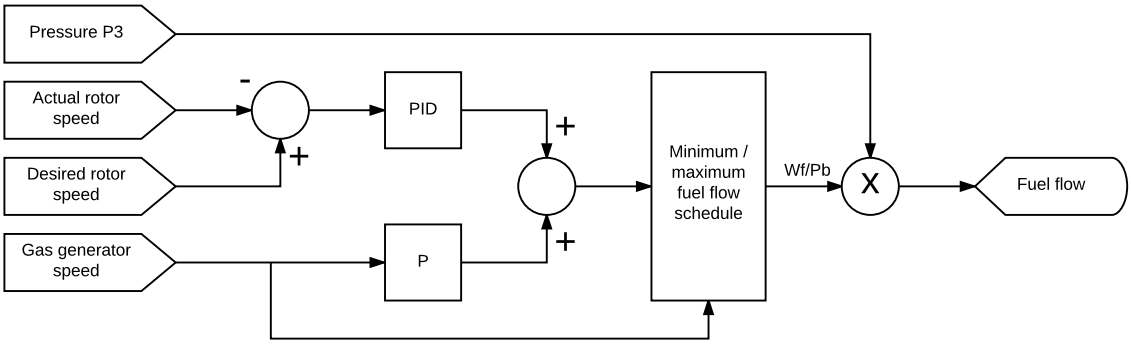

Figure C.1 – Hydro Mechanical Unit engine fuel flow controller. [59]

D

Main rotor model

The MBD MR model that is used in the UH-60 flight simulation model has been created by Dr. Voskuijl of the Flight Performance and Propulsion group at the faculty of Aerospace Engineering at Delft University of Technology . The model is inspired by the work from Pastorelli et al. [46] on MBD rotor modelling. The aim of this appendix is to provide additional technical information about the SimMechanics MBD model as presented in chapter 5 and highlight the changes that were made to the original rotor model. A detailed description of the model is given in section D.1 followed by section D.2 about the changes that have been made to the original rotor model. The main model parameters of the MBD rotor model are listed in Table D.1

D.1. Overview

The main rotor is modelled here as an articulated rotor model, with separate flap, and pitch hinges. (Lead-lag hinges not present) These components are visualised in Figure D.1a, and a diagrammatic overview of the main rotor hinges is shown in Figure D.1b. The main shaft motion actuation is applied at the MGB input gear. On the actual UH-60 torque scissors attached to the main rotor shaft are used to drive the rotating swash-plate. This is similar to the upper drag arm shown in Figure D.1a. This figure also contains a visualization of the swashplate. The rotating swash-plate moves the pitch rods which are connected to a hinge at the main rotor blades to pitch the blade.

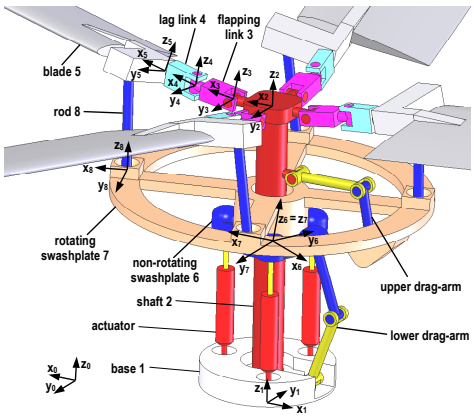

(a) Components of main rotor MBD model [46]

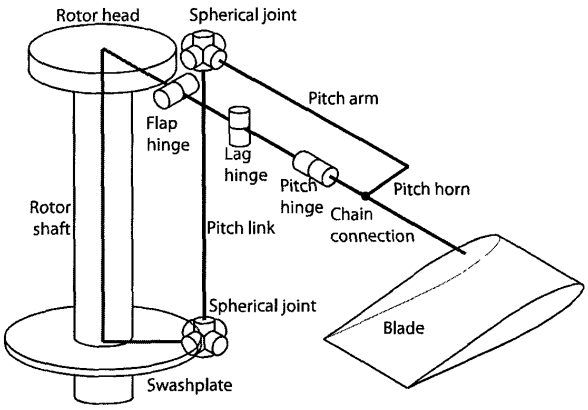

(b) Hinges and links [23]

Figure D.1 – **(a)** Main rotor MBD model, and **(b)** diagrammatic representation of rotor hinges and links.

Table D.1 – Parameters of the UH-60 main rotor model.

Parameter	Symbol	Value
Rotor blade airfoil	-	NACA0012
Number of blades [#]	$N_{b_{mr}}$	4
Calculation points per blade [#]	N_{ac}	10
Rotor blade mass [kg]	$m_{b_{mr}}$	127.8
Blade flap inertia [kg m^2]	$I_{f_{mr}}$	0.3056
Rotational speed [rad s^{-1}]	Ω_{mr}	27.018
Rotor forward tilt angle [°]	θ_{tilt}	3
Rotor radius [m]	R_{mr}	8.1778
Rotor solidity [−]	σ_{mr}	0.0821
Blade tip loss factor [−]	B	0.97
Spanwise CG station [−]	R_{cg}/R	0.586
Chordwise CG station [m]	c_{cg}/c	0.25
Chordwise AC station [m]	c_{ac}/c	0.25
Chordwise pitch hinge station [m]	c_{pitch}/c	0.25
Flap hinge radius [m]	R_{flap}	0.332
MR hub stationline [in]	STA_{mr}	341.2
MR hub waterline [in]	WL_{mr}	315.0
Collective control P gain [s]	P_{mr}	-5.82e-3
Collective control I gain [s^2]	I_{mr}	-1.0e-2
Trim collective angle [°]	$\theta_{0,mr_{\text{trim}}}$	16.50

The rotor blades are modelled as single element rigid bodies with 10 aerodynamic calculation points per blade. The aerodynamic forces and moments are computed using the Blade Element Momentum theory which assumes 2-D flow at each blade section (no radial flow is considered). Blade section velocity is measured at each calculation point. Combined with the local inflow velocity, the effective velocity vector can be determined which in turn yields the angle of attack α . Sectional aerodynamic loads are then determined using C_L, C_D, and C_M lookup tables for NACA0012 airfoils. These loads are then applied at the aerodynamic centres which are located at $c/4$.

A hard stop is included at the flap hinge of each rotor blade to prevent the blades from reaching unrealistic low flap angles. An initial condition is imposed on the main rotor speed to ensure that the rotor blades generate sufficient lift and do not fall down. This prevents the rotor blades from hitting the hard stops and greatly reduces the computational effort required to simulate the blade bounce back due to the high stiffness blade stop springs.

An overview of the SimMechanics Main Rotor model is shown in Figure D.2. This picture shows the control variables of the main rotor model: collective pitch (input 1), lateral cyclic pitch (input 2), longitudinal cyclic pitch (input 3), and engine speed (input 4). The main shaft is connected to the motion actuated MGB input gear by connection port 1 (Shaft in). The non-rotating swashplate is attached to the fuselage by connection port 2 (Base in). Motion actuation is initially supplied by a dummy engine model and afterwards by a GSP engine model. This is done to prevent rotor blades from bouncing after hitting the hard stops described in chapter 5 which requires a significant computational effort.

D.2. Adjustments

The original MBD rotor model was designed to represent the main rotor of the UH-60 in hover conditions, with aerodynamic and structural properties obtained from the FGR model. [19] A number of adjustments had to be made before the model was suitable for yaw manoeuvre simulations. These changes are outlined in the following sections.

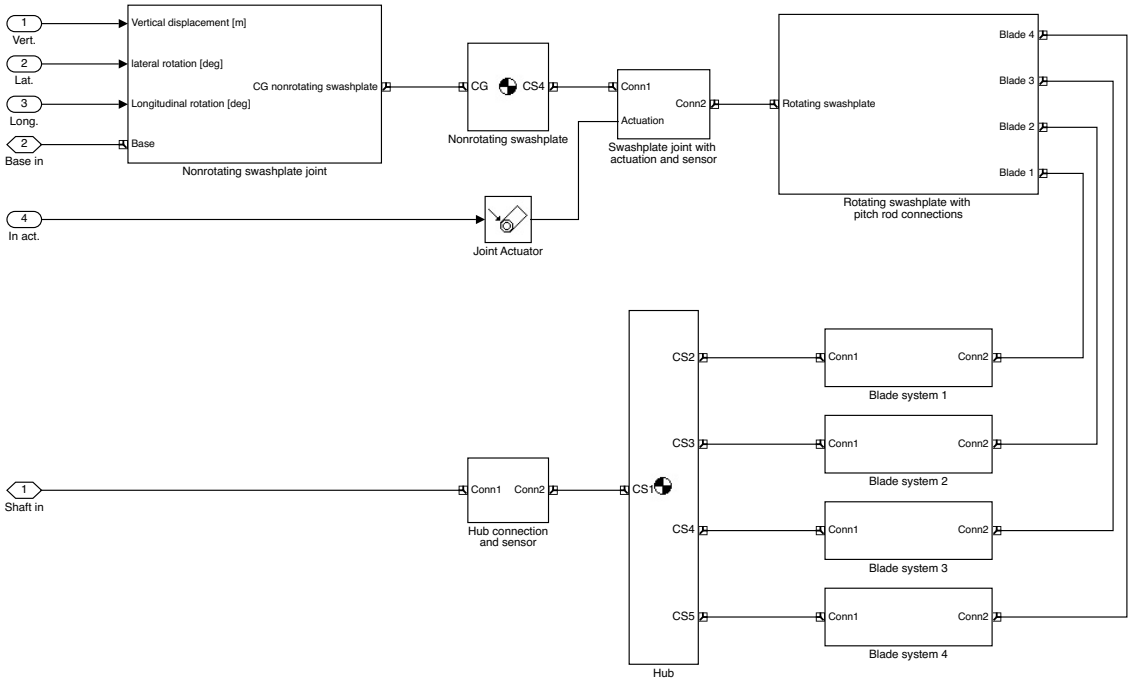

Figure D.2 – Top level components of main rotor SimMechanics model.

D.2.1. Rotor blade lay-out

The original rotor model featured rotor blades modelled with 5 equal length blade segments connected by welds. The segment CG was located spot in the middle of each segment, with mass and inertia properties derived from the FGR. Each blade segment featured a single aerodynamic calculation point at the quarter chord line $c/4$ and a pitch hinge on the half chord line $c/2$. This configuration is shown in Figure D.3a

A number of adjustments were made to the old blade layout to mimic the FGR model blade layout and prevent excessive pitch link loads. The new blade layout is shown in Figure D.3b. A single rigid body for the entire blade is introduced to limit the total number of bodies in the simulation model. It is hoped that this will reduce the computational effort required for blade motion simulation. Furthermore, now 10 equi-annular spaced aerodynamic calculation points are used per blade. This means that the aerodynamic forces and moments for each calculation point are determined with respect to an equal disk area. Lastly, the blade CG and pitch hinge line now both located at the blade quarter chord line where the aerodynamic calculations points are located also. This is done to prevent excessive loading of the pitch links and to ensure that the blade loads are transferred from the flap hinge to the main rotor hub.

D.2.2. Inflow model

A rotor generates thrust by acceleration of an amount of air through the rotor disk. The original rotor model featured an inflow model applicable to hover conditions only. Rotor thrust in hover can be determined using the Actuator Disk Theory (ADT) and assuming a uniform Glauert inflow model for induced velocity V_i at the rotor disk:

$$T = 2\rho\pi R_{MR} V_i^2 \tag{D.1}$$

During yaw manoeuvres the helicopter may experience a rate of climb or descent which affects the mass flow through the rotor. Hence the inflow model has been adjusted to account for this vertical rate. The mass flow through the rotor becomes larger for a positive Rate of Climb (RC), or $\dot{h}$, which means the induced velocity will be smaller. (For the same helicopter weight) Equation D.2 gives an expression for the rotor thrust as a function of rate of climb and induced velocity that is now used in the MR model:

$$T = 2\rho\pi R_{MR}(\dot{h} + V_i)V_i \tag{D.2}$$

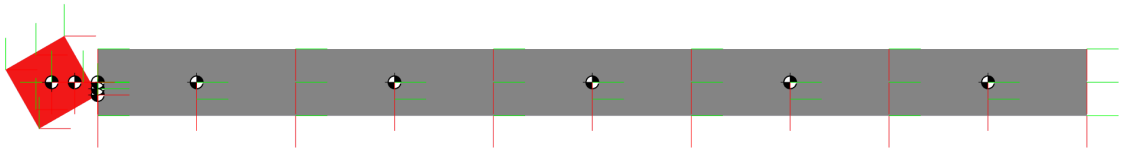

(a) Old layout

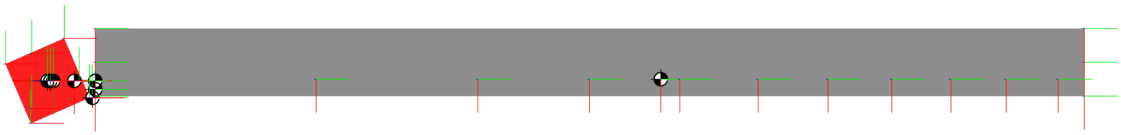

(b) New layout

Figure D.3 – **(a)** Old blade MBD model with five equispaced calculation points. **(b)** New blade model with ten equi-annular spaced calculation points. The red body represents the main rotor swashplate construction.

Lastly, it was found that the original rotor inflow model could not cope with rotor tilt (which is used on the UH-60) and did not correctly account for the effect of induced velocity at local blade sections. (Induced velocity was erroneously applied as radial flow component that is ignored in BEM calculations.) The disk inflow direction is now calculated in the rotor disk plane and then applied at local blade segments using appropriate Euler transformations.

E

Tail rotor model

This appendix gives more technical details about the Tail Rotor model that has been integrated in the UH-60 flight simulation model. This mathematical model of the UH-60 tail rotor has been developed by Hilbert [26] and is in turn based on the work done by Talbot et al. [56]. The model consists of a set of quasi-static load equations similar to a Bailey tail rotor model, [8], but besides thrust also yields rotor torque and in-plane rotor forces. Table E.1 lists the properties of the UH-60 tail rotor model. The way in which the tail rotor model is integrated in the UH-60 flight simulation model is detailed in section E.1, as well as model adjustments. Lastly, the tail rotor control limits and trim settings are discussed in section E.2.

E.1. Model integration

The mathematical tail rotor model provides a set of equations to determine rotor performance. Direct calculation of loads has been realized by setting lateral and longitudinal pitch inputs to zero and ignoring tip path plane dynamics. This yields an implicit relation for the inflow ratio λ which can be solved using the MATLAB function `fzero`:

$$\lambda_{tr} = \frac{w_{tr_C}}{\Omega_{tr} R_{tr}} - \frac{C_{T_{tr_W}}}{2\sqrt{\mu_{tr_c}^2 + \lambda_{tr}^2}} \tag{E.1}$$

Here, w_{tr_C} is the velocity along the shaft in the canted rotor axis system, Ω_{tr} is the rotational speed, R_{tr} is the rotor radius, $C_{T_{tr_W}}$ is the rotor thrust coefficient, and μ_{tr_C} is the advance ratio. Using this equation to determine the inflow ratio λ, rotor torque and in-plane forces are then calculated for a given collective input, translational and rotational helicopter body velocities, tail rotor rotational speed, and ambient conditions. The model inputs and outputs are visualized in Figure E.1. All speeds are measured using joint and body sensors connected to the SimMechanics MBD model. The ambient conditions at the pre-set flight altitude h are determined using an ISA model.

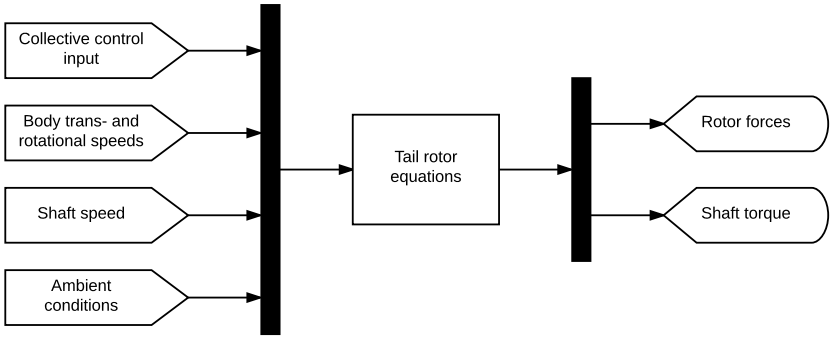

Figure E.1 – Input and output of the mathematical tail rotor model.

Table E.1 – Parameters of the UH-60 tail rotor model.

Parameter	Symbol	Value
Number of blades [#]	$N_{b_{tr}}$	4
Rotor blade mass [kg]	$m_{b_{tr}}$	5.050
Rotational inertia [kg m^2]	I_{tr}	14.195
Rotational speed [rad/s]	Ω_{tr}	124.535
Rotor radius [m]	R_{tr}	1.676
Rotor solidity [−]	σ_{tr}	0.1875
Rotor lock number [-]	γ_{tr}	3.3783
Pitch flap coupling tangent [-]	$K_{1_{tr}}$	0.7002
Rotor upward cant angle [°]	θ_{cant}	20
Rotor precone angle [°]	a_0	0.750
Linear blade twist [°]	$\theta_{t_{tr}}$	-18
Lift curve slope [1/rad]	a_{tr}	5.73
TR hub stationline [in]	STA_{tr}	732.0
TR hub waterline [in]	WL_{tr}	324.7
Proportional collective gains [s]	$P_{1,tr}$ & $P_{2,tr}$ [a]	92.0 & 61.3
Integral collective gains [s^2]	$I_{1,tr}$ & $I_{2,tr}$ [a]	160.0 & 0.15
Trim collective angle [°]	$\theta_{0,tr_{\text{trim}}}$	26.295

[a] Controller gains to trim the helicopter before the start of a yaw manoeuvre (1) and after (2).

E.1.1. Load application

In the SimMechanics implementation of the tail rotor model, the calculated forces and moments are applied to two rigid bodies as shown in Figure E.2. Tail rotor torque is applied along the shaft at the rotating body and forces are applied to the non-rotating tail rotor support body. This is done because the calculated tail rotor loads are defined with respect to the a non-rotating axis system and hence cannot be applied directly to the rotating TR body.

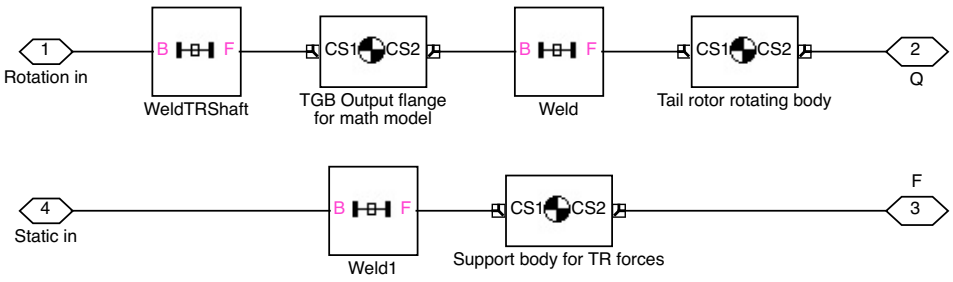

Figure E.2 – Tail rotor model bodies for application of loads.

E.1.2. Model adjustments

Two adjustments have been made to the original model by Hilbert [26] and Talbot et al. [56]. The first is a correction to an equation to calculate in-plane rotor forces. Please refer to reference [56] for an explanation of the variables in this equation. The second adjustment is that the influence of the main rotor downwash on the tail rotor is neglected.

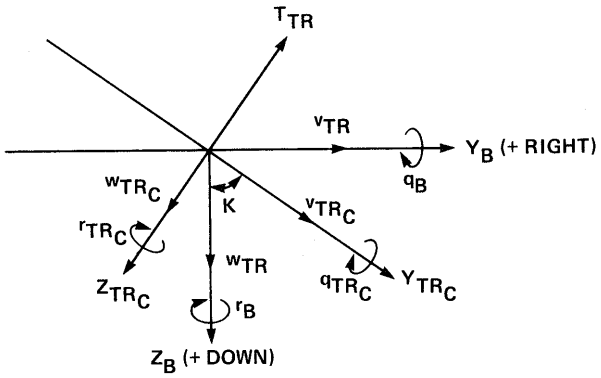

Figure E.3 – Definition of tail rotor axis systems. [26]

Correction

The first adjustment is a correction of an equation to calculate in-plane rotor force $H_{W_{tr}}$ as given by Talbot et al. [56, pp. 25]. A square bracket is missing and a wrong subscript of advance ratio μ_{tr} is used. The blue parts in Equation E.2 are new and the red part has been deleted.

$$\begin{aligned} H_{W_{tr}} =& \rho a_{tr} c_{tr} R_{tr}^2 (\Omega_{tr} R_{tr})^2 \Bigg\{ \frac{\delta_{tr}\mu_{tr}}{2a_{tr}} - \frac{1}{4}(\theta_{0_{tr}} - K_{1_{tr}} a_{0_{tr}})\left(2\lambda_{tr}\mu_{tr} - \frac{4}{3}a_{1_{tr}}\right) - \frac{\theta_{t_{tr}}}{4}(\mu_{tr}\lambda_{tr} - a_{1_{tr}}) \\ & - \frac{1}{4}K_{1_{tr}}\left[\frac{2}{3}a_{0_{tr}}a_{1_{tr}} + b_{1_{tr}}(\lambda_{tr} - a_{1_{tr}}\mu_{tr})\right] + \frac{3}{4}\lambda_{tr}a_{1_{tr}} - \frac{a_{0_{tr}}b_{1_{tr}}}{6} + \frac{mu_{tr}}{4}(a_{0_{tr}}^2 + a_{1_{tr}}^2) \\ & - \left[\frac{1}{6}(\theta_{0_{tr}} - K_{1_{tr}}a_{0_{tr}}) + \frac{\theta_{t_{tr}}}{8} + \frac{3}{16}K_{1_{tr}}b_{1_{tr}}\mu_{tr} + \frac{\lambda_{tr}}{2} + \frac{a_{1_{tr}}\cancel{\mu_{tr}}\,\mu_{tr}}{16}\right]\frac{p_{tr}}{\Omega_{tr}} \\ & - \left(\frac{1}{16}K_{1_{tr}}a_{1_{tr}}\mu_{tr} + \frac{a_{0_{tr}}}{6} + \frac{b_{1_{tr}}\mu_{tr}}{16}\right)\frac{q_{tr}}{\Omega_{tr}}\Bigg\} \end{aligned} \tag{E.2}$$

Main rotor downwash

The second change with respect to the model by Hilbert [26] is that the main rotor downwash effect on the tail rotor is neglected. In the original model, this downwash effect is included in the along shaft airspeed component w_{tr_C} in the canted rotor axis system that is used in Equation E.1.

$$w_{tr_C} = -v_{tr}\cos K + w_{tr}\sin K \tag{E.3}$$

Here v_{tr} and w_{tr} are the tail rotor hub velocities in the helicopter body axis system, K is the rotor cant angle. See Figure E.3 for a sketch of the tail rotor axes systems and local velocity components as defined by Hilbert [26]. w_{tr} in turn depends on the helicopter body translational speed w_b and rotational speeds q_b, the distance between helicopter CG and TR hub stationlines STA_{tr} and STA_{cg}, as well as the induced main rotor velocity $w_{i_{tr}}$.

$$w_{tr} = w_b + q_b(\text{STA}_{tr} - \text{STA}_{cg}) + w_{i_{tr}} \tag{E.4}$$

Talbot et al. [56] estimate the main rotor downwash velocity $w_{i_{tr}}$ for a constant location in the hub-body axis system and wake angle referred to that system based on wake measurement data. However, this is not used in the implemented tail rotor model because the complexity involved with main rotor wake estimation is outside the scope of this thesis. Furthermore no satisfying solution was found to implement the effect of a constant main rotor downwash, The model yielded unrealistically low torque values for a given thrust level when a constant downwash MR was included Because of these problems and the complexity of wake modelling it was decided not to include the effect of downwash on the tail rotor.

E.2. Control limits

The tail rotor thrust of the UH-60 Black Hawk is controlled by adjusting the blade root collective angle $\theta_{0_{tr}}$. The pilot can move pedals in the cockpit to control tail rotor blade pitch by means of a control cable system and servos connected to the tail rotor blades using pitch links. Howlett [27] lists the travel and neutral position of these pedals, this is shown in Table E.2. These limits have also been accounted for in the tail rotor model of Hilbert [26]. The sensitivity of blade pitch angle $\theta_{0_{tr}}$ to pedal input, as well as model settings for a very small forward velocity in trimmed conditions are also listed in Table E.2.

Table E.2 – UH-60 tail rotor control limits, pedal sensitivity, and trim settings.

Parameter	Symbol	Value
Pedal limit left (in)	$\delta_{p,\text{left}}$	2.69[a]
Pedal limit right (in)	$\delta_{p,\text{right}}$	2.69[a]
Pedal neutral position (in)	$\delta_{p,0}$	0[a]
Pedal sensitivity (rad/in)	$d\theta_0/\delta_p$	-0.07743[b]
Tail Rotor collective for $\delta_{p,0}$ (rad)	$\theta_{0_{\text{neutral}}}$	0.1743[b]
Pedal deflection 1kn forward trim (in)	$\delta_{p,\text{trim}}$	-1.279[b]
Minimum collective angle (rad)	$\theta_{0_{tr,min}}$	-0.127
Maximum collective angle (rad)	$\theta_{0_{tr,max}}$	0.633

[a] Values from Howlett [27, pp. 6.16]
[b] Values from Hilbert [26, pp. 13–15]

Using the data in Table E.2, the collective angle of the original tail rotor model in near hover trim conditions can be determined, as well as the minimum and maximum collective angle. The collective limits are -0.034 and 0.383 radians respectively, with a trim collective angle of 0.273 rad. This leaves a margin of 0.11 rad, or 6.3°, before the maximum $\theta_{0_{tr}}$ is reached.

However, for the implemented TR model, $\theta_{0_{tr,\text{trim}}}$ was found to be 0.4589 radians. Because the inflow of the main rotor wake at the tail rotor is neglected, a higher tail rotor collective angle is needed to achieve the desired tail rotor thrust in hover. In trimmed hover conditions, the required collective angle already exceeds the limits that follow from Table E.2. To prevent unrealistically large tail rotor collective inputs it was decided to limit $\theta_{0_{tr}}$ input in the flight simulation model to 10° above the trim collective and the same travel to the lower limit from the neutral position at 0.253 rad. This results in a collective travel from -0.127 to 0.633 rad.